Development of a Miniature and Implantable Heart Pump as the Left Ventricular Assist System: Heart Turcica Centrifugal

by

Çınar ERSANLI

A Thesis Submitted to the
Graduate School of Engineering
in Partial Fulfillment of the Requirements for
the Degree of

Master of Science
in
Mechanical Engineering

Koc University
March 2009

Koc University

Graduate School of Sciences and Engineering

This is to certify that I have examined this copy of a master's thesis by

Çınar ERSANLI

and have found that it is complete and satisfactory in all respects,
and that any and all revisions required by the final
examining committee have been made.

Committee Members:

İsmail Lazoğlu, Assc.Prof. (Advisor)

Murat Sözer, Asst.Prof.

Erdem Alaca, Asst.Prof.

Date: 27.03.2009

ABSTRACT

Heart disease is one of the most common, unexpected and number one cause of death globally; according to world health organization, approximately 17.5 million people died because of cardiovascular heart disease in 2005 which represents the 30 % of all of the deaths worldwide. In Turkey, similar situation also occurs; 55% of the total deaths is because of the heart failure problems. According to the Europe Heart Health Research, Turkey is the European leader in the number of heart failures for the ages of less than 50. In Turkey, every year approximately 500,000 patients have heart failure and 2000 to 3000 of them need urgent heart transplantation. Unfortunately, due to lack of donors, only about a few operations can be done every year.

During the long waiting time for a healthy donor heart, an artificial heart, mainly a ventricular assist device is currently the only hope and possible solution for the patients. Artificial heart pumps are known to be the best solutions for bridge-to-transplant, bridge-to-recovery and final medical solution for the patients who suffer from heart failures that result from the overfilling of the blood vessels of heart.

There are various ventricular assist devices produced in the developed countries. It is imported and used in about 20 patients in Turkey. Costs of LVAD systems are very high and not affordable by many patients in Turkey. The aim of this thesis is to develop a new ventricular assist device in Turkey. The VAD system being developed is named as “Heart Turcica”. The development process of the Heart Turcica LVAD system of five main parts: CAD (Computer Aided Design), CFD (Computational Fluid Dynamics) analyses, CAM (Computer Aided Manufacturing), precision production by Computer Numerical Control (CNC) machines and performance testing. The developed Heart Turcica LVAD system consists of a centrifugal pump, control unit and peripheral equipments. The pressure rise of the heart pump, flow rates and rotational speeds are controlled and monitored in the experiments.

Heart Turcica Centrifugal is designed and manufactured from Titanium alloy to be biocompatible with the blood tests in the hospital. In this thesis, the design process of the heart pump, the performance curves of several designs, and the results of in-vitro experiments carried out are presented.

ÖZET

Kalp rahatsızlıkları tüm dünyada en beklenmedik ve yaygın ölüm nedenlerinin başında gelir. Dünya Sağlık Örgütü'nün istatistiklerine göre, 2005 yılında kardiyovasküler kalp rahatsızlıkları nedeniyle tüm dünyada 17,5 milyon kişi hayatını kaybetmiştir ve bu rakam tüm ölümlerin %55'ine tekabül etmektedir. Benzer durum Türkiye'de de vardır, Avrupa Kalp Sağlığı Araştırmasına gore, 2007 yılında 50 yaş altı kalp rahatsızlığı sıralamasında Avrupa lideri olmuştur. Türkiye'de her yıl yaklaşık 500.000 kişi kalp rahatsızlığı geçirmekte ve bu hastalardan en az 2000 ile 3000 tanesine acil kalp nakli yapılması gerekmektedir. Ne yazık ki donör azlığından ötürü her yıl oldukça az sayıda operasyon yapılmaktadır.

Sağlıklı bir donör beklemek için geçen uzun süre boyunca, yapay bir kalp, başlıca karıncık destek aygıtı, şimdilik hastalar için tek ümit verici ve mümkün çözüm olarak öne çıkmaktadır. Yapay kalp pompaları kalp nakli için bekleme esnasında ve iyileşme için bekleme sırasında kullanılırlar ve damarları kanla aşırı dolmuş, pompalama yetisi azalmış hasta kalpler için son medikal çözümdürler.

Gelişmiş ülkelerde üretilmiş çok sayıda karıncık destek aygıtları bulunmaktadır. Türkiye'de bugüne kadar 20 hasta için ithal edilmiş ve takılmıştır. Sol karıncık destek aygıtları oldukça pahalı sistemlerdir ve Türkiye'de birçok hasta tarafından ücreti karşılanamaz. Bu tezin amacı Türkiye'de yeni bir sol karıncık destek aygıtı geliştirmektir. Geliştirilen cihaz "Santrifüj Türk Kalbi" olarak adlandırılmaktadır. Santrifüj Türk Kalbi'nin gelişim süreci beş ana bölümden oluşmaktadır: BDT (Bilgisayar Destekli Tasarım), HAD (Hesaplamalı Akışkanlar Dinamiği) analizleri, BDÜ (Bilgisayar Destekli Üretim), BNC (Bilgisayarlı Sayısal Denetim) makineleri ile hassas üretim ve performans testleri. Geliştirilen Santrifüj Türk Kalbi sistemi bir santrifüj pompa, kontrol ünitesi ve enerji yan birim aygıtlarından oluşmaktadır. Kalp pompasının basınç değişimi, debisi ve dönme hızı deneyler sırasında kontrol edilir ve gözlemlenir.

Santrifüj Türk Kalbi, hastanede yapılacak kan testlerinde canlılıkla uyumlu olabilmesi için titanyum alaşımından üretilmiştir. Bu tezde, kalp pompasının tasarım süreci, çeşitli dizaynların performans grafikleri ve yapılan deneylerin sonuçları sunulmuştur.

ACKNOWLEDGEMENTS

I would like to thank all people who have helped and inspired me during my master's study.

I would like to express my deep and sincere gratitude to my advisor, Associate Professor Ismail Lazoglu for his expert guidance, support, and patience throughout this study. His wide knowledge, detailed and constructive comments and personal guidance have provided a good basis for my thesis. I am grateful to Emel Yılgör for her kindful help and academic support during viscosity experiments. I would also like to thank the members of my thesis committee, Asst. Prof. Murat Sozer and Asst. Prof. Erdem Alaca.

During this study, I have collaborated with my colleagues, Onur Demir and Emre Bıyıklı, for whom I have great regard, and I wish to extend my warmest thanks to them.

I wish to express my warm and sincere thanks to my dearest cousins Güliz Alkaya and Filiz Alkaya for their unflagging love and support throught my life.

My colleagues Tolga Bayrak, Bilal Örün, İlkin Kokal, İsmail Filiz, Özgür Sönmez and Ilgar Veryeri were always together with me from the beginning of my master's study. Without their help and support, I would not have the chance of enjoying both social and academic life. My warm and sincere thanks are for Merve Gürsoy and Kübra Çürüksulu for helping me get through the difficult times, and for all the emotional support they gave.

I want to thank to Koc University College of Engineering and TUBITAK for providing the necessary equipment and conditions to accomplish this project. I also appreciate the valuable contributions of Yeditepe University Hospital Faculty.

At last, but not at least, I would like to thank to my family for their great guidance, supports, patience and help during my whole academic and social life. This study may have not been possible without my father, Berkan Ersanlı, my mother, Güler Ersanlı and my brother, Çağlar Ersanlı.

TABLE OF CONTENTS

LIST OF TABLES

LIST OF FIGURES

NOMENCLATURE

β_1	Inlet Blade Angle [rad]
β_2	Exit Blade Angle [rad]
ρ	The density of blood [kg/m^3]
σ	The slip coefficient (dimensionless)
ψ	The head coefficient (dimensionless)
Φ	The flow coefficient (dimensionless)
η	The target efficiency of the pump (dimensionless)
B	The width of impeller blades [mm]
B_1, B_2	The width of impeller blades at the inlet and outlet [mm]
C_1, C_2	Absolute velocity at the inlet and outlet of impeller [m/s]
C_{r1} , C_{r2}	Absolute radial velocity at the inlet and outlet of impeller [m/s]
C_{t1} , C_{t2}	Absolute tangential velocity at the inlet and outlet of impeller [m/s]
D_1	Impeller eye diameter [m]
D_2	Impeller diameter [m]
g	Gravitational acceleration [m/s^2]
H	The desired head rise of the pump [m]
H_{th}	The theoretical head rise of the pump [m]
n	Rotational speed of the impeller [rpm]
N	Pump specific speed (dimensionless)
P	Power [Watt]
r_1	The radius of the eye of impeller [m]
r_2	The outer radius of impeller [m]
Q	Flow rate of the pump [liters/s]
U_1, U_2	The tangential velocity of impeller at the inlet and outlet[m/s]
V_{pipe}	Inlet pipe velocity [m/s]

W_1, W_2	The relative velocity of fluid wrt the impeller at inlet and outlet [m/s]
W_{r1} , W_{r2}	The radial velocity of fluid relative to the impeller at the inlet and outlet [m/s]
W_{t1} , W_{t2}	The tangential velocity of fluid relative to the impeller at inlet and outlet [m/s]
w	Rotational speed of the impeller [rad/s]
T	The torque applied to the fluid by the impeller [Nm]
Z	The number of blades

Chapter 1

INTRODUCTION

Centrifugal pump is a kind of pump which uses a rotating impeller to obtain a higher fluid pressure at the exit of the pump. In a centrifugal pump, flow and pressure are generated dynamically. Centrifugal pumps work with the principle of converting the rotational kinetic energy that is gained usually from an electric motor, to increase the static fluid pressure up to the desired value. They generate pressure by accelerating and then decelerating the movement of the fluid through the pump. About %90 of the pumps used in industry, including the heavy industry, mining, petroleum refining, pulp and paper production, potable water, manufacturing, etc., centrifugal pumps are used [34]. They are also commonly used as ventricular assist devices because they can achieve large discharge pressures through smaller heads.

A ventricular assist device can be defined as the mechanical pump that helps a weak heart to pump the blood with the desired pressure and flow rate, and is used to partially or completely replace the function of a failing heart. They are used as a permanent clinical solution to heart failure. They are mainly used for two purposes; as a bridge during heart transplantation and as a bridge to recovery. During heart operations, the heart does not pump the blood to the body at the needed pressure value; so a ventricular assist device helps the heart during the transplantation. If a donor heart cannot be found for the weak heart, a ventricular assist device is implanted into the patient and is used until a healthy donor is found. It is important to realize that a VAD does not replace the heart. Instead, it

works with the patient's own heart to pump sufficient blood throughout the body. A VAD is grouped according to the area of the heart it helps into three: left ventricular assist devices, right ventricular assist devices and bi-ventricular assist devices. Left ventricular assist devices (LVAD) help the left side of the heart push blood to the aorta, the body's main blood vessel. They are the most common type of heart pumps. Right ventricular assist devices (RVAD) pull blood from the right side of the heart and send it to the lungs and bi-ventricular assist devices (BVAD) help both sides of the heart to pump blood.

The VAD consists of a pump, a control system and energy supply units. All VADs use an inlet cannula, which connects the pump to the heart. Blood that leaves the heart flows through this tube and into the pump, so the heart does not have to work as hard. The pump then sends the blood to a major artery, such as the aorta or pulmonary artery. The energy supply and the control system are located outside the body; the pump can be either inside or outside the body. A VAD can be grouped according to the position of the pump: the VAD pump can either be placed outside the body (external) or inside the body (implantable). Both external and implantable VADs are attached to a microprocessor controller which controls the rotational speed of motor based on sensor (such as flow meter) feedback. The patient can often wear the controller around his waist, attached to the belt.

The aim of this thesis is to design and develop the first left ventricular assist device in Turkey. This thesis gives brief information about the design process of LVAD starting by detailed literature review and ending with the production and experimental processes.

Chapter 2 gives the background information for ventricular assist devices. The main four categories of ventricular assist systems, the parameters affecting the blood flow through the pump and some important ventricular assist devices that are being used today are illustrated.

Chapter 3 describes the design procedure of the centrifugal pump. The main steps taken through the designing of impeller are clearly explained. The effects of the blade angles on the impeller are analyzed. The design criteria for the impeller are listed. The necessary calculations for the design of impeller are performed.

Chapter 4 provides the information about the computer aided design of the centrifugal pump. The impeller, volute, upper and lower casings of Heart Turcica are designed with respect to calculated parameter. Many different designs are studied to analyze the performances with simulations and experiments. Moreover, the computational fluid dynamics simulations that were carried out for the different designs of Heart Turcica centrifugal are presented.

Chapter 5 is about the computer aided manufacturing of Heart Turcica. The parameters for the processing of the pump, the experimental set-up, experimental procedure, the results of in-vitro experiments and performance curves obtained by experiments are introduced.

Chapter 6 is a review of the results regarding Heart Turcica and tells about the future work that will be done until Heart Turcica will be implanted into a human.

Chapter 2

LITERATURE REVIEW

Heart disease is one of the most common, unexpected and number one cause of death globally; approximately 17.5 million people died because of cardiovascular heart disease in 2005 which represents the 30 % of all of the deaths worldwide [1]. In Turkey, similar situation also occurs; 55% of the total deaths is because of the heart failure problem [2]. According to the Europe Heart Health Research, 3. EuroAspire, Turkey is the European leader in the number of heart failures for the ages of less than 50 [3]. In Turkey, every year 500,000 patients have heart failure and every year 2000 to 3000 of them need heart transplantation [4]. Unfortunately, due to lack of donors, only about 20 operations can be done every year. During the long waiting time for a healthy donor heart, an artificial heart, mainly a ventricular assist device is currently the only hope and possible solution for the patient. Artificial blood pumps are known to be the best solutions for bridge-to-transplant, bridge-to-recovery and final medical solution for the patients who suffer from heart failures that result from the overfilling of the blood vessels of heart [5]. The purpose of using an artificial organ is to replace the function of the defective organ with adequate patient comfort. It is a must to consider three different features in the case of using an artificial organ replacing a living organism; the immune response, the adaptability to new conditions and interdependence of structures and functions [6].

The concept of blood pumps, their features and clinical applications have developed since 1960s, more than 50 years, and can be divided into four main categories: (1) First-

generation blood pumps, (2) Second-generation blood pumps, (3) Third-generation blood pumps, (4) Fourth-generation blood pumps.

First-generation blood pumps were characterized by the shaft-seal and purge systems for mainly extracorporeal usage, for 48 hour-2 weeks in-hospital use. At the first examples of first-generation blood pumps, the most of the research was done on pulsatile devices imitating the pumping mechanism of a normal heart. The main problems faced were mechanical trauma and thrombogenicity. Hemadyne Medtronic, BioPump BP-80, Hemopump, the Thoratec biventricular assist devices, the Novacor VAD, Kyocera Gyro are examples of first-generation blood pumps [7]. The second-generation blood pumps which are represented by continuous blood pumps with contact bearings and sealless structures were used to improve the inadequacies of first-generation blood pumps and lengthen their performing lives. They were designed for both in and out-of-hospital uses with performance lives of 4-5 years. They were driven by magnetic couplings. MicroMed DeBakey VAD, Jarvik 2000, Thoratec HeartMate II, Nedo Pump, Impella Recover, TinyPump can be listed as the examples of second-generation blood pumps [7]. The third-generation blood pumps have arrived in both axial and centrifugal types where the rotor impeller is being levitated magnetically or hydrodynamically. They own noncontact bearings and are driven by magnetic couplings. They are designed for permanent usage and are guaranteed to use more than 10 years out of hospital. They serve benefits for both bridge to transplantation and bridge to recovery situations. Mainly, four different 3rd generation left ventricular assist devices are being developed, which are VentrAssist of Ventracor (US), NASD:THOR of Thoratec (US), Japan's Terumo Heart Inc. and Germany's Berlin Heart AG [13]. Hydrodynamic levitation is used in VentrAssist, however magnetic levitation is used in the other three pumps. The Berlin Heart and Thoratec companies use axial pump to assist the pump where Japanese company uses a centrifugal pump. Fourth generation blood pumps have been developed also for right ventricular assist

devices (RVAD), not only for left ventricular assist devices (LVAD). These pumps can be converted from a LVAD to a RVAD with no difficulty [8].

Continuous flow blood pumps were evolved by DeBakey, Gibbons and Kantrowitz; who can be told as the forerunner professors in the subject of heart-lung machines [9]. In 1955, Dr. Wesolowski has made research on the role of the pulse in the maintenance of normal physiology in the systemic circulation during heart-lung bypass [10]. The earliest article on continuous blood pumps was published by Saxton and Andrews in 1960 which was “An ideal heart pump with hydrodynamic characteristics analogous to the mammalian heart” [11]. This article stated that rotary blood pumps have potential advantages compared to positive displacement pulsatile devices. Ventricular assist devices can either be pulsatile or dynamic systems. Pulsatile pumps that are actuated by a positive displacement mechanism are pumps such as the TCI HeartMate can drive pump, Novacor spring decoupled solenoid and the Penn State roller screw pump. These are all controlled by virtue of adjusting the stroke volume or pump rate. Today, in fact the pulsatile VAD is still the most prevalent heart assist device in use [12]. One of its pluses is the fact that pulsatile pumping action probably imitates the natural pumping rhythm of the heart more closely than continuous flow. The biggest advantage of pulsatile pumps is they have been effective for short-term implantation, but unfortunately they are bulky and have large power requirements. However, a rotary pump may be more suitable for late-stage heart failure patients and it has a smaller size, operates quieter than pulsatile devices, achieves a higher level of biocompatibility and due to the fact that rotary pumps operate at lower RPM ranges, it has less mechanical wear than a pulsatile device.

However, two main disadvantages of rotary blood pumps were identified by these studies. The first one is that the blood cell damage may occur because of the unknown shear stresses within the pumping chamber. The second one is the requirement of higher output volumes by continuous flow than pulsatile flows.

Excessive blood cell injury caused by high shear stresses within the pumping chamber may result in hemolysis. Hemolysis can be defined as the breakage of the red blood cell's membrane, causing the release of the hemoglobin and other internal components into the surrounding fluid. One of the most important things that affect the hemolysis rates is the roughness of the blood contacting surface. In order to be able to have an antitraumatic and antithrombogenic surface as in blood vessels, the surface smoothness must be less than 0.2 µm after a good polishing process [14]. Takami et al. investigated the effect of surface finish on hemolysis and found out that under cardiopulmonary bypass conditions (5 liters/min and 350 mmHg) surface finish from 5 µm average roughness value to 0.06 µm average roughness value is relevant but this is not applicable under left ventricular assist conditions (5 liters/min and 100 mmHg) [16]. For left ventricular assist conditions, they found out that less than 0.2 µm average roughness value must be provided.

There are some important issues to be considered when blood flow is considered, such as "how much plasma-free hemoglobin is too much within the pumping chamber?" and "what is the toxicity of high plasma-free hemoglobin within the organism?".

In 1938, Ottenberg stated that for a healthy human, the renal threshold for hemoglobin was above 150 mg%. Renal threshold can be defined as the concentration of a substance dissolved in the blood above which the kidneys begin to remove it into the urine. This can be summarized as, if the plasma-free hemoglobin is higher than 150 mg%, then it is discharged into the urine. In 1964, Bernstein et al. tried to figure out the maximum plasma-free hemoglobin that could be endured in animals by giving a continuous dose of 0.1 mg/kg*min of hemoglobin without increasing the blood urea nitrogen, i.e. the plasma-free hemoglobin within the urine [9].

One of the most parameters to be considered during blood flow through a ventricular assist device is the normalized index of hemolysis (NIH). Normalized Index of Hemolysis

(NIH) can be defined as the clinical measure of hemolysis as per the ASTM standards and can be calculated by the flowing formula (ASTM F1841-97):

$$NIH = \delta fHb \; x \, V \; x \, \frac{100 \;\; Ht}{100} \, x \, \frac{100}{Q \; x \; T} \quad \left[gr / liters \right] \tag{2.1}$$

In this formula, δfHb stands for the increase in plasma (gr/liters) and can be measured by spectrophotometer, Ht stands for the hematocrit ratio in blood (%), Q is the flow rate of the blood (liters/min), T is the driving time duration (min) and V stands for the total blood volume in the circuit (liters).

NIH can also be stated as the amount of plasma-free hemoglobin released per pass of blood volume through the blood pump. Typically, if the NIH of a pump becomes smaller than 0.01 gr/100 liters at a pressure head of 100 mm Hg, the pump remains antitraumatic [14]. This is the design objective for a ventricular assist device. If it is smaller than 0.02, this means that the ventricular assist device is clinically acceptable, if it is smaller than 0.04, this means the device is physiologically acceptable. However if NIH exceeds 0.04, this means that blood transfusion is needed despite the fact that there is no increase in the plasma-free hemoglobin. If NIH is greater than 0.06, this is an alarm for danger and indicates that the plasma-free hemoglobin is increasing. Araki et al. studied the in vitro performance (by using heparinized fresh bovine blood) of three turbo pumps they designed; a centrifugal pump, a mixed flow pump and an axial flow pump, and calculated NIH for all of these pumps [15]. The minimum value of NIH; (1) for centrifugal pump was 0.038, achieved at 5000 rpm, 38 mmHg and 4.60 liters/min; (2) for mixed flow pump was 0.01, achieved at 7000 rpm, 100 mmHg and 8.22 liters/min; (3) for axial flow pump was 0.033 achieved at 7000 rpm, 48 mmHg and 2.84 liters/min.

The earliest design of first-generation blood pump designs with shaft seal and purge systems was invented by Drs. Blackshear and Bernstein by cooperation of University of California, the University of Minnesota and Medtronic Inc. in 1965 [17]. The device was called Hemadyne Medtronic pump. This pump had only one moving part, the rotor-impeller section, where the centrifugal force propelled blood by imparting kinetic energy from the rotating impeller. It was driven by an external rotating magnetic field which rotated a magnet within the pump based on the magnetic coupling between the drive source and rotor impeller. This device was evaluated for duration of 24 hours with low hemolysis and nonthrombogenic performance in calves. Bernstein et al. went on experiments with Hemadyne and achieved the running of the continuous flow pump for 24 hours. The plasma-free hemoglobin did not exceed 21 mg% but the number of platelets has decreased, there was normal slotting of the blood and because of the seal failure an increase of plasma-free hemoglobin in excess of 300 mg% was observed [18].

The following studies on Hemadyne Medtronic Pump were done by Golding's group at Cleveland Clinic Foundation. Golding et al. worked in a clinic and provided a detailed statement of good hemodynamic support with plasma-free hemoglobin of 39 mg% in 24 hours time interval [19]. In the early 1980s, Medtronic Inc. stopped the support for the design and production of Hemadyne pumps, however BioMedicus Inc., which is a part of Medtronic Inc., begin to develop a new pump, called Bio-Pump, since 1970s. They developed it and designed BP-80 which can be counted as the pioneer of cardiopulmonary assist and also for short-term support to patients who suffer of cardiogenic shock after having an open heart operation [20]. In order to compare their pump VentrAssist, James et al. calculated NIH for BP-80 for comparing the values with their pump and to be able to use BP-80 as a control [21].The NIH for the BioMedicus BP-80 was approximately 0.0040±0.0023 gr/liters for pooled red blood cell suspensions and 0.00053±0.0002 gr/liters

in whole blood. These values are well-accepted as they are in safety conditions as told above.

One of the most widely used left ventricular assist devices in the world is the MicroMed-DeBakey ventricular assist device. The MicroMed-DeBakey VAD was designed in the 1980s for the first time with the collaboration of Dr. Michael DeBakey and Dr. George Noon from Baylor College of Medicine and engineers from NASA. Their aim was to develop a very small axial pump which will serve as a left ventricular assist device and meet the needs of the failing heart. In 1996, MicroMed Technology, Inc, has got the license for this ventricular assist device and they have continued to research to develop this device for usage in clinics [22]. This device is an electromagnetically actuated axial pump made of titanium and can pump at a flow rate of 10 liters/min with a pressure difference of 100 mmHg where the rotor speed is 10000 rpm and the power given to the system is smaller than 10 W. Its diameter is 30.5 mm and its weight is only 95 grams. The first clinical use of the device was reported in Europe in 1998 [23] with subsequent trials starting in United States in June of 2000 [22]. In the first clinical experience of MicroMed DeBakey, the pump is implanted into two different patients with left heart failures. The average value of the flow rate of the pump was 3.9±0.5 liters/min which results in an average cardiac index of 2.3±0.2 L/m^2 per min. The normal range of cardiac index is 2.6 - 4.2 L/m^2 per min. If the cardiac index falls below the value of 1.8 L/m^2 per min, the patient may have a cardiogenic shock. However, in the recovery time which is the 8-12 days after the operation, as the pulse pressures increased, the flow rate also increased to the 4.5±0.6 liters/min and also the cardiac index rose up to 2.7±0.2 L/m^2 per min, but still in safety conditions. The same safety conditions were also seen in hemolysis; since the plasma-free hemoglobin has rose from 2.1±0.8 mg/dliters to 3.3±1.8 mg/dliters 6 weeks after the operation, which cannot be counted as a significant increase [23]. In the first weeks after the pump is implanted to both of the patients, VAD was characterized by completely

nonpulsatile blood pressure, where the mean arterial blood pressures were kept in the range of 70 to 90 mmHg. After this period, pulsations with low-amplitude frequencies started, but at any time nonpulsatile flow patterns could be obtained by increasing the speed of the pump. Regarding to results of subsequent clinical trials in US which were evaluated from 32 patients, the chance of living was 81% and this result suggested that MicroMed DeBakey VAD can provide the needed support to the left ventricle as a bridge-to-transplantation [22].

Coming to the late 1980s, at the start of 1990s, it became so difficult to find a donor for heart transplantation because the number of patients having heart failure was increasing day by day. This required a more efficient artificial heart technology with 5-years durability and emerging new technology like tissue engineering and regenerative medicine. In order to achieve this goal, second-generation designs were carried out. One of these new innovative pumps was Thoratec HeartMate II developed by Nimbus-TCI. It is an axial flow pump made of titanium and has a rotor that produces flow rates greater than 10 liters/min at rotational speeds higher than 10000 rpm. It has been tested many times on animals and has been implanted on a patient in Israel in 2000. Following this operation 6 more patients received this device and now its usage area is getting larger [26]. In this first clinical usage of HeartMate II in United States, the range of the number of plasma-free hemoglobin was around 7 mg/dliters, which tells us that HeartMate II offers a low level of hemolysis during the support.

One of the best examples of second-generation blood pumps, Jarvik 2000, by Jarvik Heart, Inc., is designed mainly to offer ventricular assistance in stead of replacing the heart. It is the third and similar flow pump to MicroMed and HeartMate II. It assists the pumping action of the left side of the heart. In other words, it can be said that this pump is used as a bridge-to-transplant until a new donor can be found. It is driven by a direct current motor, and owns a rotor supported by two ceramic bearings and there is one single moving part; a

small, spinning titanium impeller which helps to pump the blood at 7 liters/min. This impeller is capable of working between ranges of 8000-12000 rpm. This device is controlled manually by an external controller. It has relatively a simple design. As a second-generation blood pump, Jarvik 2000 was expected to serve for 4-5 years, but Jarvik 2000 implanted in 2000 has lasted for 6 years [24]. In order to get rid of the thromboembolism risk, Jarvik 2000 is implanted directly into the left ventricle without using an inflow cannula. In order to test the performance of Jarvik 2000 and evaluate the surgical results, Jarvik 2000 was implanted in two patients who suffer of heart failure with a cardiac index of 1.8±0.3 liters/m^2 per min [25]. The cardiac index increased from 3.7±1.5 liters/ min per m^2 at 8000 rpm to 5.9±2.9 liters/m^2 per min at 12000 rpm. All the patients did have mild hemolysis but it was not harmful and did not require any transfusion. After 49 days, patients were discharged home. The total result gave that Jarvik 2000 appears to be safe.

By the start of 2000s, the technologies of rotary blood pumps have increased very fast and the second-generation pumps with bearings immersed into the blood became unpreferable compared to third-generation blood pumps which are mechanical non-contact devices with magnetic suspension mechanisms. The most commonly used third-generation blood pumps are Terumo DuraHeart, HeartMate III, HeartQuest, MiTiHeart, Berlin Heart INCOR system, VentrAssist VADs. Hoshi et al. studied on all types of the third-generation blood pumps and reviewed their properties and clinical outcomes [28]. Third-generation blood pumps can be classified into three groups regarding to their magnetic-levitation systems: (1) external-motor driven system (2) direct-drive motor system (3) bearingless motor system. Teruma DuraHeart is an example of external motor-driven magnetic-levitated system. The speed range of the pump is between 1200 and 2600 rpm and it pumps at flow rates between 2 and 10 liters/min. The pump was implanted to 20 patients and the average flow rate was measured as 4.94±0.36 liters/min, the average cardiac index was

calculated as 2.60±0.21 liters/m^2 per min and the average plasma-free hemoglobin was found as 7.35 mg/dliters [29]. For direct-drive mechanism pumps, Berlin Heart INCOR can be a good example with axial levitation. The impeller of this pump can rotate between 5000 and 10000 rpm and this device can pump at flow rates up to 5 liters/min with a pressure difference of 100 mmHg. Berlin Heart has been implanted in 212 patients in all over the world and in all of these patients, no trauma of blood cells was observed and any hemolysis incident was not seen in any of the patients [30]. Levitronix Centrimag extracorporeal magnetic-levitation pump can be an example for the system driven by bearingless motor. Its pump works at rotational speeds up to 5500 rpm and can achieve flow rates of up to 10 liters/min with a pressure difference of 600 mmHg. Between the years 2003 and 2005, the device was implanted to 150 patients and all of the patients had low hemolysis which did not cause any traumatic blood cell creation [31].

The ventricular assist devices' usage has become a big era in cardiac transplant because of the huge number of patients suffering from heart failures. By the year 2004, there were 30000 patients waiting for a donor heart immediately worlwide [32]. The important thing to be considered is that not all of these patients can receive a ventricular assist device. Because of the physiological considerations with serious tachycardia, patients having a cardiac index of less than 2 liters/min need mechanical support immediately [33].

Chapter 3

DESIGN PROCEDURE OF THE PUMP

3.1 Introduction

The design of the centrifugal pump of the left ventricular assist device is quite important for the performance of the pump. When designing a rotary blood pump for a LVAD, there are some important performance parameters that have to optimized and clearly considered during design process, such as the pressure rise, flow rate, input torque and rotational speed. Moreover, for the biocompatibility of the pump, the viability of cellular components of the blood should be well-analyzed.

A centrifugal pump is composed of a casing, a volute, a bearing housing and an impeller (see Figure 3.1). The fluid enters into the eye of the impeller and is captured in the cavities between the blades. The impeller blades push the fluid and give it a significant speed as the fluid passes from the impeller eye towards the outside diameter of the impeller, i.e. the rotating impeller pushes fluid on the back of the impeller blade, imparting circular and radial motion. Regarding to the Bernoulli principle, as the fluid speed increases at the eye of the pump, a low pressure zone occurs at this section. This is the reason why the fluid must enter into the pump with a sufficient energy. The fluid leaves the impeller at the outer diameter of impeller with a relatively high speed gained by blades. It strikes to the internal section of the volute with a sudden force. At this point, the centrifugal component of the fluid velocity suddenly comes to zero value and the reverse of Bernoulli principle occurs and the velocity is converted into pressure.

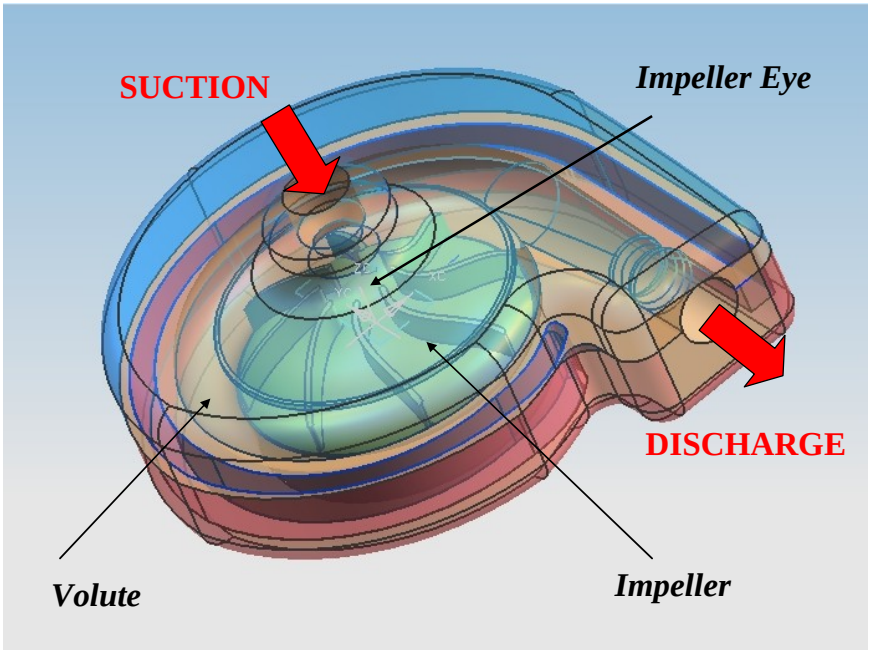

Figure 3.1: The main units of a pump

Bernoulli principle gives information that, as the velocity of the fluid goes up; the pressure of the fluid goes down. At this time, the motor goes on spinning so the velocity has also a rotary component. The volute channel area increases as the fluid follows the pathway. The rotary velocity component decreases because of the increasing pathway and as explained by the Bernoulli principle, the pressure again increases because of the decreasing velocity. At the exit of the pump, the pressure comes to the desired discharge pressure to overcome the resistance in the whole system. The flow rate inside the pump is affected by the rotational speed of the driver and the height of the blades, which affects the inside volume of the pump. The pressure difference across the pump is affected mainly again by the rotational speed of the driver and the impeller diameter. There are some other parameters affecting the flow rate and the pressure difference, such as the number, the pitch and thickness of the blades, the clearance values, etc. but they don’t have significant roles.

3.2 Impeller Design

Impeller is the rotating element of a pump that contains a disk with curved vanes. The impeller imparts movement and pressure to the fluid. Impeller design is so important because it determines the performance and the efficiency of the pump and also the hemolysis index and thrombogenicity ratio is affected by the impeller. The number of vanes on an impeller affects the efficiency, in common more number of vanes mean being more efficient. Moreover, the number of vanes affects the steepness of the characteristic curve.

Impellers can be grouped into three classes whether they are: (1) open, (2) semi-open (or semi-closed), (3) closed (see Figure 3.2).

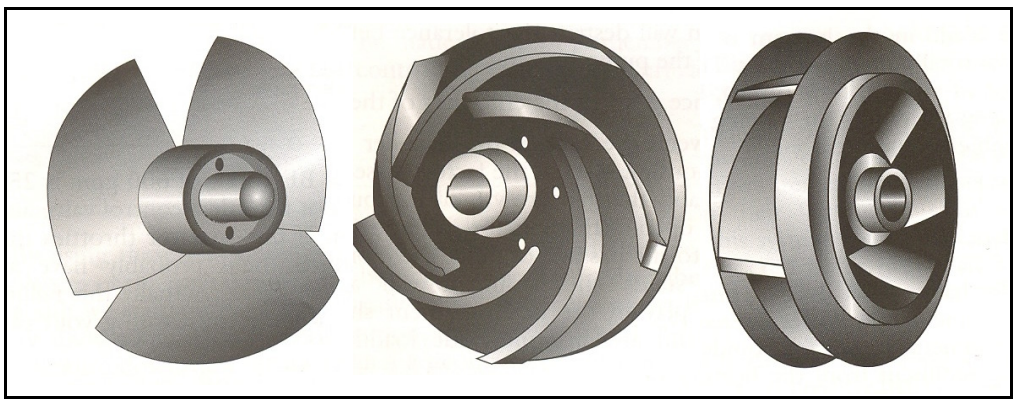

Figure 3.2: Open, semi-open and closed type impellers [34]

Closed impellers have embedded blades between two support shrouds or plates. Because of this reason, manufacturing of closed impellers is quite complicated. In a closed impeller, the fluid enters the impeller eye and the vanes add energy to the fluid and direct it to the discharge nozzle. There is no impeller to volute or back plate clearance to set.

The open impeller contains blades attached to a hub. In an open impeller, the impeller vanes are open and the edges of the vanes are not constrained by the hub. Compared to closed impellers, their biggest disadvantage is the loss of efficiency.

The semi-open impeller contains a circular plate attached to one side of the blades. Although they show higher axial hydraulic thrust than closed impellers, they are more efficient because the disk friction caused from the shroud is eliminated. Heart Turcica Centrifugal involves a semi-open impeller because it is more efficient and it is easier to manufacture it by the vertical machining center at Manufacturing & Automation Research Center at Koç University.

3.3 Design Procedure

When it comes to design of an impeller for a centrifugal pump, a detailed design and layout procedure has to be followed. In this section, detailed information for designing a centrifugal pump impeller is presented.

First thing to be done is to calculate the pump specific speed. For that reason, a best efficiency point should be selected. We are designing a centrifugal pump that will help a weak heart to pump the blood to the body with a sufficient pressure at a desired flow rate, which is approximately 100 mm-Hg at 5 liters/min. this condition can be used as a best efficiency point.

The pump specific speed is calculated with the following formula:

$$N = \frac{n*(Q)^{1/2}}{(H)^{0.75}} \tag{3.1}$$

When the head is multiplied by the gravitational acceleration, g, the pump specific speed becomes dimensionless.

Once the pump specific speed is determined, the vane number and the discharge angle must be selected. The following graph can be used to select the number of vanes and the discharge angle:

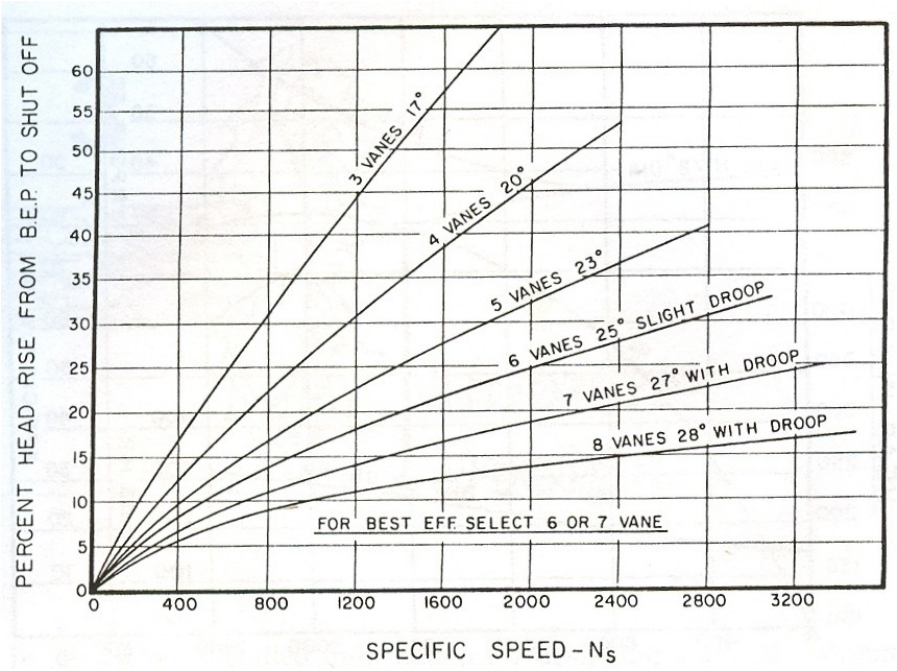

Figure 3.3: Percent Head Rise [36]

In order to produce the required head rise, the number of vanes could be determined from the graph above which is based on a theoretical approach and many years of collecting thousands of performance tests in various specific speeds. The discharge angle of the vanes can also be found by using this graph.

By using the specific speed calculated, a target efficiency η can be estimated by using the chart efficiency graph drawn by Oak Ridge, shown in Figure 3.4. This efficiency is assumed to eliminate the effect of the losses.

Impeller is the only rotating part in the pump and includes radial flow passages which are directed towards the axial direction that are formed by rotating blades in a circle. As this is a semi-open impeller, the blades are covered by a shroud on the back side and another disk, hub, connects the impeller assembly to the shaft. At the inlet, i.e. the eye of the impeller, flow enters axially and inside the impeller it turns in the radial direction.

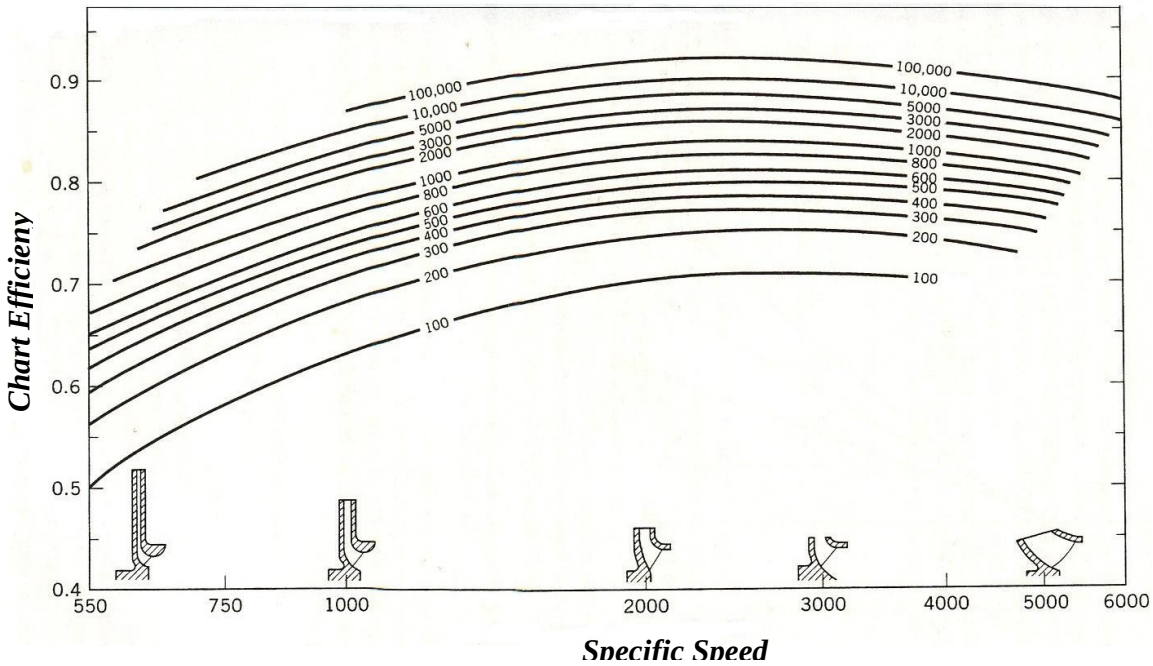

Figure 3.4: Chart efficiency of pumps versus specific speeds [37]

In stead of using cartesian coordinates, flow conditions, velocities and pressures in the impeller are expressed in cylindrical coordinates: *r, θ and z*; which are the radial, circumferential and axial directions in the impeller. The rotational speed of the impeller is shown by ω, which is given by ω(rad/s)=n(rpm)(2π/60). Figure 3.5 shows the absolute velocity components, C_r and C_t , and the relative components, W_r and W_t .

How much energy is transferred by an impeller and how efficiently a pump works is determined by mostly the shape of the blades of the impeller and the flow pattern in the pump. Conservation of angular momentum, calculated by $\rho r C_t$, can be applied to find the theoretical energy increase in the pump and the theoretical head rise through the impeller. The only assumption done to be able use conservation of momentum is that flow is behaved as one-dimensional flow.

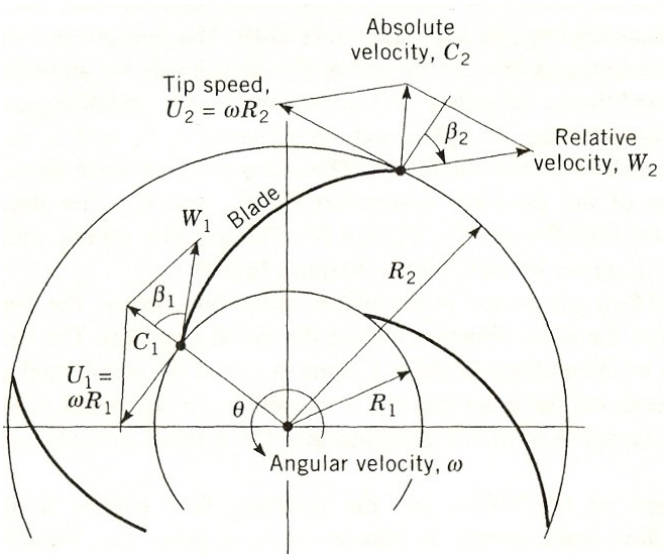

Figure 3.5: The relative and absolute flow velocity vectors in an impeller [37]

A control volume has to be selected to apply conservation of momentum. For the sake of simplicity, an annular shape with an inner radius r_1 and outer radius r_2 is selected; where the index *"1"* refers to the condition at the inlet of impeller and index *"2"* refers to the exit of the impeller. The torque applied to the fluid by the impeller is equal to the difference between the angular momentum entering the control volume, $\rho r_1 C_{t1}$, and the angular momentum leaving the control volume, $\rho r_2 C_{t2}$, *:*

$$T = Q\,(\rho r_2 C_{t2} - \rho r_1 C_{t1}) \tag{3.2}$$

It is a well know formulation that the power applied is equal to the multiplication of torque and the velocity. If this formulation is applied to the pump:

$$P = Tw = \rho Q H_{th} g \tag{3.3}$$

$$\Rightarrow H_{th} = \frac{Tw}{\rho Q g} = \frac{\rho Q (C_{t2} r_2 - C_{t1} r_1) w}{\rho Q g} = \frac{(C_{t2} r_2 - C_{t1} r_1) w}{g} \tag{3.4}$$

This expression is known as Euler's Equation and the theoretical head is also referred as Euler Head. In practice, the total head across the pump is less than this due to energy dissipation in eddies and in friction. The term $C_{t1}r$ is assumed as equal to zero because pumps are designed for no angular momentum at the inlet. So, the theoretical, or Euler head becomes:

$$H_{th} = \frac{U_2 C_{t2}}{g} \tag{3.5}$$

where U_2 stands for the tangential velocity at the impeller exit and formulated as:

$$U_2 = wr_2 \tag{3.6}$$

The velocity vectors at the inlet and outlet sections of blades can be seen in Figure 3.6:

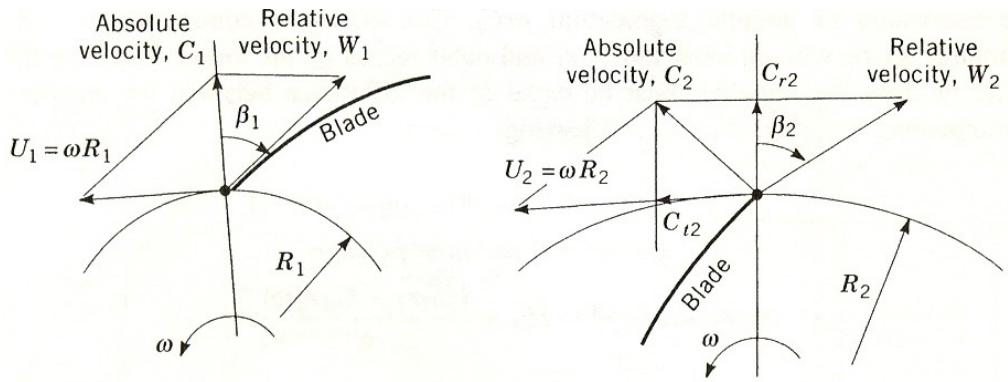

Figure 3.6: Velocity vectors at the inlet and outlet of the blades [37]

The Equation 3.4 can be written in terms of absolute velocities rather than their components using velocity triangles. Assuming that fluid enters at absolute velocity C_1 at an angle of α_1 and leaves at absolute velocity C_2 at an angle of α_2:

$$C_{t1} = C_1 \cos\alpha_1 \tag{3.7}$$

$$C_{t2} = C_2 \cos\alpha_2 \tag{3.8}$$

$$H_{th} = \frac{C_{t2}u_2 - C_{t1}u_1}{g} = \frac{u_2C_2\cos\alpha_2 - u_1C_1\cos\alpha_1}{g} \tag{3.9}$$

Using the cosines theorem, the following formulations are obtained:

$$u_1C_1\cos\alpha_1 = \frac{C_1^{\,2} + u_1^{\,2} - W_1^{\,2}}{2} \tag{3.10}$$

$$u_2C_2\cos\alpha_2 = \frac{C_2^{\,2} + u_2^{\,2} - W_2^{\,2}}{2} \tag{3.11}$$

Replacing equations 3.10 and 3.11 into the equation 3.9 gives:

$$H_{th} = \frac{1}{2g}\left[(C_2^{\,2} + u_2^{\,2} - W_2^{\,2}) - (C_1^{\,2} + u_1^{\,2} - W_1^{\,2})\right] \tag{3.12}$$

$$H_{th} = \frac{1}{2g}(C_2^{\,2} - C_1^{\,2}) + \frac{1}{2g}(u_2^{\,2} - u_1^{\,2}) + \frac{1}{2g}(W_1^{\,2} - W_2^{\,2}) \tag{3.13}$$

Substituting " $u=wr$ " into the equation above,

$$H_{th} = \frac{1}{2g}(C_2^{\,2} - C_1^{\,2}) + \frac{\omega^2}{2g}(r_2^{\,2} - r_1^{\,2}) + \frac{1}{2g}(W_1^{\,2} - W_2^{\,2}) \tag{3.14}$$

In the final equation for the theoretical head rise, the first term denotes the increase in kinetic energy of the fluid in impeller, the second term denotes the energy used to circulate fluid about impeller and the third term denotes the regain of static head due to reduction of relative velocity.

In order to find the values of the exit angular momentum, the velocities should be found at the inlet of the impeller, i.e. the leading edge of blades and at the exit of the impeller, i.e. the trailing edge of the blades. The relative velocity at the inlet of impeller, W_1, is obtained

from the vectorial sum of the absolute velocity approaching the pump inlet, C_1, and the rotational velocity, i.e. the tangential velocity of the impeller at the inlet, U_1, as shown in Figure 3.5. Like this, the relative velocity at the exit of impeller, W_2, is obtained from the vectorial sum of the absolute velocity leaving the pump exit, C_2 , and the rotational velocity, i.e. the tangential velocity of the impeller at the exit, U_2. The components C_{t2} and C_{r2} in the circumferential and radial directions make up the resultant absolute velocity C_2 since

$$C_2^{\,2} = C_{t2}^{\,2} + C_{r2}^{\,2} \tag{3.15}$$

At this point, some assumptions must be done to calculate the velocities and to draw the velocity vectors as in Figure 3.5. The flow is assumed to be incompressible flow. This means, the flow through the impeller is a flow with no density change in. The tangential flow velocity, C_{t1}, is assumed to be zero at the inlet. This means there is no whirl at the inlet. This leads to the result that the radial flow velocity at the inlet is equal to the absolute velocity. So, the local flow angle, β_{F1} will be equal to the β_1, which is the inlet blade angle. The blade angle meets the relative velocity tangentially. This situation is called as no-shock condition. At the exit, it is assumed that the fluid leaves with relative velocity tangential to the blade, i.e. the local flow angle, β_{F2} will be equal to the β_2, which is the exit blade angle.

From the velocity triangle in Figure 3.5, it is simply seen that the circumferential component of the absolute velocity can be defined as a function of the radial velocity component and local flow angle, which is measured from the radial direction in the sense opposite to the direction of rotation:

$$C_{t2} = U_2 - W_{t2} = U_2 - W_{r2} \tan \beta_{F2} \tag{3.16}$$

Substituting this equation in Equation 3.5, the theoretical head, i.e. the energy added to a unit mass of fluid by the pump, can be written as:

$$H_{th} = \frac{U_2 C_{t2}}{g} = \frac{U_2^{\,2} - U_2 W_{r2} \tan \beta_{F2}}{g} \tag{3.17}$$

It is known that the blades curve backwards, so there is a negative sign in the formulation since the relative velocity, W_{r2}, points in the direction opposite to the direction of rotation. This expression is very important for designing new pumps and calculating the pump performance.

But the assumption made is for the ideal case. There is a miscellaneous situation that the flow does not follow the blades exactly, which means that the local flow angle is not equal to the exit blade angle because the relative exit velocity W_2 is somewhat more inclined opposite to the direction of rotation. This is because the fluid remains its orientation in the absolute reference frame and tends to rotate in an opposite direction with respect to the impeller. To compensate this situation, a correction factor is added to Equation 3.16, named as slip coefficient and shown by σ:

$$C_{t2} = U_2 - W_{r2} \tan \beta_{F2} = U_2 \sigma - W_{r2} \tan \beta_2 \tag{3.18}$$

Hence the theoretical head becomes,

$$H_{th} = \frac{U_2^{\,2} \sigma - U_2 W_{r2} \tan \beta_2}{g} \tag{3.19}$$

Wiesner et al. has derived an expression for the slip coefficient:

$$\sigma = 1 - \frac{\sqrt{\sin\left(90^\circ - \beta_2\right)}}{Z^{0.70}} \tag{3.20}$$

In this equation, Z stands for the number of blades. It is important that slip does not mean a loss in energy, it only affects the value of the head that a given size impeller can produce.

There are two important coefficients that have to be taken into account during designing a centrifugal pump; head and flow coefficients. These coefficients are defined because they make a connection between the theoretical head and the energy input of the pump with the absolute tangential velocity at the exit of impeller and the flow rate with the radial velocity at the exit of impeller. These coefficients are dimensionless. The head coefficient, represented by ψ, is calculated by dividing the absolute tangential velocity at the impeller exit by the tangential velocity of the impeller and the flow coefficient, represented by Φ, is calculated by dividing the radial velocity of the exit of impeller by the tangential velocity of the impeller exit:

$$\varphi = \frac{C_{t2}}{U_2} = \frac{gH_{th}}{\eta U_2^{\,2}} \tag{3.21}$$

$$\phi = \frac{C_{r2}}{U_2} = \frac{Q}{\pi D_2 B_2 U_2} \tag{3.22}$$

where B_2 stands for the width of the blades at the outlet. By using these formulations, the tangential velocity at the impeller exit can be calculated, and hence the diameter of the impeller at the exit can be found out, since:

$$U_2 = \omega r_2 = \frac{\omega D_2}{2} \tag{3.23}$$

These two coefficients and the slip coefficient are related with each other with the following formulation:

$$\varphi = \sigma - \phi \tan \beta_2 \tag{3.24}$$

The radial components of absolute and relative velocities are equal to each other because the rotation affects only the tangential components. The radial velocity components at the exit are calculated by:

$$W_{r2} = C_{r2} = \frac{Q}{\pi D_2 B_2} \tag{3.25}$$

The relative velocity of the fluid at the inlet of the impeller should be at the minimum level because low losses at the inlet can be achieved by only low velocities [38]. Low relative velocities at the inlet minimize the diffusion, the ratio of the inlet relative velocity to exit relative velocity, W_1/W_2, that can cause to flow separation if excessive. So the diameter of the impeller at the impeller eye should be optimized by considering this.

Utilization between two opposite trends, the absolute and the relative velocities at the inner of impeller, can optimize an inlet diameter. The vectorial sum of the circumferential velocity U_1 and the axial velocity C_1 adds up to the relative inlet velocity W_1. If it is assumed that any prerotation exits,

$$W_1^2 = U_1^2 + C_1^2 \tag{3.26}$$

$$U_1 = \omega r_1 = \frac{\omega D_1}{2} \tag{3.27}$$

$$Q = C_1 A = C_1 \frac{\pi D_1^2}{4} \quad \Rightarrow \quad C_1 = \frac{Q}{\pi D_1^2 / 4} \tag{3.28}$$

The circumferential velocity U_1 at the inlet of the impeller increases with the inlet diameter, while the axial inlet velocity C_1 decreases with the square of the inlet diameter

for a specific flow rate. A tolerance value has to be given for blockage from the blade thicknesses at the inlet, which is more critical than at the impeller exit. These opposing trends balance and make the inlet relative velocity a minimum, hence the optimal inlet diameter is found as:

$$D_1 = \left(\frac{8\sqrt{2}}{\pi}\right)^{1/3}\left(\frac{Q}{\omega}\right)^{1/3} = 1.533\left(\frac{Q}{\omega}\right)^{1/3} \tag{3.29}$$

Once the inlet diameter is calculated, the tangential velocity at the inlet can simply be calculated, since:

$$U_1 = \left(\frac{2\pi n}{60}\right)\frac{D_1}{2} \tag{3.30}$$

One more assumption has to be done to calculate the absolute tangential velocity of fluid. It is assumed that the inlet pipe velocity is equal to the absolute tangential velocity of the fluid. The inlet pipe velocity can be calculated from the definition of mass flow rate where,

$$Q_m = V_{pipe}\ A = V\frac{\pi D_1^{\,2}}{4} \tag{3.31}$$

$$C_1 = V_{pipe} = \frac{Q_m}{\pi D_1^{\,2}/4} \tag{3.32}$$

Again assuming that there is no inlet whirl condition, the inlet blade angle is calculated as:

$$\beta_1 = \tan^{-1}\left(\frac{U_1}{C_1}\right) \tag{3.33}$$

As seen from the above equation, the values of the inlet diameter and the velocities at the inlet of the diameter, C_1 and U_1, affect the value of the inlet blade angle, β_1. However, there is one important thing to be considered that the inlet blade angle usually is not constant along the leading edge of the pump and should be calculated at several locations. When there is a radial leading edge, the circumferential velocity decreases with decreasing radius along the leading edge.

The desired suction head and correct incidence at the pump inlet determine inlet blade angle β_1 and the desired pump head determines the exit blade angle β_2. The most important dimensions of the impeller are the inlet diameter, the exit diameter and the exit width of the blades and these all are fixed. The detailed contour of the hub and shroud and the blade angle distribution from inlet to exit is on the choice of the designer.

3.4 Affinity Laws

When the rotational speed of a pump changes, the operational characteristics of this pump also change. These changes can be calculated by using the Affinity Laws. The affinity laws used in hydraulics are a series of equations that manage the pump. These rules briefly tell that the energy transfer in turbomachines is based on hydrodynamic processes for which all pressure and energy differences are proportional to the square of the square of the rotational speed.

What affinity laws express can simply summarized as:

- Flow changes directly proportional to a change in rotational speed.
- Head changes directly proportional with the square of a change in rotational speed.
- Power changes directly proportional with the cube of a change in rotational speed.

The affinity laws are expressed by the three following relationships formulated below where Q denotes the flow rate, n the rotational speed of the pump, H the total head and P

the power. Anyone can predict the operating condition for point 2 based on the knowledge of the conditions at point 1 and vice versa.

$$\frac{Q_1}{Q_2} = \frac{n_1}{n_2} \tag{3.34}$$

$$\frac{H_1}{H_2} = \left(\frac{n_1}{n_2}\right)^2 \tag{3.35}$$

$$\frac{P_1}{P_2} = \left(\frac{n_1}{n_2}\right)^3 \tag{3.36}$$

The affinity laws can be used if only it is assumed that the two operating points that are being compared are at the same efficiency. With a small change in velocity (i.e. 20 to 50 rpm), the efficiency would not be affected but for example, doubling the rotational speed will result in a small change in efficiency, like 2 or 3% increase [35]. So, the assumption is made for the ideal case.

If the rotational speed of a pump remains constant, the values of head and power will change when the impeller diameter changes. The affinity laws relate the impeller diameter and the flow rate, the head and the power as follows:

- Flow changes directly proportional to a change in diameter.
- Head changes directly proportional with the square of a change in diameter.
- Power changes directly proportional with the cube of a change in diameter.

This relationship is formulated as follows:

$$\frac{Q_1}{Q_2} = \frac{D_1}{D_2} \tag{3.37}$$

$$\frac{H_1}{H_2} = \left(\frac{D_1}{D_2}\right)^2 \tag{3.38}$$

$$\frac{P_1}{P_2} = \left(\frac{D_1}{D_2}\right)^3 \tag{3.39}$$

The formulations above are valid if only speed changes while the diameter remains constant in the first case and if only diameter changes in the second case while the speed remains constant. If both of them change at the same time, then the formulations below can be used:

$$\frac{Q_2}{Q_1} = \frac{D_2}{D_1} \times \frac{n_2}{n_1} \tag{3.40}$$

$$\frac{H_2}{H_1} = \left(\frac{D_2}{D_1} \times \frac{n_2}{n_1}\right)^2 \tag{3.41}$$

$$\frac{P_2}{P_1} = \left(\frac{D_2}{D_1} \times \frac{n_2}{n_1}\right)^3 \tag{3.42}$$

3.5 Volute Design

Volute is one of the most important parts of the impeller. A volute is the stationary housing, in which the impeller rotates, that collects, recirculates and discharges water that enters into the pump. It acts like a diffuser and transforms some of the kinetic energy of the flow coming from the impeller into pressure energy by slowing down the flow velocity. Simply, a volute is a curved funnel increasing in area to the discharge port. As the area of the cross section increases, the volute reduces the speed of the liquid and increases the pressure of the liquid. The volute casing and the parts of a volute can be seen in Figure 3.7.

As seen in the figure, a volute is constructed by distributing its cross sectional area on a base circle that touches the tongue or cutwater and is meridionally removed from the impeller exit by a gap.

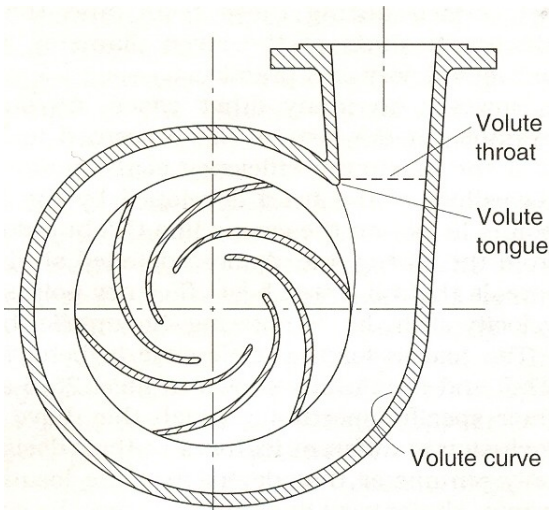

Figure 3.7: Nomenclature of certain volute parameters [39]

The geometry of volute tongue has a great effect on the performance of the pump. Unfortunately, there isn't any theory that explains the reason for this great effect of tongue geometry on performance [39]. However, there is a encouraging reality that a problem that causes from volute tongue can be simply solved by cutting away or removing a part of the volute tongue. The volute curve's shape doesn't play an important role in the performance of the pump. But it is possible to overcome high radial loads by modifying the shape of the volute curve. The circle, centered on the axis of rotation and tangent to the volute tongue, is called the base circle. Its diameter is about %10 greater than the impeller diameter. At flow rates smaller than the designed flow rate, some of flow returns into the volute, passing between the impeller and the tongue, in stead of leaving through the volute throat. Because of this reason, the space between the impeller and the tongue must not be very small.

Centrifugal pumps can be classified in two different categories according to the volute designs; single and double volute centrifugal pumps as shown in the following figure:

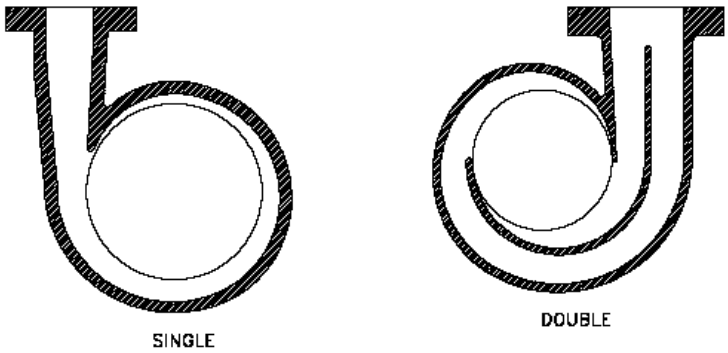

Figure 3.8: The single and double volute pumps [40]

Single volute pumps are less difficult to manufacture and more economical to produce because all of the areas around the impeller periphery are open. Double volute centrifugal pumps are built in such a manner that result in two distinct volutes, each receiving the fluid that is discharged from a 180 degrees region of the impeller at any given time. This way, all areas exposed to velocity and pressure around the volute casing are equal. The second cutwater and volute channel create an additional obstruction to the flow through the pump and this reduces the efficiency at a small degree. The double volute pump is designed to operate over a wide range of flows and heads.

Chapter 4

COMPUTER AIDED DESIGN
&
COMPUTATIONAL FLUID DYNAMICS

4.1 Introduction

In order to accomplish the design of the heart pump, mainly two software programs are used in this thesis; the first one is the Unigraphics Design program and the other one is the Blade Modeler Module of CFX Ansys Workbench 10. This project is a group project, in which both doctors and mechanical engineers are involved. As a mechanical engineer, our first purpose is to design a centrifugal pump that achieves the best performance in terms of the flow rate and the pressure difference across the pump. A normal human heart pumps approximately 4-5 liters/min with a pressure of 100 mm-Hg in normal conditions. So, the pump to be designed must achieve this criterion.

4.2 Design of the Impeller

The most important part of a centrifugal pump that affects the performance is the impeller. The design of Heart Turcica Centrifugal consists of the designs of the impeller and volute. This thesis is constructed mainly on the comparisons of many impeller designs.

Impeller design has many parameters to deal with, such as the inlet diameter, the outlet diameter, the inlet and outlet blade angles, the blade thicknesses, etc. During designing

different impellers, the inlet and outlet diameter were held at constant values, in other words, the effect of changing the diameter was not analyzed. Different impeller designs were established by changing the blade parameters.

The design procedure explained in Chapter 3 is carefully applied to obtain the impeller diameters. The diameter of the eye of impeller is calculated by using the equation 4.1. In order to use this equation, the flow rate is selected to be 5 liters/min and the rotational speed is designed as 3000 rpm.

$$D_1 = 1.533\left(\frac{Q}{\omega}\right)^{1/3} = 1.533\left(\frac{5 liters/\min \times 1m^3/1000 liters}{3000 rpm \times 2\pi}\right)^{1/3} = 9.849 * 10^{-3}\ m$$

$$= 9.849\ mm \tag{4.1}$$

The inlet diameter of the impeller is selected to be 10 mm for the sake of simplicity. The outer diameter of the impeller is found by several calculations which are carried out to find out the velocities at the tip of the impeller with the definition of theoretical head:

$$U_2 = \left(\frac{H_{th}\ g}{\varphi}\right)^{1/2} = \frac{\omega\ D_2}{2} \tag{4.2}$$

The outer diameter is found out to be approximately 48.3 mm.

The other important thing to consider is to decide whether to have a straight or a tapered inlet. The difference between a straight inlet and a tapered inlet can be seen in Figure 4.1.

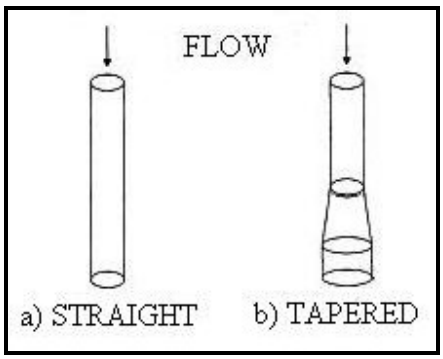

Figure 4.1: The two types if inlets of pump: a) straight b) tapered

The tapered inlet has found out to be achieve a lower normalized index of hemolysis (NIH) compared to the straight shape [41]. Moreover, the flow velocity within a tapered inlet is found out to decrease as the fluid path becomes larger because of the increasing area. However, the flow enters at a greater velocity into a straight inlet because of the small diameter. For blood trauma and hemolysis are main concerns to be minimized, Heart Turcica Centrifugal is designed with a tapered inlet as shown in Figure 4.2:

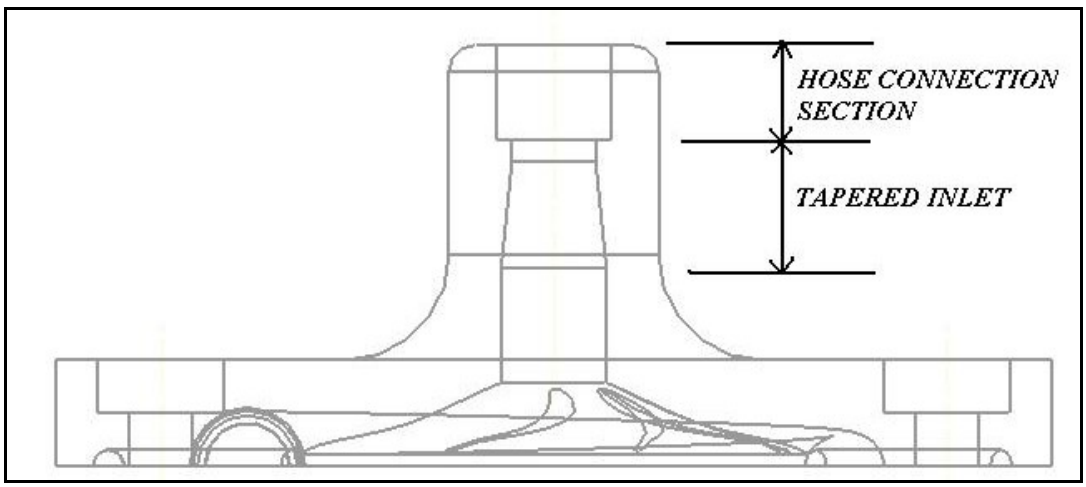

Figure 4.2: The tapered inlet of Heart Turcica Centrifugal

The main difference between the impeller designs is carried out by changing the blade angles, mainly the inlet and outlet blade angles. During this thesis, the changes within the blade angles are made by using the Blade Modeler software of Ansys Workbench. The blade angles have to be determined in optimum values to gain the maximum head. Figure 4.3 shows the main window of Blade Modeler and the parameters that have been changed to obtain new designs.

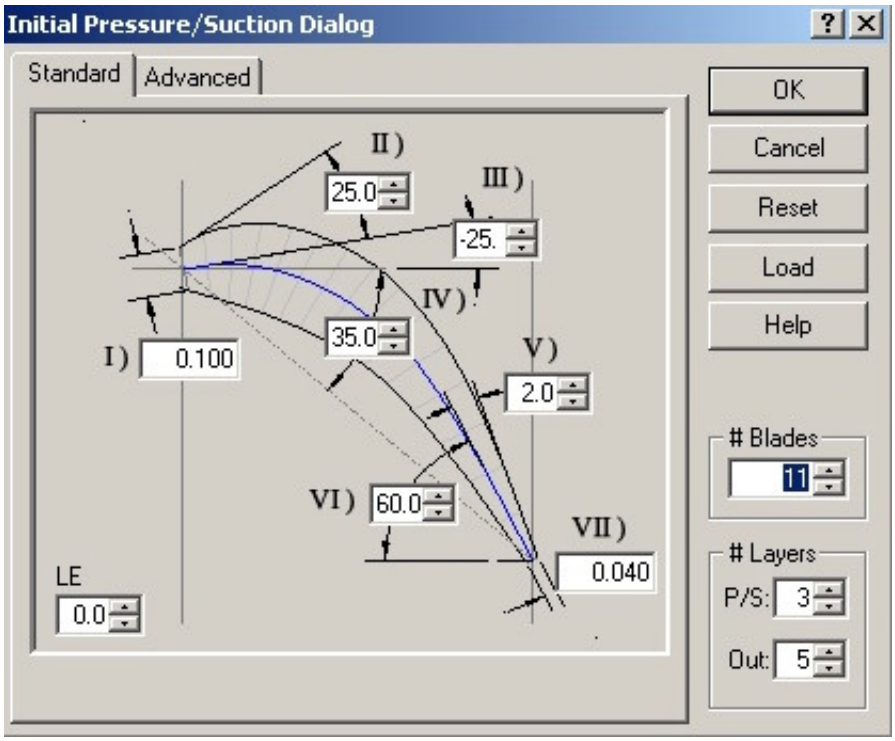

Figure 4.3: The blade parameters given as inputs in ANSYS Blade Modeler

According to the calculations done based on the procedure explained in Chapter 3, the number of blades is fixed at 8. All of the impellers designed contain 8 blades. Default parameters for the inlet and outlet blade angles are calculated as 25˚ and 60˚. Given a

specific tolerance value for each angle value, 17 different designs were constructed. Table 4.1 is the design matrix that shows the values of blade angles for all of these designs. Gökhan Yıldız has performed the computational fluid dynamics simulations of these designs to see which one achieves a higher head with a larger flow rate. Figure 4.4 the corresponding head pressures of 17 designs found by CFD results are shown. The best performing design was Model 13 with inlet blade angle of 25˚ and outlet blade angle of 70˚, and was manufactured by Gökhan Yıldız.

CHANGING PAR.	21 DIFFERENT DESIGNS				
II	II) 15	II) 20	II) 25	II) 30	II) 35
	III) -25	III) -25	III) -25	III) -25	III) -25
	IV) 35	IV) 35	IV) 35	IV) 35	IV) 35
	VI) 60	VI) 60	VI) 60	VI) 60	VI) 60
III	II) 25	II) 25	II) 25	II) 25	II) 25
	III) -15	III) -20	III) -25	III) -30	III) -35
	IV) 35	IV) 35	IV) 35	IV) 35	IV) 35
	VI) 60	VI) 60	VI) 60	VI) 60	VI) 60
IV	II) 25	II) 25	II) 25	II) 25	II) 25
	III) -25	III) -25	III) -25	III) -25	III) -25
	IV) 25	IV) 30	IV) 35	IV) 40	IV) 45
	VI) 60	VI) 60	VI) 60	VI) 60	VI) 60
VI	II) 25	II) 25	II) 25	II) 25	II) 25
	III) -25	III) -25	III) -25	III) -25	III) -25
	IV) 35	IV) 35	IV) 35	IV) 35	IV) 35
	VI) 50	VI) 55	VI) 60	VI) 65	VI) 70

Table 4.1: The design matrix containing different designs with different blade angles

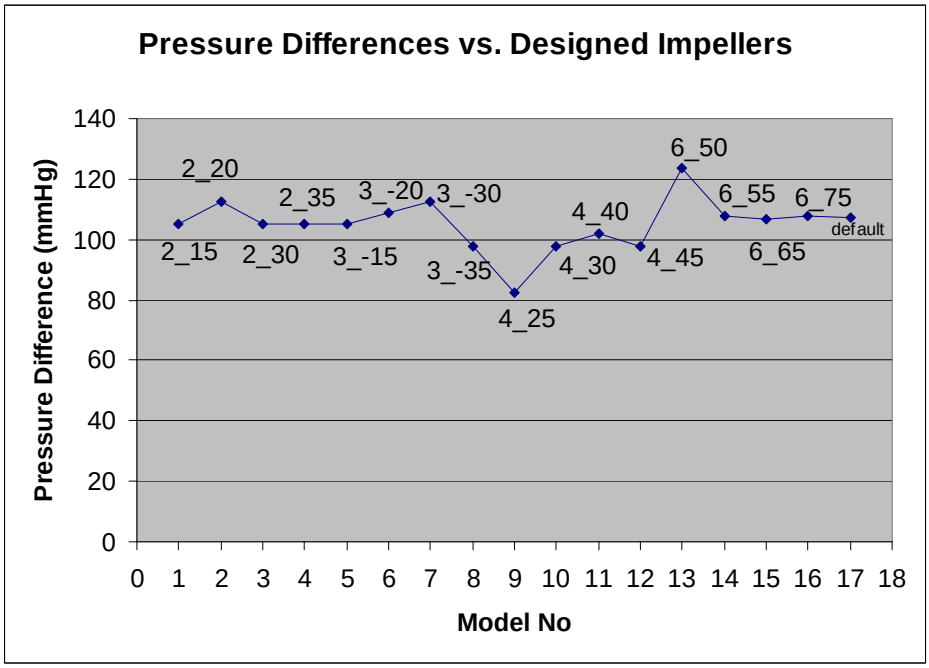

Figure 4.4: CFD prediction of the different impeller designs

Beyond these 17 designs, after Model 13, the pump that achieves the largest pressure head is Model 2. Model 2 has constant blade height of 5 mm. The inlet blade angle is 20˚ and the exit blade angle is 60. CFD simulations of Model 2 have been completed and a prototype of it has been manufactured. On the back side of impeller, 9 holes are drilled; eight of them are for the cylindrical magnets and one for the radial bearing. The diameter of the cylindrical magnets used is 5 mm and their height is 8.1 mm, so the shaft on the back side of impeller is designed to be 10 mm. 1.9 mm thickness is left between the magnet holes and the back side of the hub so that any possible failures that may result with fracture are avoided. Figure 4.5 shows the 3D CAD data of the impeller of Model 2 and Figure 4.6 shows the dimensions of the magnets and the bearings.

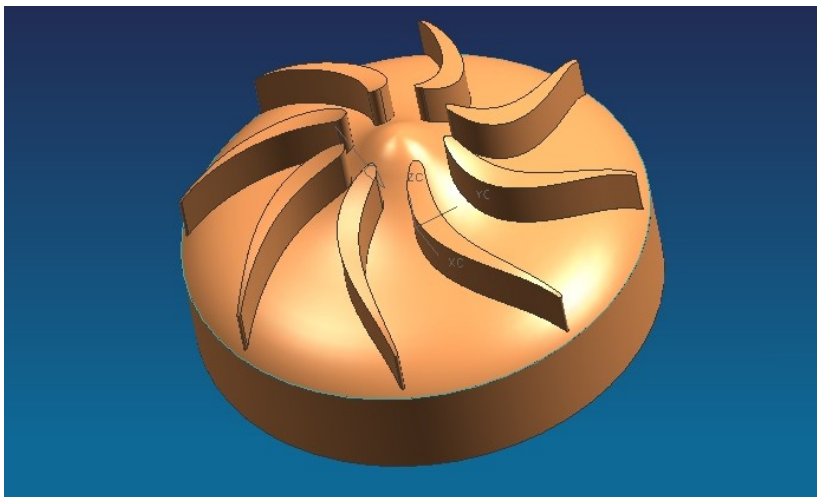

Figure 4.5: The 3D CAD modeling of the impeller of Model 2

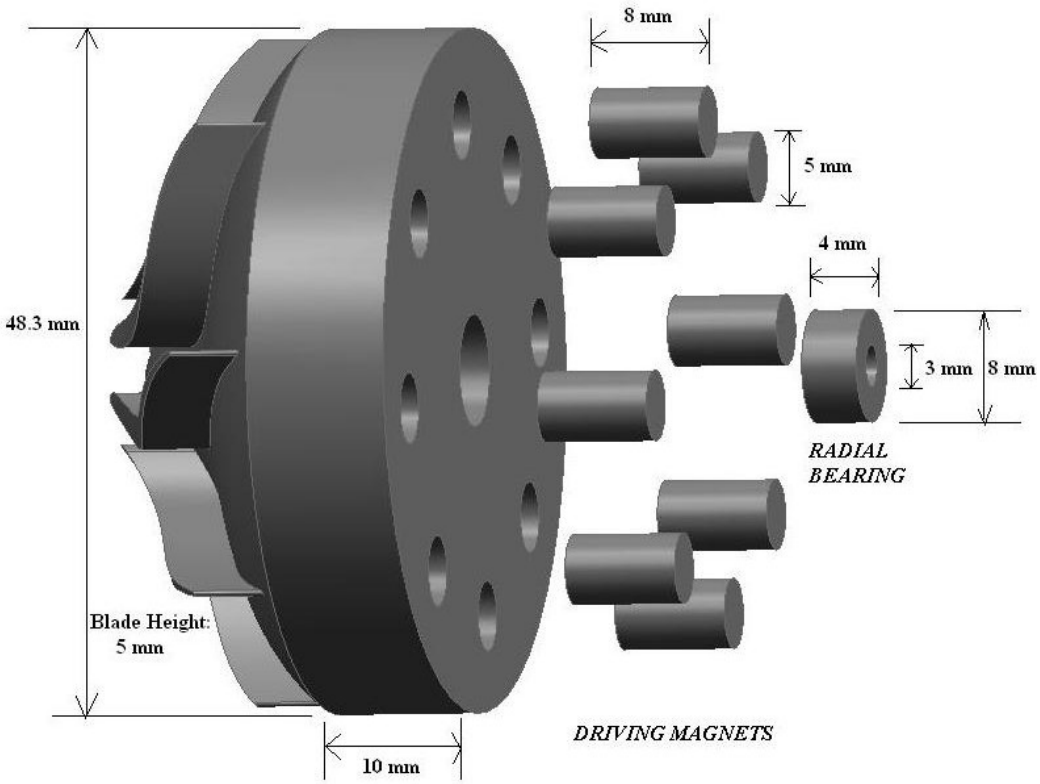

Figure 4.6: The dimensions of the impeller, the magnets and the radial bearing

The height of the shroud of model 2 is 14 mm. A new hub design has been made with 8 mm shroud height to see the effect of a smaller volume inside the pump and to obtain the comparison of performance curves of the pumps with different shroud heights. Figure 4.7 shows the 3D CAD modeling of model 2 with a shroud height of 8 mm.

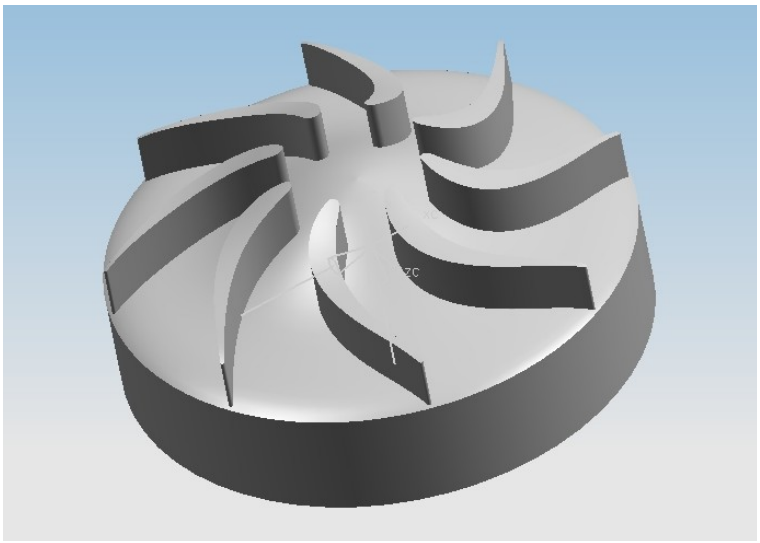

Figure 4.7: 3D CAD data of impeller of pump Model 2 with 8 mm Hub Height

A new design is made by changing the height of the blades of Model 13 in order to observe the effect of the volume inside the pump once more. In addition, the effect of the blade height on the performance of the pump is investigated. In the first version of Model 13, the blade height was designed as 5 mm but in my new design, the blade height is increased to 10 mm. In Figure 4.8, 3D CAD modeling of this new pump with blade height of 10 mm can be seen.

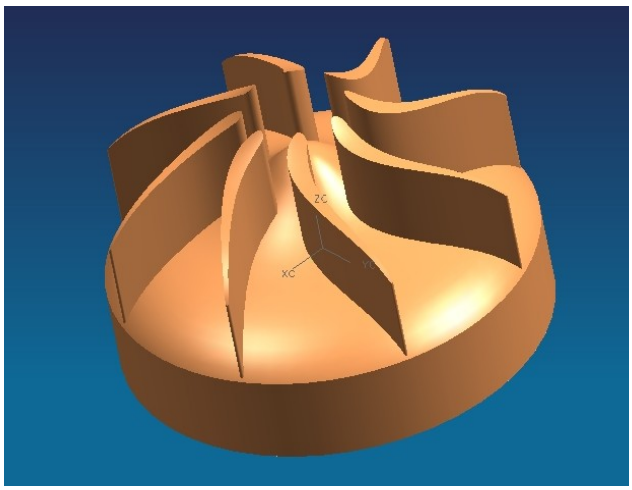

Figure 4.8: 3D CAD data of impeller of pump Model 13 with 10 mm blade height

Model 13 is re-manufactured with hydrofoil shaped blades that have constant blade thickness because hydrofoil geometry can increase pressure efficiently despite its small cross sectional area. . Figure 4.9 shows the 3D CAD modeling of the modified pump model 13.

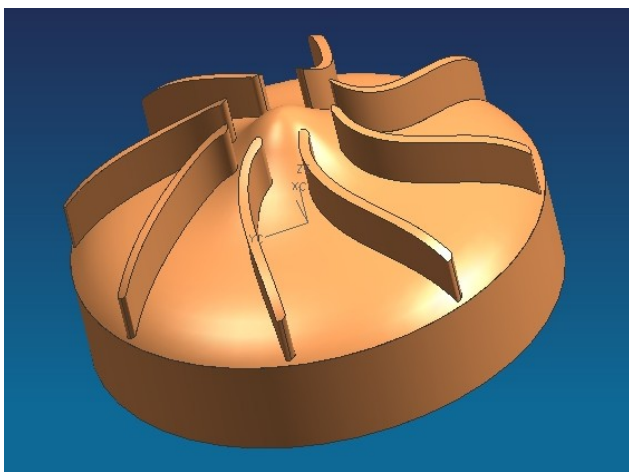

Figure 4.9: 3D CAD data of impeller of pump Model 13 with 10 constant blade thickness

4.3 Design of the Volute

Volute is the spiral-shaped flow passage where the impeller discharges directly into. It is usually of circular or trapezoidal cross section. Its cross section increases gradually around the impeller periphery, starting from the volute tongue and ending at the volute throat. The duty of the volute tongue is to direct the total flow, that is collected from around the impeller, through the throat to the pump exit flange.

A volute can be designed in two different ways according to the shape of the volute tongue: a sharp tongue and a rounded tongue (Figure 4.10).

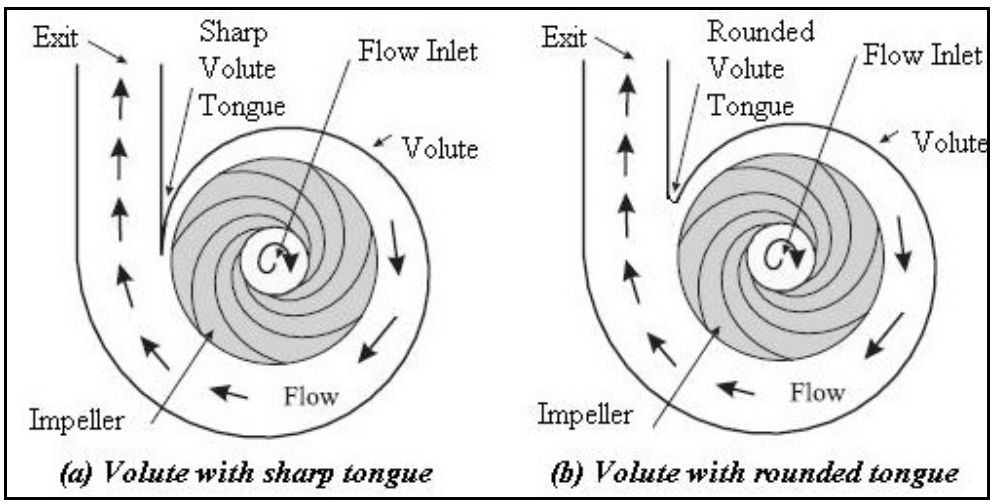

Figure 4.10: Two different volute designs according to the volute tongue [48]

Onur Demir has studied the effect of volute tongue, whether rounded or sharp, on the effect of performance and resulted that the first type of the volute with the sharp tongue is more suitable for a centrifugal blood pump [44]. For that reason, all of the pumps designed own a volute with a sharp tongue.

The gradually increasing volute flow cross sections are calculated from the flow rate and from an average velocity at the volute cross section center. The volute was divided into

twelve equal parts and the cross section of the volute was computed for twelve locations. Figure 4.11 shows the division of the volute and all these 12 sections.

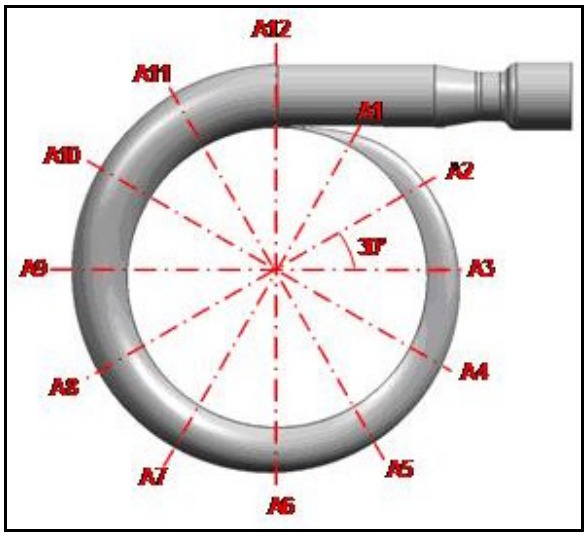

Figure 4.11: The cross section illustration of spiral geometry [44]

The radius of each of these sections, R_j, was calculated according to the formula below where A_c and h represent the cross section area of the volute and the height of the blade. A_i stands for the inlet area and can be calculated simply by multiplying the square of the inlet radius with the pi number. Table 4.2 shows the calculated areas of each section and the corresponding radius values.

$$A_i = \pi R_i^2 \tag{4.3}$$

$$A_{c_j} = \pi R_j^2 - \left[R_j^2 \sin^{-1}\left(\frac{h}{2 R_j} \right) \right] + \frac{h}{2} \sqrt{\left(R_j^2 - \frac{h^2}{4} \right)} \tag{4.4}$$

A_c (mm^2)			R (mm)
A1	A_i / 12	6.545	1.527
A2	2 A_i / 12	13.090	2.081
A3	3 A_i / 12	19.635	2.526
A4	4 A_i / 12	26.180	2.906
A5	5 A_i / 12	32.725	3.243
A6	6 A_i / 12	39.270	3.548
A7	7 A_i / 12	45.815	3.830
A8	8 A_i / 12	52.360	4.092
A9	9 A_i / 12	58.905	4.339
A10	10 A_i / 12	65.450	4.572
A11	11 A_i / 12	71.995	4.794
A12	A_i	78.540	5.006

Table 4.2: The cross section area calculation of spiral geometry

The diameter of the base circle tangent to the volute tongue is designed to be 10% larger than the impeller diameter. It is important that pressure fluctuations at the tongue when the individual blades pass by will decrease with increasing base circle diameter.

4.4 The Assembly of the Pump

The final thing to do is to design the upper and lower casings of the pump, after the impeller and volute are designed. The casings are obtained by subtracting the volute and impeller geometries from the rectangular blocks. While the hub of impeller is subtracted to construct the upper casing, 200 μm clearance is given to prevent any frictional problem that will cause energy loss. The hole for the radial bearing is drilled on the back side of impeller in stead of on the bottom surface of the lower casing; hence the shaft is manufactured

united with the bottom surface of the lower casing in stead of attaching it to the impeller. This makes the manufacturing process much easier. The two casings are assembled via the M6 bolts at the three corners of casings except the corner at the exit of the pump. At that corner, the distance is 10 mm between the exit and the side of casing, so at this point M4 bolt is used to assemble the casings. In order to prevent the possible leakage problem during experiments, the casings are also glued by using silicone on the adjacent surfaces. At this point, there is a risk that the silicone may flow into the volute and may become an obstacle for the fluid. Concerning this possible problem, channels are made with a depth of 0.5 mm on the sides of both casings, shown in Figure 4.12.

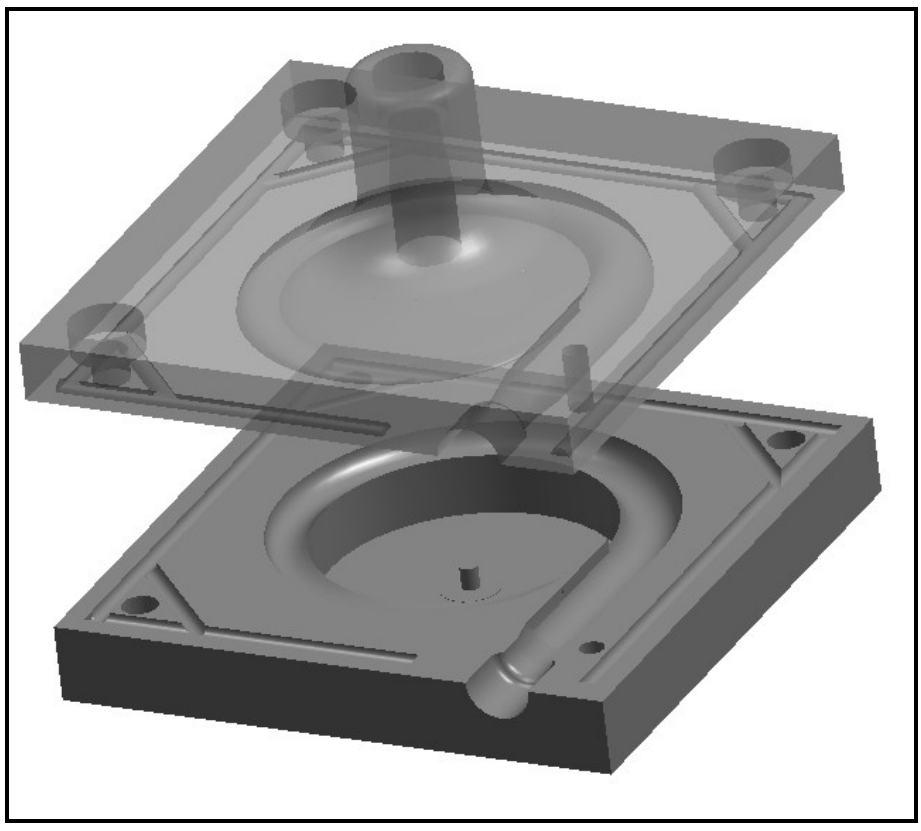

Figure 4.12: 3D CAD modeling of upper and lower casings

The driving system for the pump is not a shaft-driving mechanism; in stead a magnetic driving mechanism is used to get rid off the uncontrollable and unstable flow disturbance within the pump that will cause because of the misalignment of the impeller and the motor shaft. This also eliminates a possible leakage problem that would cause because of the interaction between the impeller and the shaft. The important thing here is that the distance between the driving magnets and the magnets at the end of the impeller must not be large because the force between these magnets is inversely proportional to the fourth power of the distance. Moreover, the distance must not be so small because the material used is acrylic glass and when the thickness is small, it might quickly crack. The distance is designed to be 1 mm. The total thickness of the lower casing becomes 13 mm with the magnets that are 8 mm in height. The clearance value between the lateral side of the impeller and the lateral surface of the lower casing is 100 μm. The thickness of the upper casing is 10 mm and with the 30 mm inlet design for the hose connection, the total height of the upper casing becomes 40 mm. The clearance between the hub surface of the impeller and the top casing is 200 μm. The CAD modeling of the assembly of the pump and the casings with the impeller is given in Figure 4.13.

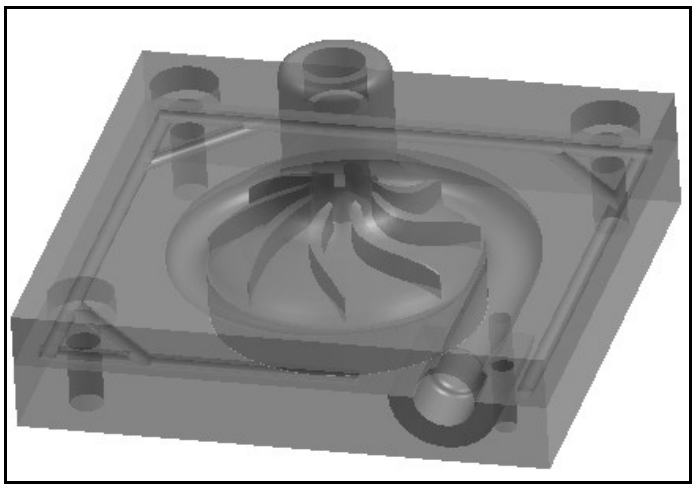

Figure 4.13: 3D CAD modeling of the assembly of the pump

4.5 Computational Fluid Dynamics

Computational Fluid Dynamics (CFD) has become one of the most important parts of the engineering design and analysis because by the help of CFD simulations anyone can predict the performance of new designs or processes before they are ever manufactured or implemented. This process can be called as Computer Aided Engineering (CAE). Design engineers use CAE tools at the concept stage to test and check the design they have made before manufacturing it. This process is cost friendly because major changes may be relatively expensive to re-produce the pump.

The fluid motion across the pump can be determined by analyzing the CFD simulation results without doing any experiments. In the studies, CFD results have been used to validate the experimental results with simulation results. ANSYS Workbench has been used. CFX-Mesh, Advanced CFD and Blade Modeler modules of ANSYS Workbench were utilized to analyze the performance of the pump. The data obtained from simulations is processed via Matlab to obtain the performance graph of the pump. The flowchart followed during CFD simulations is shown in Figure 4.14.

The sharp and violent activation of blood that is the main cause of thrombosis formation in the pump can occur because of oppose, contrary flow characteristics which include turbulence, recirculation stasis, and high shear stress [42]. CFD simulations give the chance to calculate the distribution of the fluid flow velocity, see the velocity and pressure streams across the pump and observe whether there is turbulence in the pump by calculating the turbulence kinetic energy of fluid flow. The pump can be re-designed with respect to the results obtained by CFD to achieve better performances.

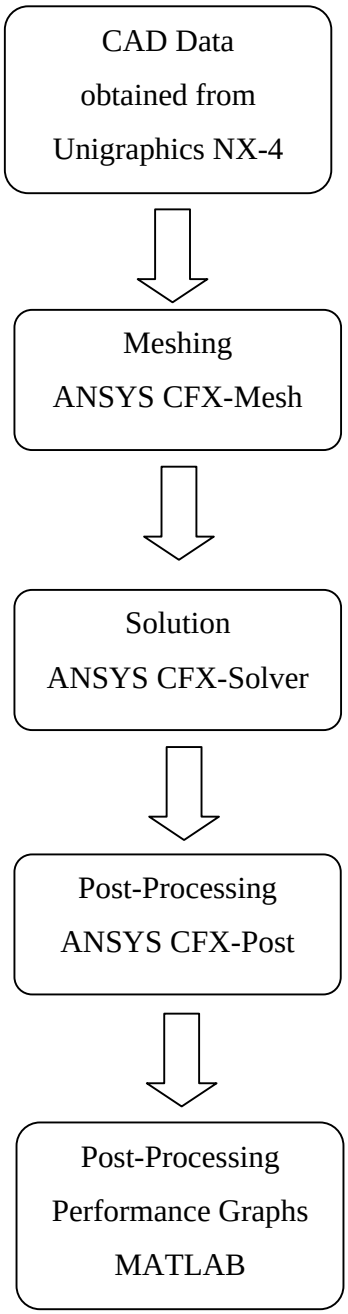

Figure 4.14: The flowchart of the CFD process

The simulation starts by importing the flow geometries to the meshing software. The important point here is that the CAD data of the pump is not meshed, the design that the CFD simulations are held is the geometry of pump where fluid passes through. The pump geometric data can be easily read by meshing the fluid geometry.

The pump consists of 4 parts to analyze in CFD: the inlet, the center zone, impeller and the volute with the exit zone (Figure 4.15). In Unigraphics, the inverse of the impeller CAD geometry is constructed, i.e. the geometry where the fluid flows is designed as solid, because the geometry being analyzed in CFD is the flow geometry.

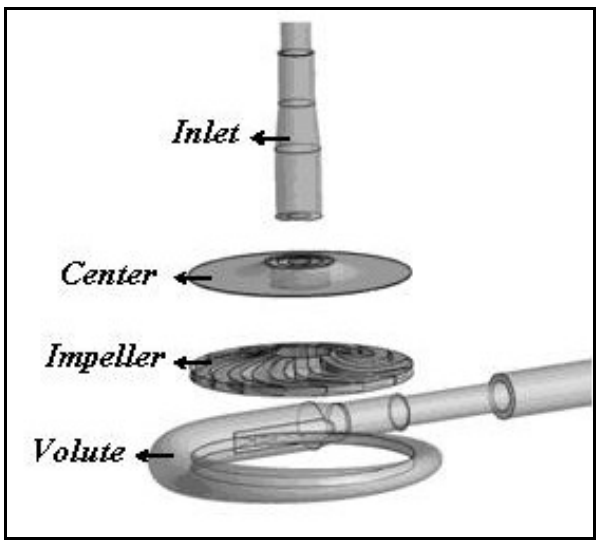

Figure 4.15: CAD modeling of the pump transferred to CFX-Mesh

The inlet and the flow are modeled with respect to the position of the pressure sensors at the inlet and exit of the pump because the pressure may fall down because of the resistance shown by the connectors, tube and the hose; and this will lead to get inaccurate values of pressure by CFD simulations. The center part is created because there is 200 μm clearance between the hub and the upper casing. Fluid fills these spaces during flow, so this clearance must also be considered.

The CFD simulation starts with the mesh generation. Mesh generation can be defined as generating a polygonal or polyhedral mesh that approximates a specific geometric domain. Once the geometry is imported from Unigraphics, there may be unconnected surfaces, so virtual faces are created to unite the whole part. Structured tetrahedral elements are used to characterize the geometry. Minimum size of these elements is specified as 0.1 mm and maximum size is introduced as 0.65 mm. Smaller size cannot be achieved because the computers used were not capable of generating higher number of grids and performing the simulation. An example of the meshing, the virtual face creation and the final situation of meshing of the impeller is shown in Figure 4.16.

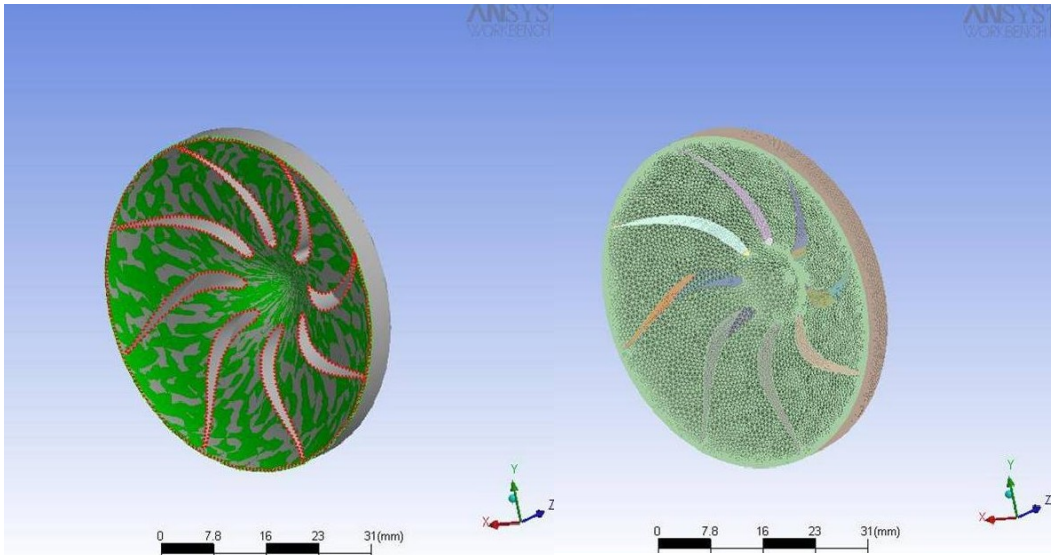

Figure 4.16: Meshing of the impeller in CFX-Mesh

After the meshing of all parts is done separately, these parts have to be assembled together. The assembly is constructed in CFX-Solver Module. Impeller and the center zone are introduced as rotating domains and the volute with the exit and the inlet zones are introduced as static domains. The final situation of the assembly in CFX-Solver is shown in Figure 4.17.

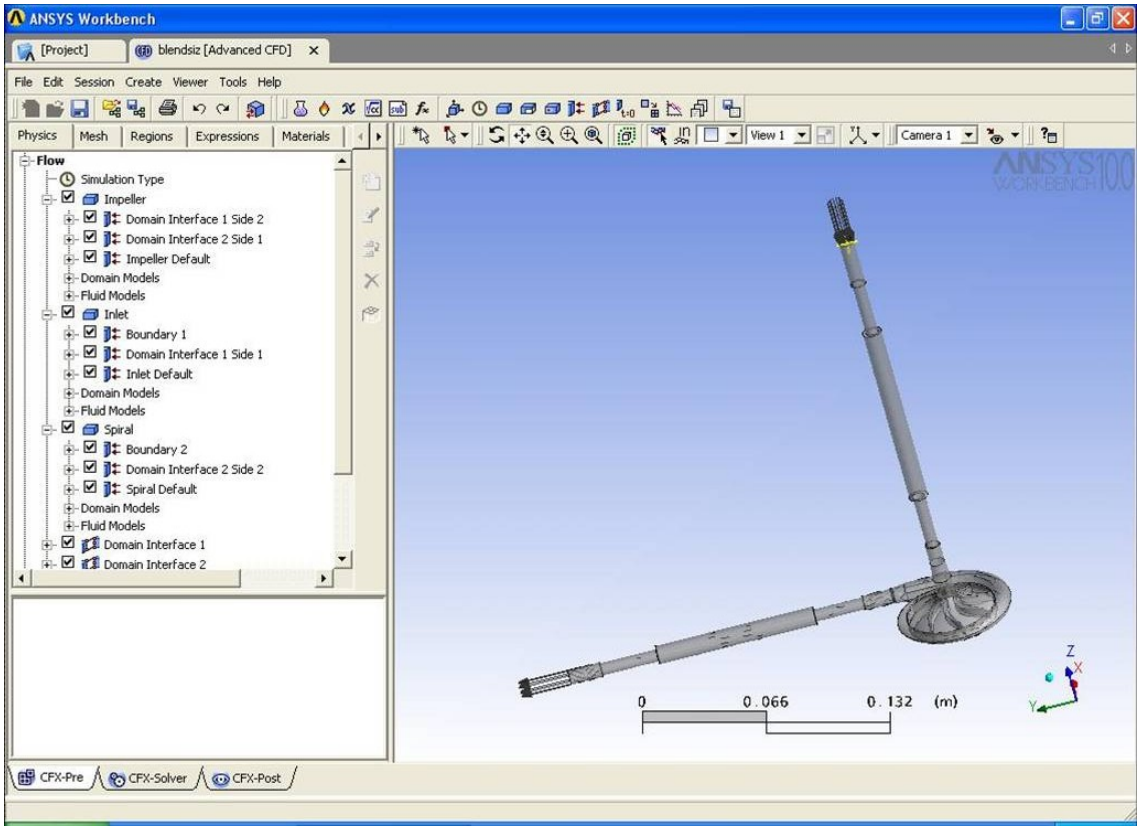

Figure 4.17: The assembly of the pump in CFX-Solver

Boundary conditions have to be specified to be able to simulate the flow across the pump. The type of the boundary condition depends on what sort of boundary or interface boundary condition is placed on. In order to obtain accurate results at the end of simulations, boundary conditions must be set properly. Inlet, outlet and wall boundary conditions are used in simulations. The inlet boundary condition is given via the pressure value at the inlet. As the inlet is free of air, the inlet static pressure is given as 0 atm. The outlet boundary condition is given via the mass flow rate and is specified by giving the mass flow rate as an input parameter. The upper surface of the clearance is introduced as counter-rotating wall to achieve no-slip boundary condition at the impeller surface. All

other surfaces are assigned to be wall with no-slip condition. The four domains are connected carefully so that there is not any transformation or rotational offset between the domains.

The fluid is chosen to be water with a density of 997 kg/m^3 and with a viscosity value of 0.001 kg/m-s in order to be able to compare the results of experiments with the simulations. It is assumed that there is not any temperature difference across the pump.

Auto timescale option is selected for the convergence control of the simulation and the maximum number of equations is introduced as 1000. The convergence criteria is described such that the residual error is 0, 0001. If the error falls below this value, the simulation stops. Simulation type is steady state. k-ε turbulence model is used for the simulations because it is the most popular and suitable two-equation model for centrifugal pumps [49].

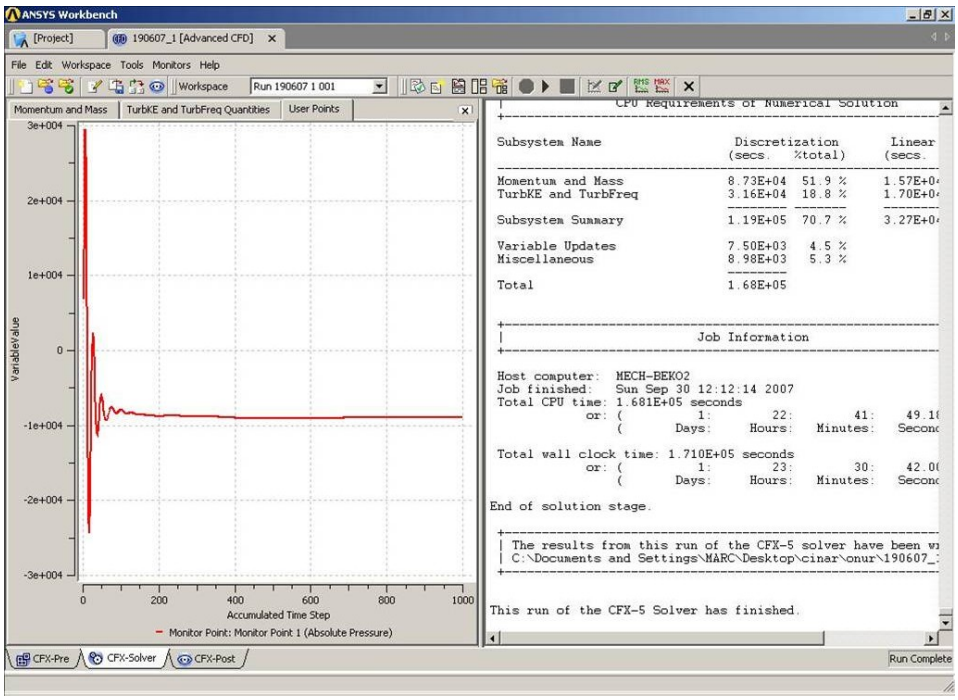

Figure 4.18: Pressure vs. time graph for the monitor point

During the simulations, a monitor point is placed at the exit of the pump, so that the pressure value at this point will give the pressure difference across the pump because the pressure at the inlet is set to zero. In order to see the pressure distribution, pressure contours are analyzed at the end of the simulation. Velocity streamlines are drawn to see if there is any swirl within the pump or not. The most important thing to be considered in the design of a blood pump is the blood trauma. The prediction of blood trauma can be done by checking the shear stress and the swirl within the pump. Amy L. Throckmorton et al. stated that shear stress below 300 Pa means that hemolysis will occur at low levels which is acceptable. Hydraulic performance of the pump is predicted by checking the pressure contours and velocity streamlines.

For this thesis, CFD simulations are performed for pump Model 2 because the other pumps designed are based on a significant change on a previous model and so it can be compared with the experimental data of that pump. The simulations were held for 2000 rpm, 2250 rpm, 2500 rpm, 2750 rpm and 2998 rpm, which are the rotational speeds worked during experiments. Simulations were done at four different flow rates for each speed and performance curve was plotted by fitting these data. Minimum of 3 data points is enough to fit a second order polynomial to the results. Figure 4.19 shows the performance graph of pump Model 2 that is plotted with the simulation data. Figures 4.20-4.24 show the pressure distribution within the pump at the maximum value of the flow rate given for the simulation at the specific rpm. Figures 4.25-4.29 give information about the shear stress distribution within the pump. The results were not well because in all of the cases the maximum value of shear stress was above 300 Pa, which means danger for blood trauma. Figures 4.30-4.34 show the velocity streamlines across the pump.

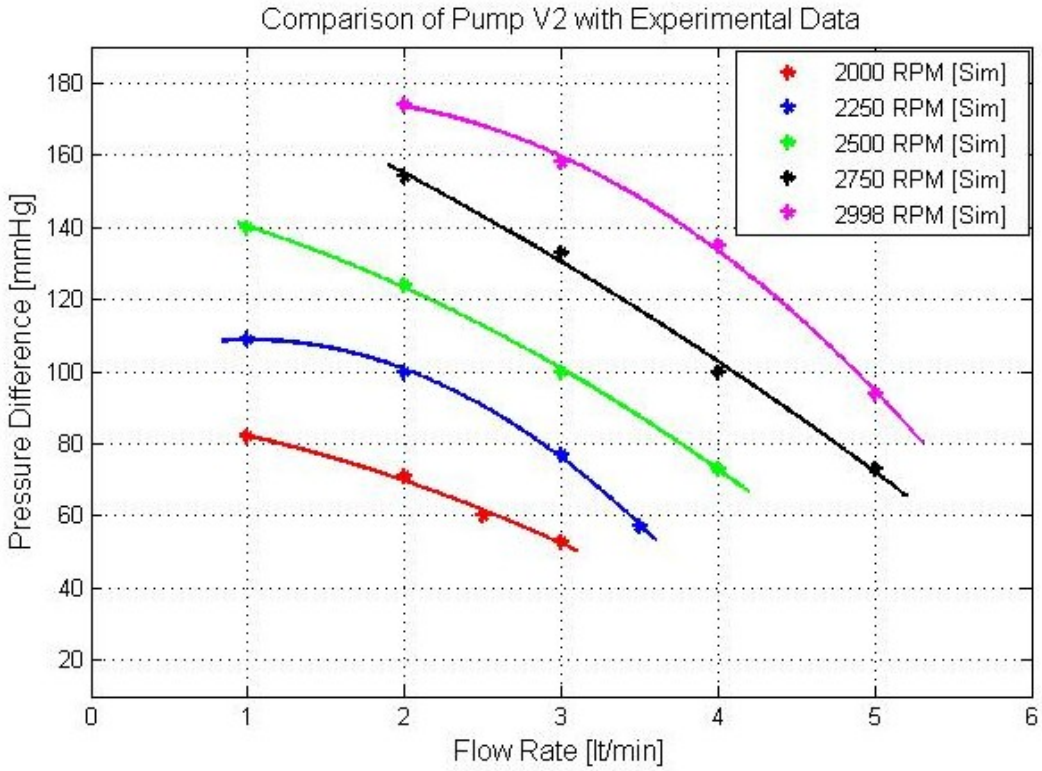

Figure 4.19: The performance curve of pump Model 2 plotted with respect to the simulation results

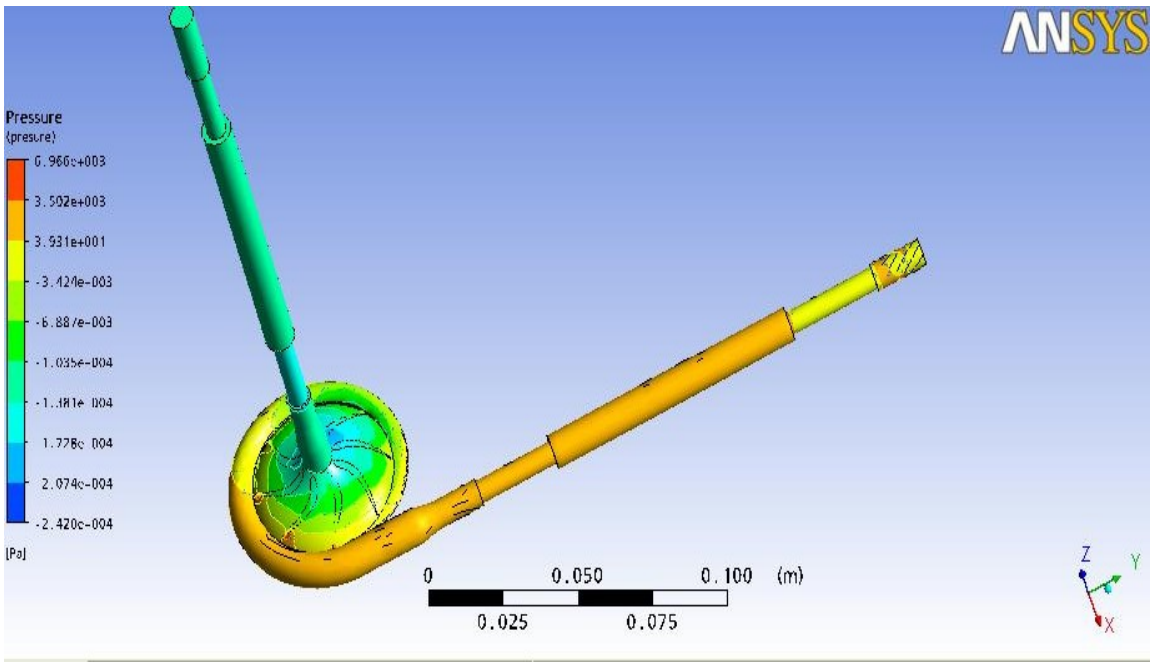

Figure 4.20: Pressure distribution within the pump at 2001 rpm and 3 liters/min flow rate

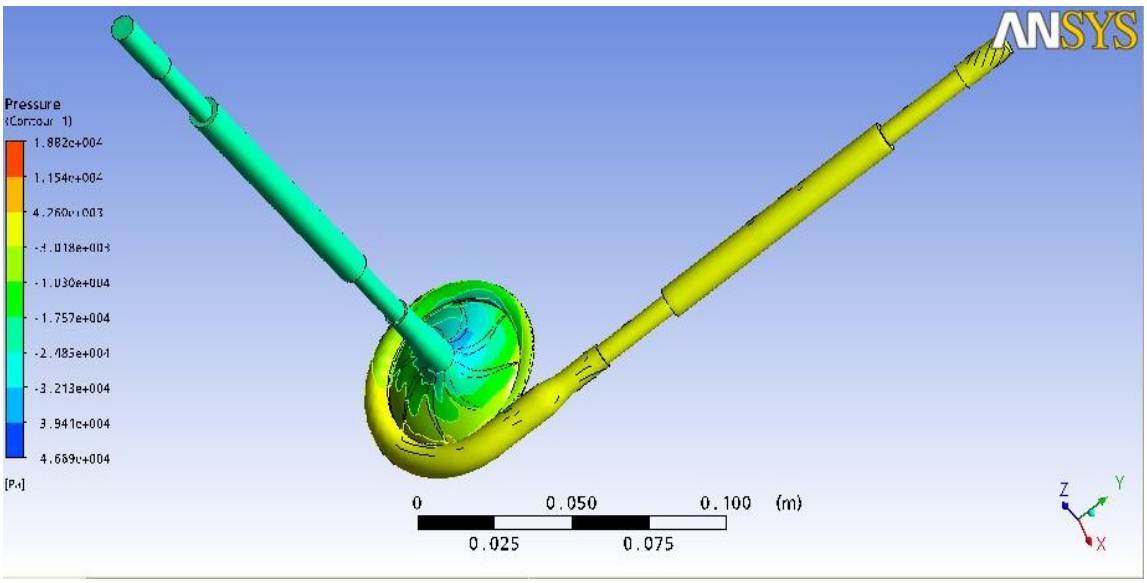

Figure 4.21: Pressure distribution within the pump at 2250 rpm and 3.5 liters/min flow rate

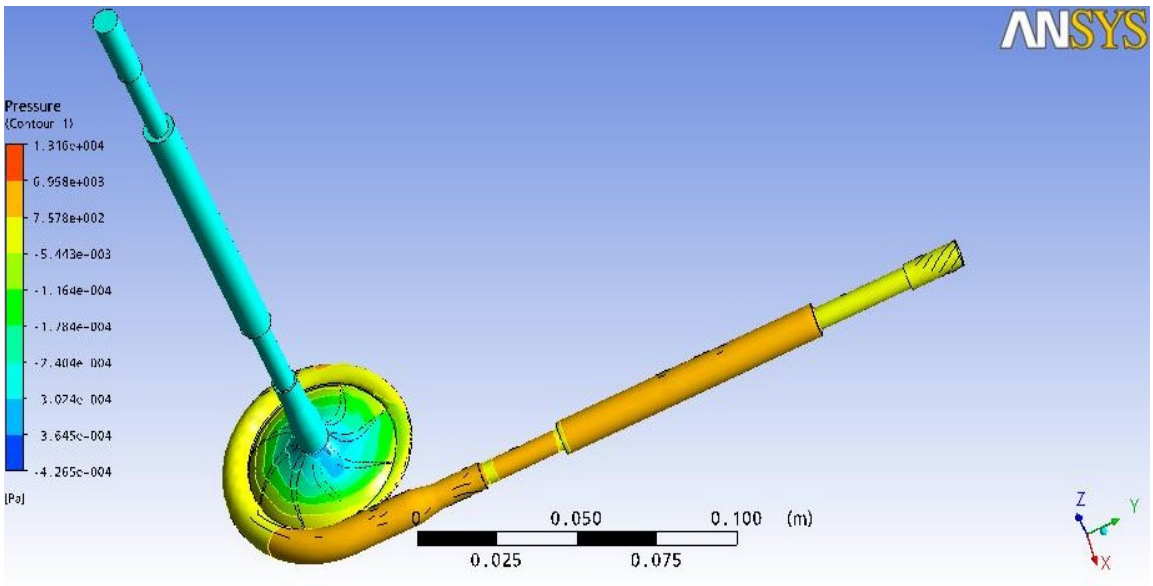

Figure 4.22: Pressure distribution within the pump at 2500 rpm and 4 liters/min flow rate

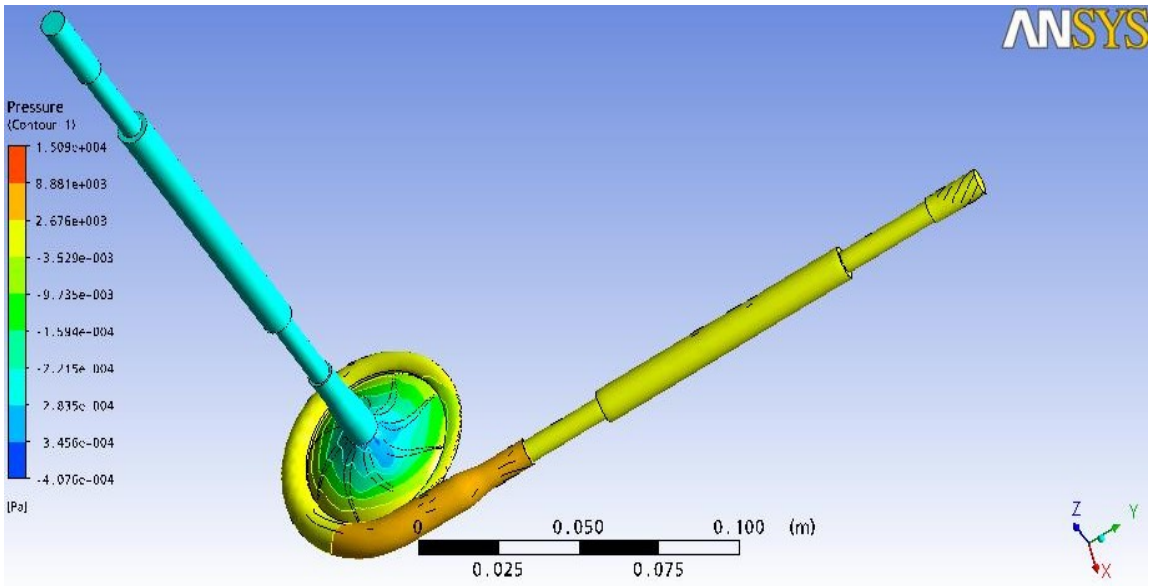

Figure 4.23: Pressure distribution within the pump at 2750 rpm and 5 liters/min flow rate

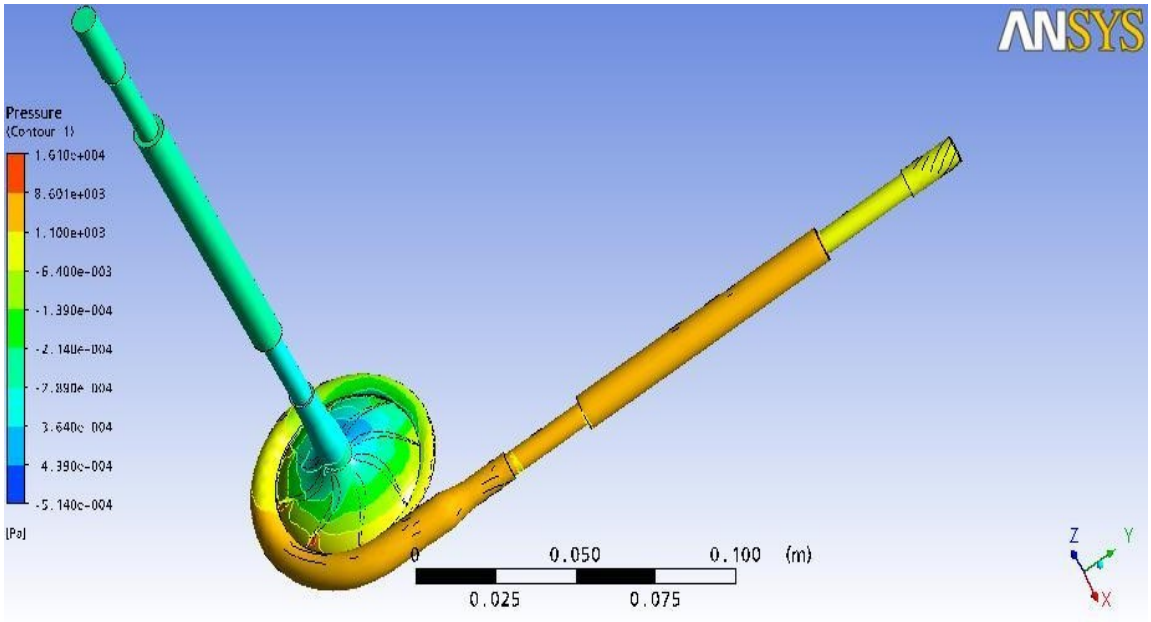

Figure 4.24: Pressure distribution within the pump at 2998 rpm and 5 liters/min flow rate

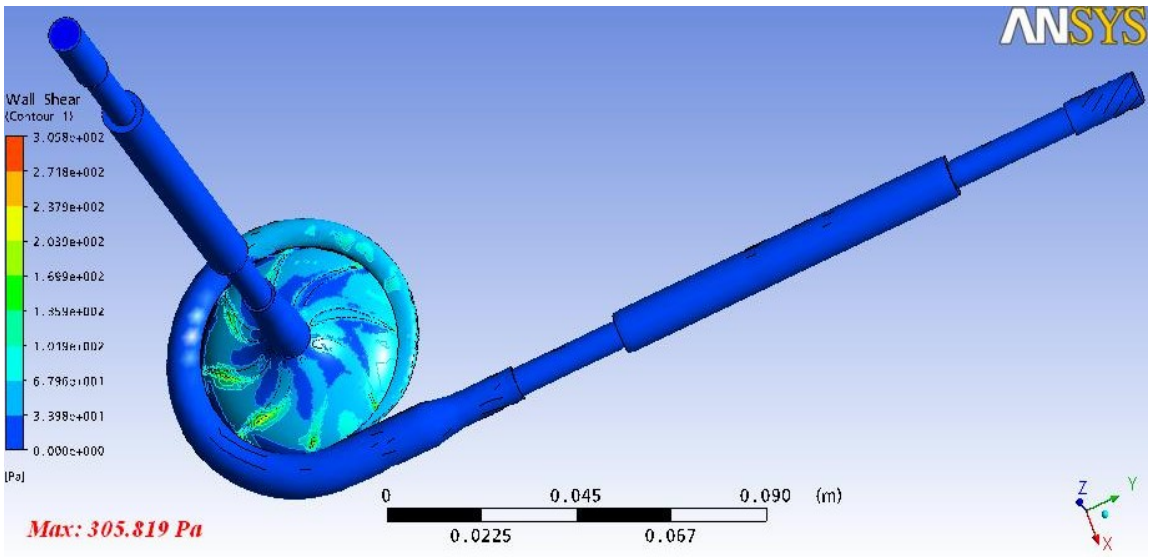

Figure 4.25: Wall shear stress distribution within the pump at 2001 rpm and 3 liters/min flow rate

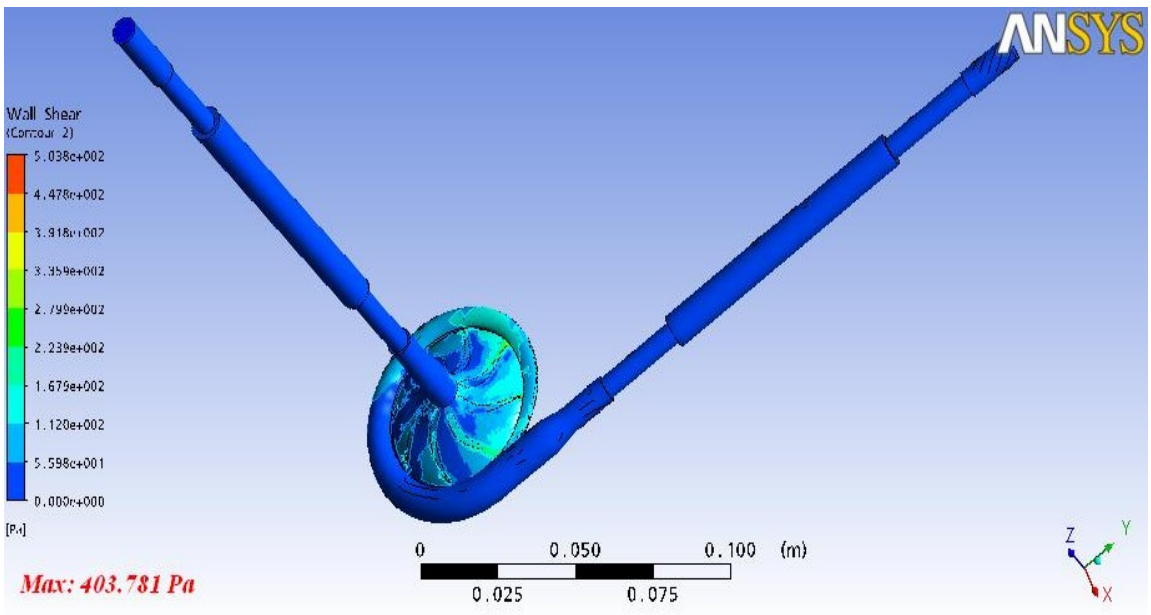

Figure 4.26: Wall shear stress distribution within the pump at 2250 rpm and 3.5 liters/min flow rate

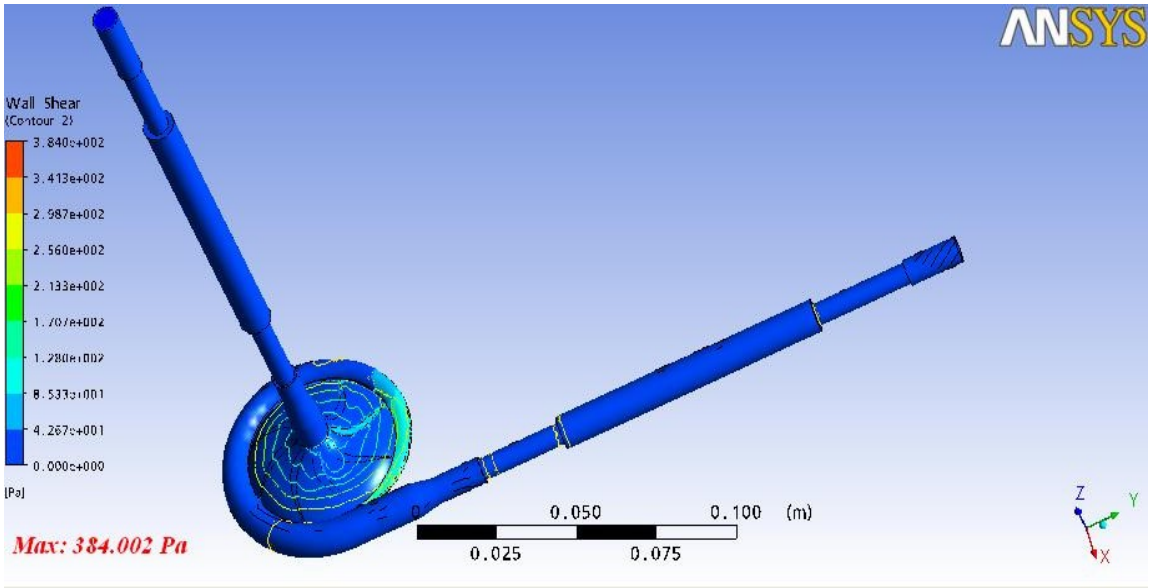

Figure 4.27: Wall shear stress distribution within the pump at 2500 rpm and 4 liters/min flow rate

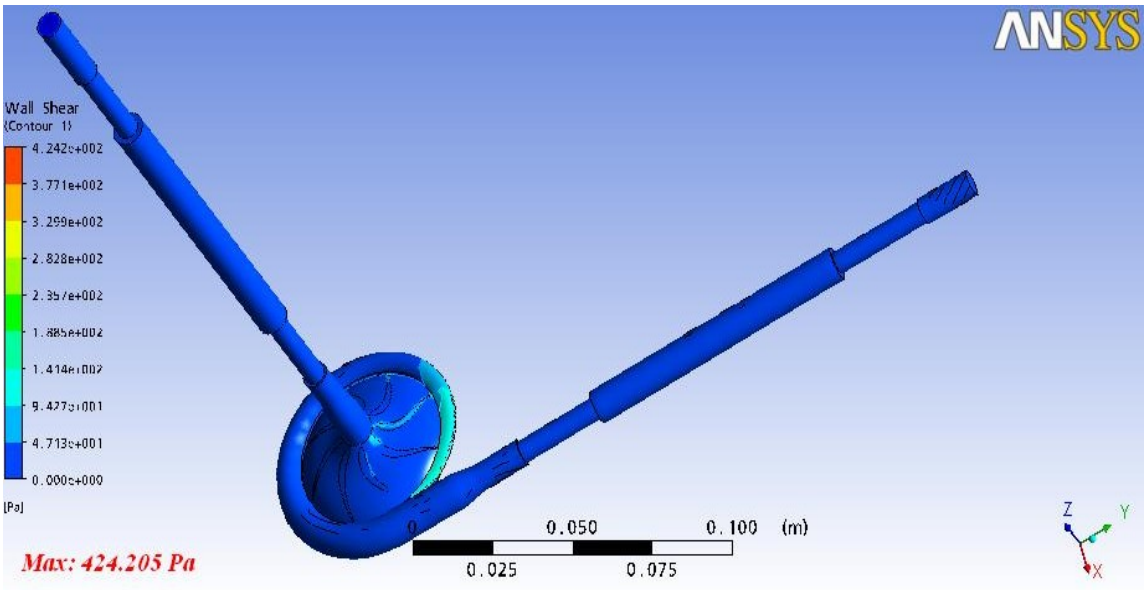

Figure 4.28: Wall shear stress distribution within the pump at 2750 rpm and 5 liters/min flow rate

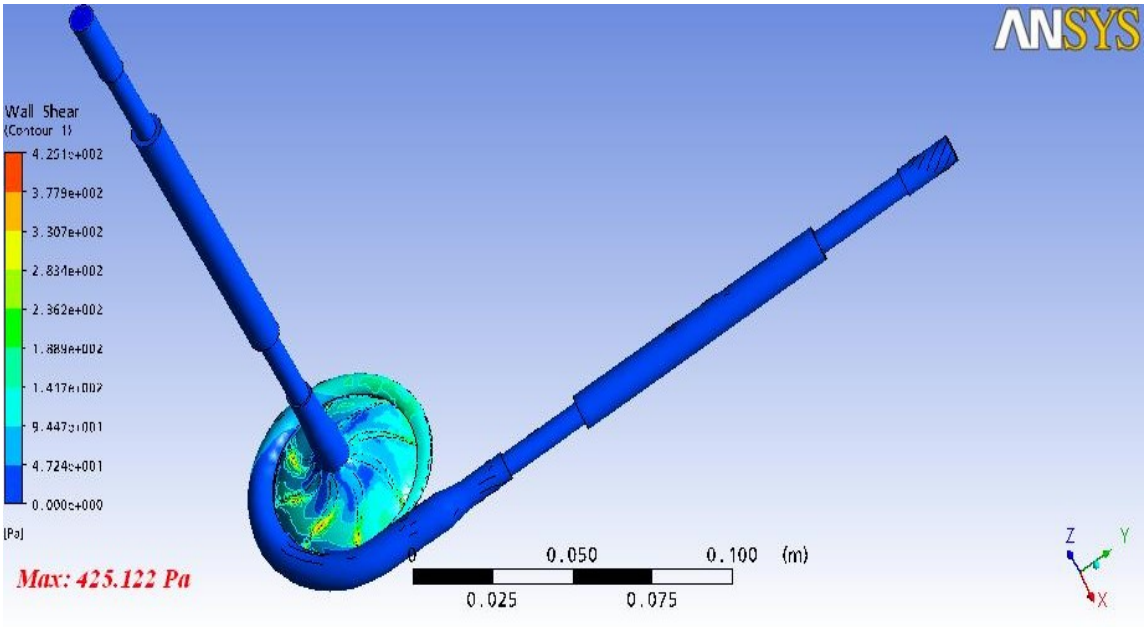

Figure 4.29: Wall shear stress distribution within the pump at 2998 rpm and 5 liters/min flow rate

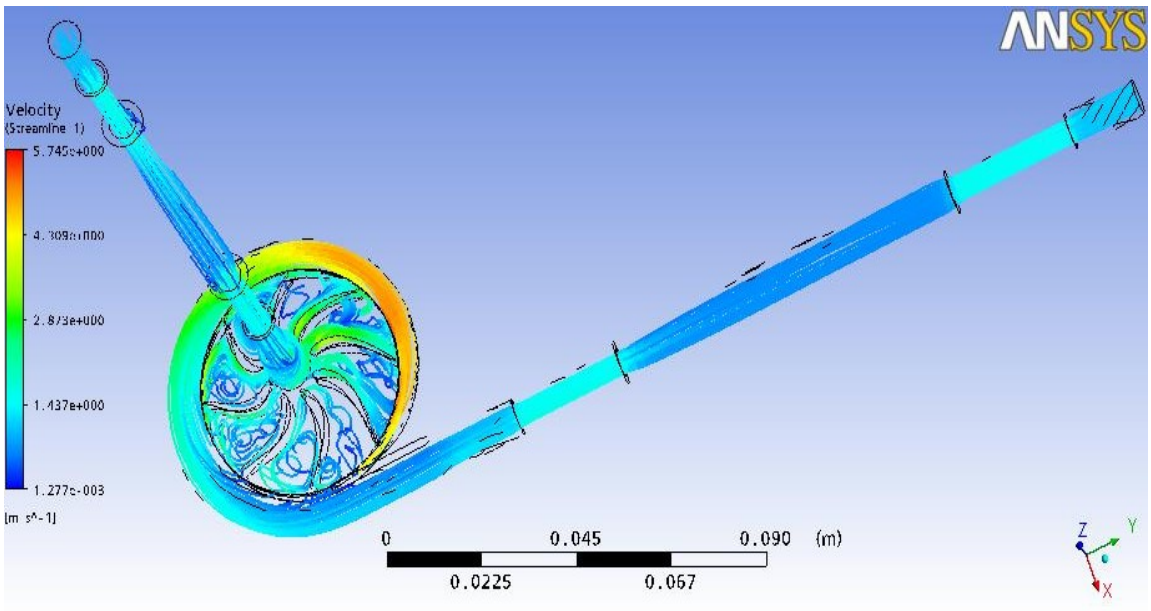

Figure 4.30: Velocity streamlines within the pump at 2001 rpm and 3 liters/min flow rate

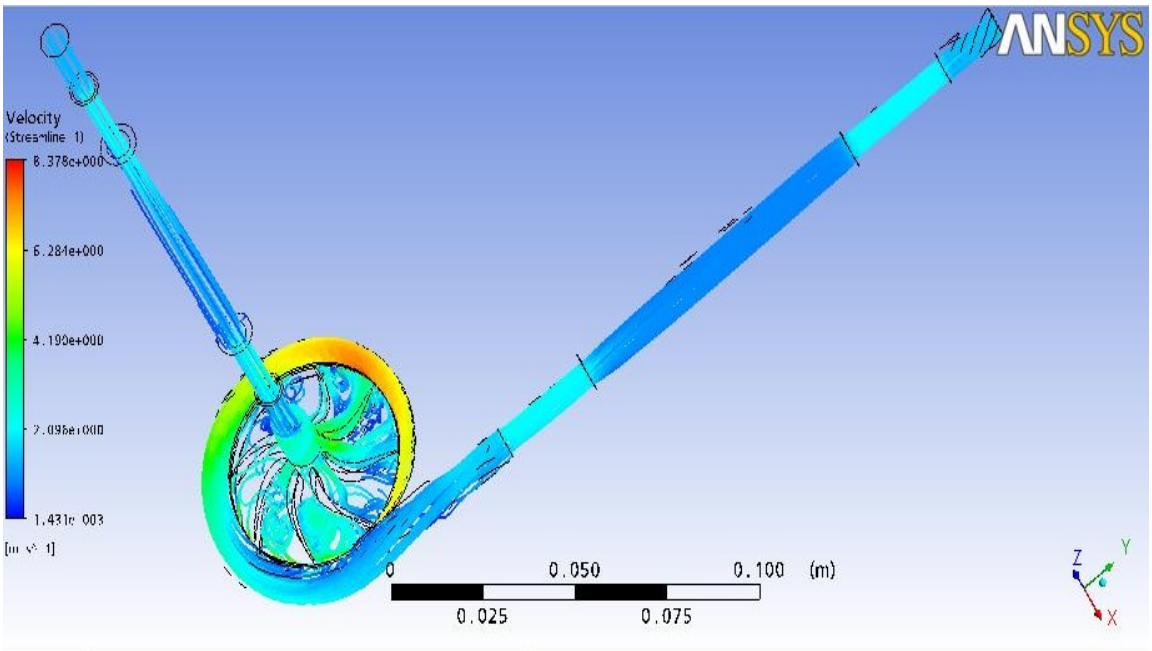

Figure 4.31: Velocity streamlines within the pump at 2250 rpm and 3.5 liters/min flow rate

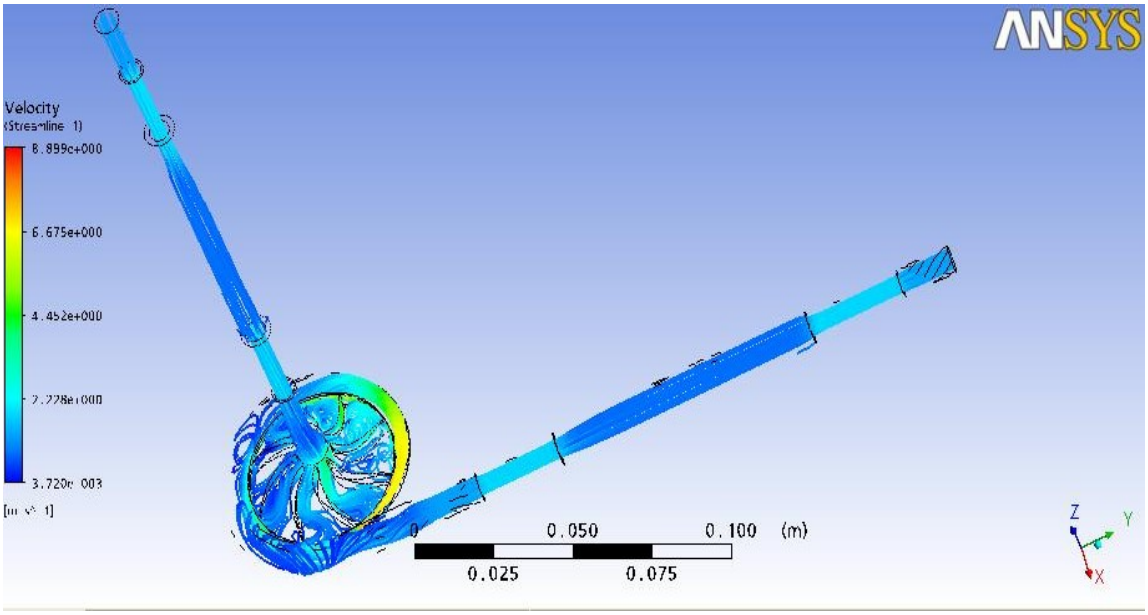

Figure 4.32: Velocity streamlines within the pump at 2500 rpm and 4 liters/min flow rate

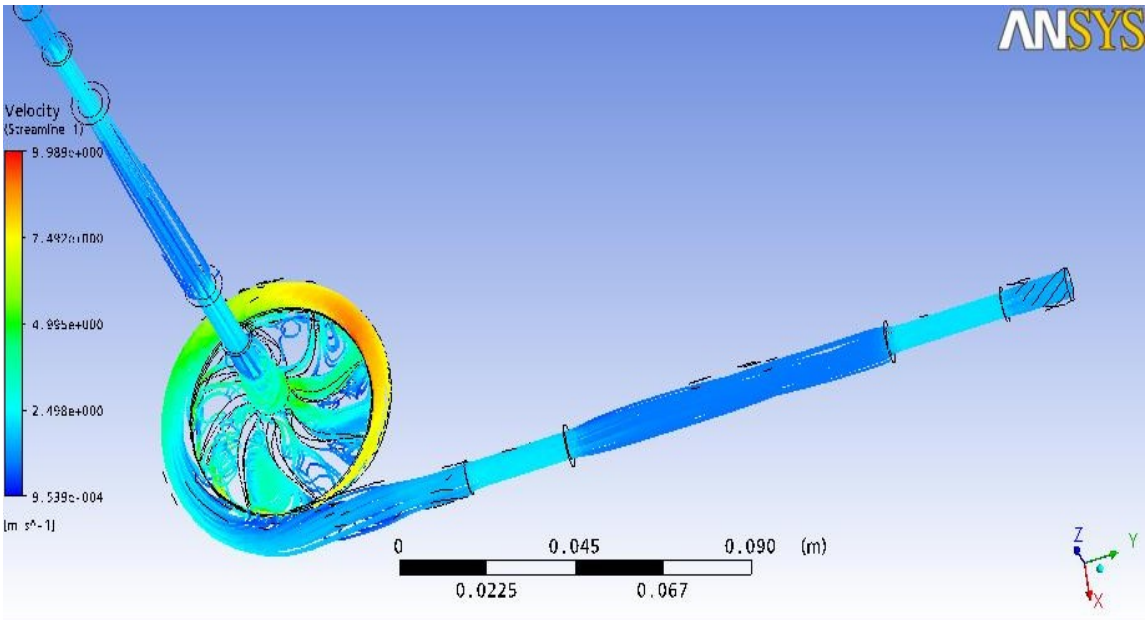

Figure 4.33: Velocity streamlines within the pump at 2750 rpm and 5 liters/min flow rate

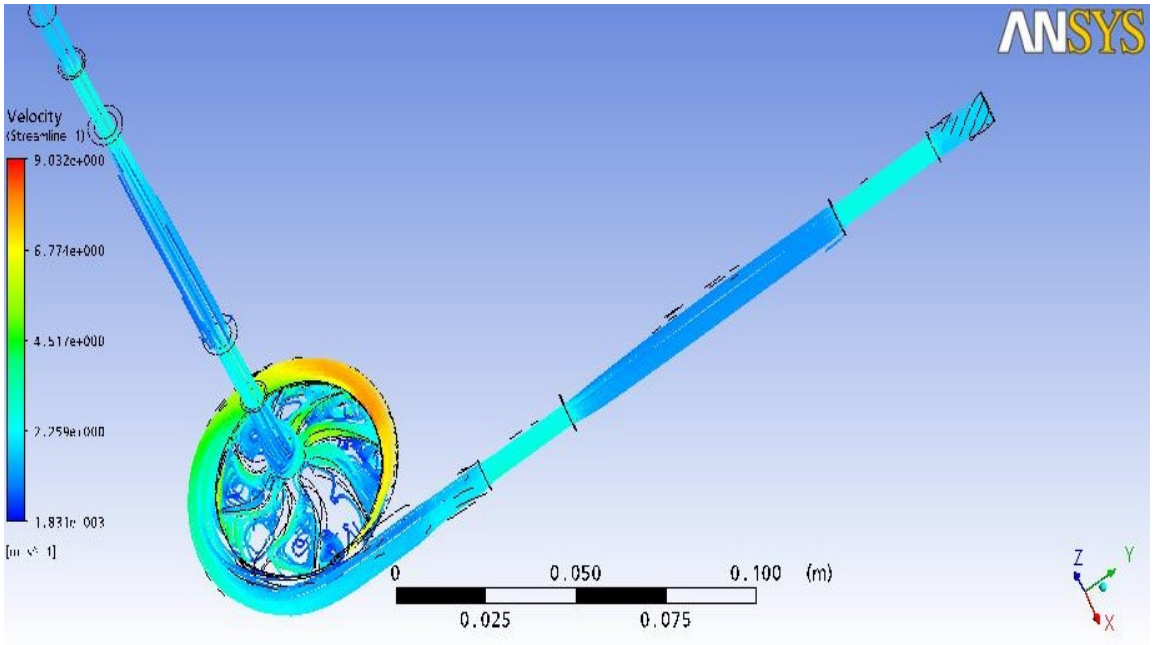

Figure 4.34: Velocity streamlines within the pump at 2998 rpm and 5 liters/min flow rate

In order to be able to see the velocity vectors within the pump, small strings with lengths smaller than the gap between two blades are glued on the pressure side of the blade. A stereoscope is used to see the impeller as non-rotating. The only moving part that is seen is the fluid and so the strings. At each rpm, the experiment was carried out and in all situations the strings were tangent to the blade which shows us that there is not swirl and so much disturbance within the pump. One example from the experiment at 2998 rpm is shown in Figure 4.34.

Figure 4.35: The string experiment at 2998 rpm

Chapter 5

COMPUTER AIDED MANUFACTURING & EXPERIMENTATION OF THE PUMP

5.1 Introduction

Behind the design and Computer Aided Engineering processes, next come the manufacturing process, and the experimental tests of the manufactured pump. This chapter briefly gives information about the manufacturing of all the components (lower and upper casings and the impeller) of the Heart Turcica Centrifugal; the cutting conditions, cutting materials; and the results of the experiments done by the manufactured pumps to obtain the performance curve for each pump. During this thesis study, many prototypes of different Heart Turcica designs were manufactured; and the one selected beyond these designs was manufactured from titanium alloy.

5.2 Computer Aided Manufacturing

Computer Aided Manufacturing (CAM) is a programming tool in which computers send work instructions directly to the machine that will do the manufacturing process. CAM assists engineers and machinists in manufacturing to make 3D models using CAD. Because each of the many manufacturing processes in a CAM system is controlled by the computer, a high degree of precision can be achieved that will not be possible with a human control alone.

Computer Aided Manufacturing is commonly linked to Computer Aided Design systems. The resulting integrated CAD/CAM system takes the computer-generated design, and feeds it directly into the manufacturing system; the design is then converted into multiple computer-controlled processes, such as drilling or turning [43]. The output of the CAM software is a text file, G-code which is the programming language of the numerical control. G-codes are the codes that position the tool and do the actual work and tell the manufacturing machine to perform the process.

In this study, Unigraphics NX-4 is used to perform both CAD and CAM processes. When the CAM module of Unigraphics is used, the first thing to be done is to select the manufacturing type. Commonly, “cavity milling” or “z-level follow core milling” are selected for rough milling process and “contour area milling” for finishing. The tools to be used in the manufacturing process are introduced and selected in the CAM program. Mainly, 5mm and 12 mm end mills are used for rough milling, and 3 mm, 2 mm and 1 mm ball-end mills are used for finish and semi-finish processes during the manufacturing of Heart Turcica. There are so many inputs to be defined for a manufacturing process in the CAM such as; type of the tool, the cut method, step-over, the depth of cut, and the tool path to be defined (see Figure 5.1).

Once all the parameters are entered into the program, the tool path verification must be done and 3D simulation of the whole machining process is done to check if everything is all right and to be sure that there will be no collision between the tool, the tool holder and the work piece. Figures 5.2 and 5.3 show the tool path and 3D simulation of the machining process for the impeller Model 2 during the rough milling process with a 5mm end mill and the tool path and 3D simulation of the machining process for the same impeller during the semi-finish process with a 3 mm ball-end mill.

Figure 5.1: The parameters to be defined for the CAM process

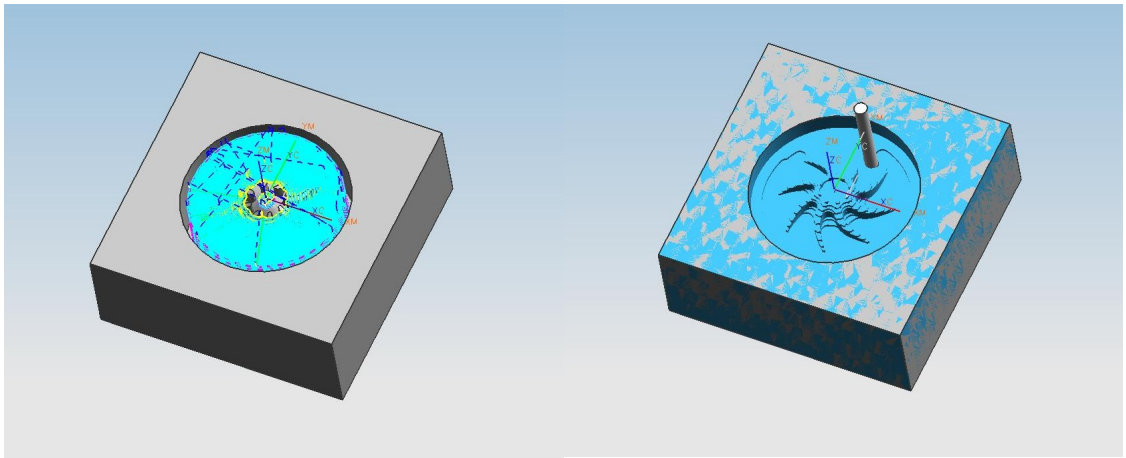

Figure 5.2: Tool path and 3D simulation of the machining process for the impeller Model 2 in the rough milling process with a 5mm end mill

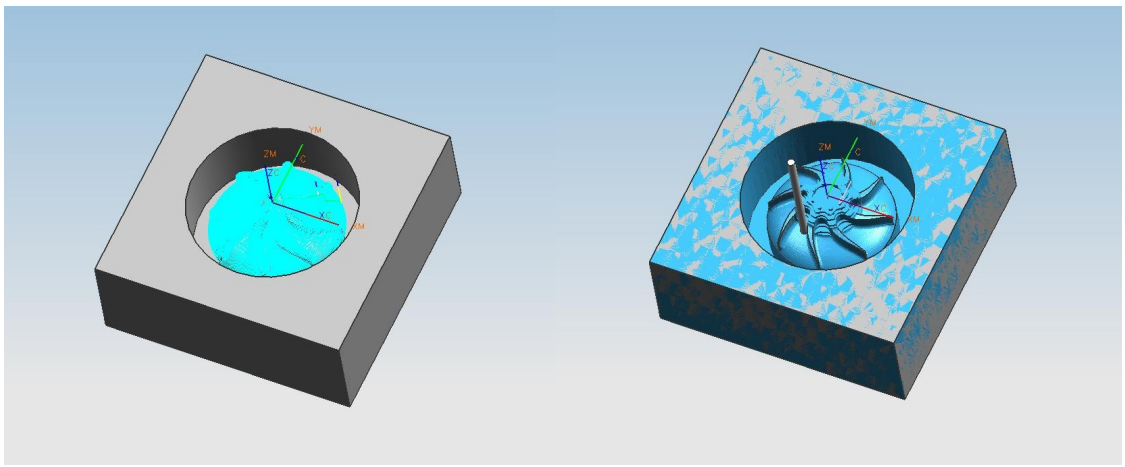

Figure 5.3: Tool path and 3D simulation of the machining process for the impeller Model 2 in the semi-finish milling process with a 3 mm ball-end mill

As the G-codes are obtained from the CAM process, they are transferred to the CNC milling machine and the manufacturing process starts. The machining operations are done on Mazak FJV-200 UHS Vertical Machining Center (VMC) which owns a 25000 rpm spindle motor and ±2.5 micrometers sensitivity (Figure 5.4).

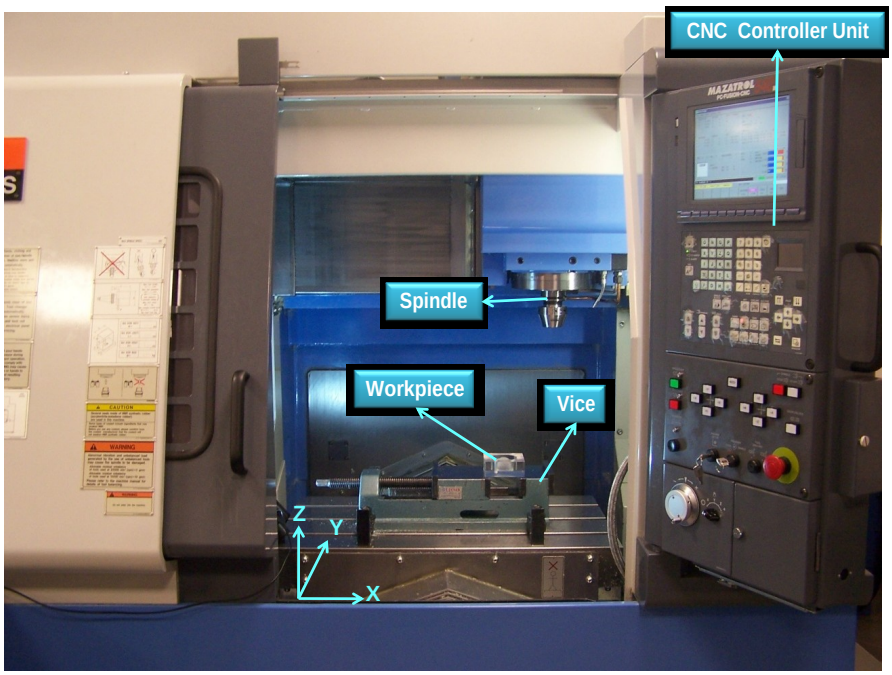

Figure 5.4: Mazak FJV-200 UHS Vertical Machining Center (VMC)

Acrylic glass is used as the raw material for the manufacturing of the prototypes of Heart Turcica because it is easy to process hence takes less time for machining. Moreover, the transparency of epoxy glass gives the chance to observe the flow inside the pump. Rectangular blocks with dimensions of 100 mm x 100 mm x 40 mm are used. Both the lower and upper casings and the impeller are processed through 3 operations: rough milling, semi-finishing and finishing. The spindle speed was set to 10000 rpm for rough milling and the tool was moving with a 1000 mm/min feed rate and for the finishing

operations, the spindle speed was set to 7000 rpm and the tool was moving with a 700 mm/min feed rate.

A detailed literature review is done for selecting the right material for manufacturing Heart Turcica that will be tested with blood and will be used in in-vivo tests. Many researches have been investigated done on the failure of using stainless steel on orthopedic devices. This lead to the result of usage of stainless steel would be impractical [45]. Titanium alloys, mainly Ti-6Al-4V and Ti-6Al-7Nb are mainly used in medical applications because these materials have good corrosion resistance and biocompatibility when used in human body. Ti-6Al-4V alloy is selected as the raw material of Heart Turcica because of its superior biocompatibility.

The dimensions of the raw materials of titanium alloy are: 29 mm x 95 mm x 95 mm rectangular block for upper casing, 8 mm x 95 mm x 95 mm rectangular block for lower casing, Ø 65 mm x 30 mm cylindrical block for impeller (Figure 5.5).

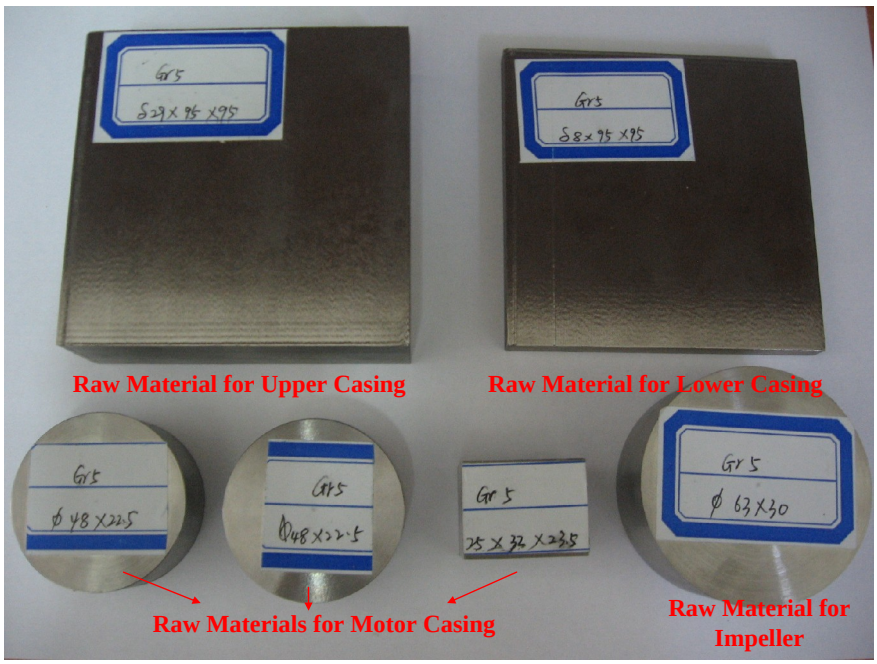

Figure 5.5: The Ram Materials of Titanium Alloy for Heart Turcica

The outer profiles of lower and upper casings are processed by water-jet cutting method. Water jet cutting is a cutting method where metals are sliced and manufactured by means of a jet of water and an abrasive material mixture at high pressure and high velocity. The water jet system can be clearly seen in Figure 5.6.

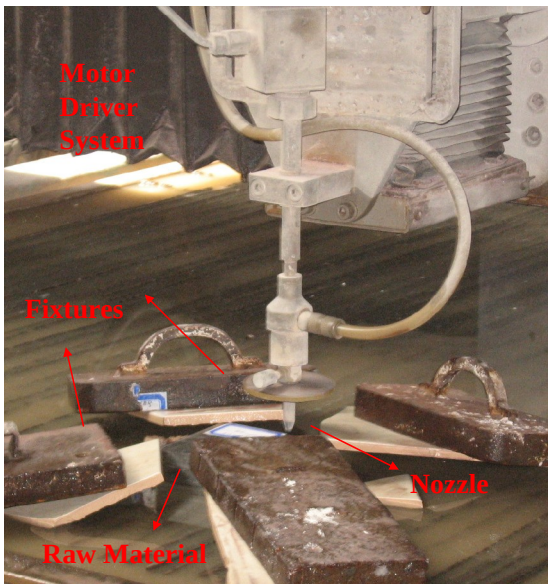

Figure 5.6: The processing of outer profile of the lower casing by a water-jet

Figure 5.7: The outer profile of lower casing processed by a water-jet

The machining of titanium is considerably harder than acrylic glass, so the spindle speed and the feed rates must be different from the previous values. The cutting parameters used for cutting titanium are shown briefly in Table 5.1.

	IMPELLER		
Operation Type	*Rough*	*Semi-finish*	*Finish*
Tool Type	End-mill	Ball end-mill	Ball end-mill
Tool Diameter [mm]	5	3	1
Number of Flutes	2	2	2
Spindle Speed [rpm]	3000	3000	5000
Feed Rate [mm/min]	75	50	100
Feed per Tooth [mm/rev]	0,0125	0,0083	0,01
Depth of Cut [mm]	0.5	0,1	0,05
Stepover [mm]	0,5	0,1	0,01
	LOWER CASING		
Operation Type	*Rough*	*Semi-finish*	*Finish*
Tool Type	End-mill	Ball end-mill	Ball end-mill
Tool Diameter [mm]	5	3	2
Number of Flutes	2	2	2
Spindle Speed [rpm]	5000	6000	7000
Feed Rate [mm/min]	100	100	150
Feed per Tooth [mm/rev]	0,01	0,0083	0,0107
Depth of Cut [mm]	0,5	0,1	0,05
Stepover [mm]	0,5	0,1	0,05
	UPPER CASING		
Operation Type	*Rough*	*Semi-finish*	*Finish*
Tool Type	End-mill	Ball end-mill	Ball end-mill
Tool Diameter [mm]	12	3	2
Number of Flutes	4	2	2
Spindle Speed [rpm]	2000	6000	7000
Feed Rate [mm/min]	60	150	200
Feed per Tooth [mm/rev]	0.0075	0,0125	0,014
Depth of Cut [mm]	0,7	0,1	0,05
Stepover [mm]	1,2	0,1	0,05

Table 5.1: The cutting parameters of TiAl6V4 alloy

5.3 Experimental Setup

All the parts are assembled together by using bolts and nuts for connecting the upper and lower casings after the manufacturing of the prototype of Heart Turcica is completed. The impeller sits on the shaft by means of a miniature ball bearing with 3 mm inside diameter. The experimental setup is shown in Figure 5.8.

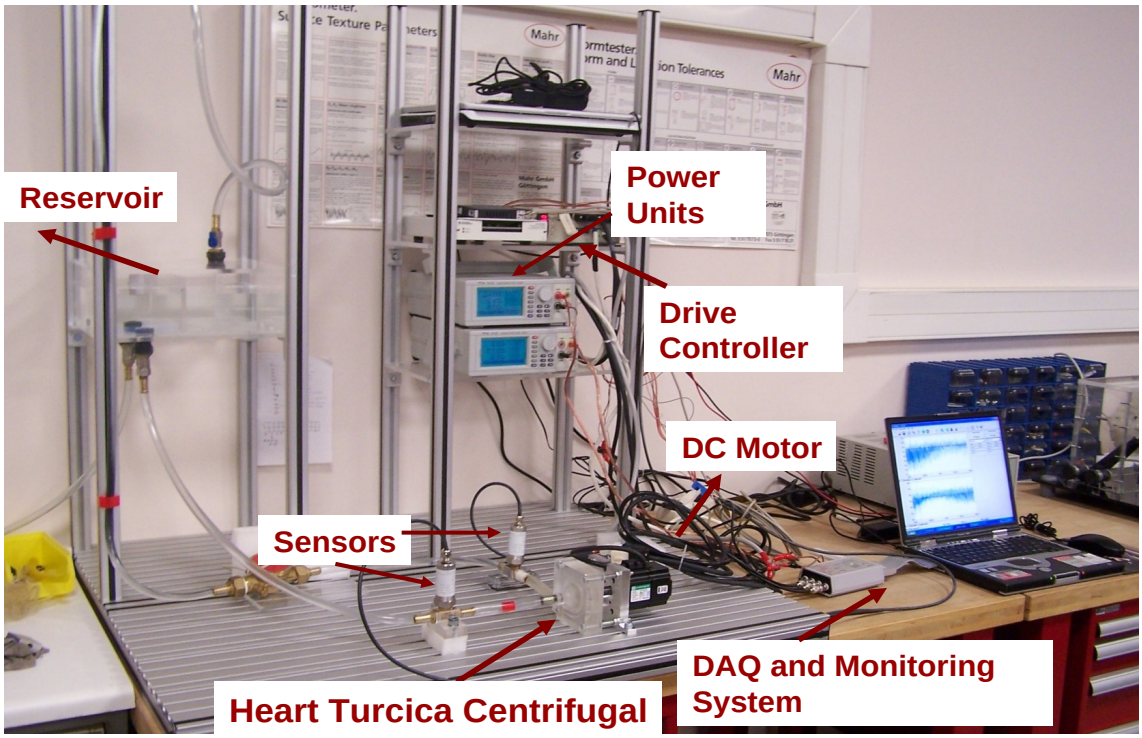

Figure 5.8: The experimental set-up

The characteristic of a pump is investigated by its performance curve; which shows the change of pressure difference across the pump versus the flow rate. In order to measure the pressure, there are 2 pressure sensors in the setup; one located at the inlet of the pump, the other one located at the exit of the pump. The pressure difference across the pump is

calculated by subtracting the measured inlet pressure from the measured exit pressure value. Sensitivities of the sensors are 15.001 mmHg/mV for the inlet pressure sensor and 37.503 mmHg/mV for the outlet pressure sensor. The data from these sensors is collected at the computer by using a data acquisition card via CutPRO software. There are some parameters to be given for this software, such as the sampling rate, number of samples, the sensitivities of the sensor. The output screen of CutPRO is shown in Figure 5.9. The pump is driven by a 100 watt DC motor. Maximum 3000 rpm of rotational speed can be achieved with this motor. The size of the actuator is not a big deal for the experiments, but in reality, it is obvious that this motor cannot be used in the body. For real applications, a brushless 50 watt micro motor which has a 45 mm diameter will be used. The picture of the micro motor to be used is shown in Figure 5.10.

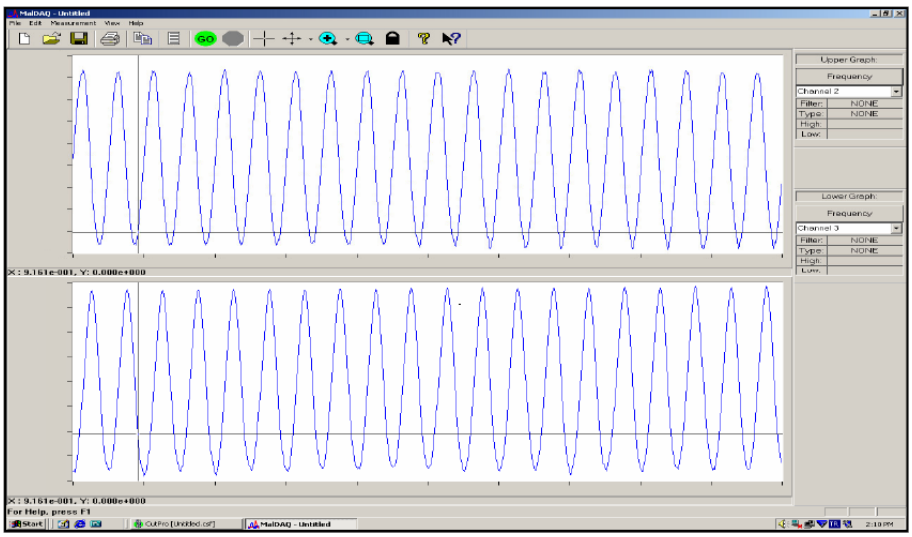

Figure 5.9: The output screen of CutPRO

The motor drives the centrifugal pump by means of neodium magnets embedded at the end of the impeller. The same type magnets are also embedded on a disk replaced on top of the motor shaft. The magnets are arranged in a row such that the north pole of the magnet is

near the south pole so that the risk of missing poles is minimized. The magnetic force between two particles is reversely proportional to the fourth power of the distance between particles. For this reason, the distance between the disk on top of the motor shaft and the lower casing of the pump is essentially kept lower than 0.5 mm. Moreover, the distance between the back of the impeller and the back of the lower casing is important, but it cannot be so thin because it can be torn and broken. After several trials, it has been observed that 0.5 mm distance between the impeller and the back of the lower casing is ideal. At first, 8 magnets have been used but as the performance of the pump increases, the flow rate also increases and so this causes a larger friction force and creates a larger torque. Using 16 magnets in stead of 8 solved this problem.

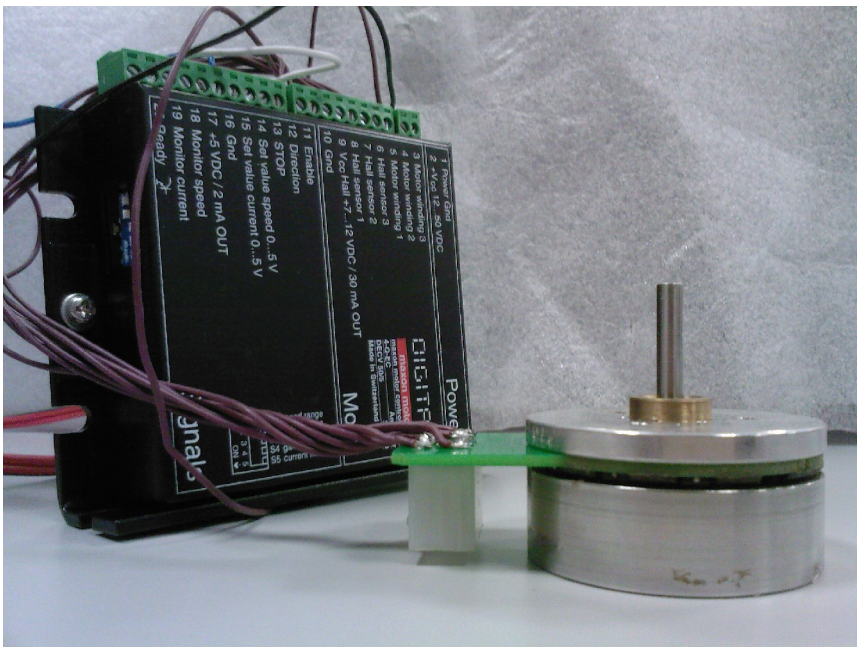

Figure 5.10: The brushless Φ 45 mm flat micro motor

5.4 Results of In-Vitro Experiments done with Water

Before the motor begins to rotate and actuates the system, the vane connected to reservoir is opened and the pump and all of the pipes are filled with water. The most essential thing before starting the experiment is to be sure that there will be no air trapped inside the pump and vanes. The water flow is disturbed very much with the air trapped inside, so all the air is taken out of the system. When there is no air inside the system, the motor starts to rotate slowly. The rotational speed is set to a specific value and different measurements are done at different flow rates. The performance curve at a specific rotational speed is obtained by this way. The collected data via CutPRO is processed in Matlab and the graph; pressure difference versus time is drawn in Matlab as in Figure 5.11.

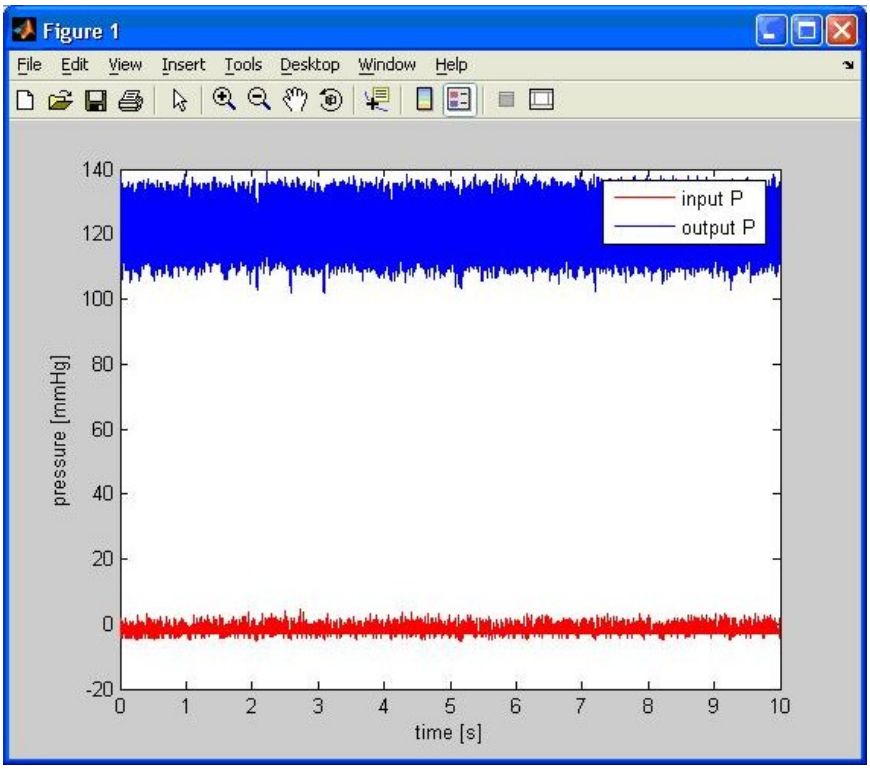

Figure 5.11: The pressure vs. time graph; obtained from the data of pressure sensors

For model 2, 8 different rotational speeds were set: 1502 rpm, 2002 rpm, 2252 rpm, 2501 rpm, 2751 rpm, 2751 rpm, 2800 rpm, 2900 rpm and 2998 rpm. Measurements smaller than 1500 rpm were not tried because this not a pediatric pump, so it will not meet the needs of a normal heart. The performance curve of Model 2 can be seen in Figure 5.12.

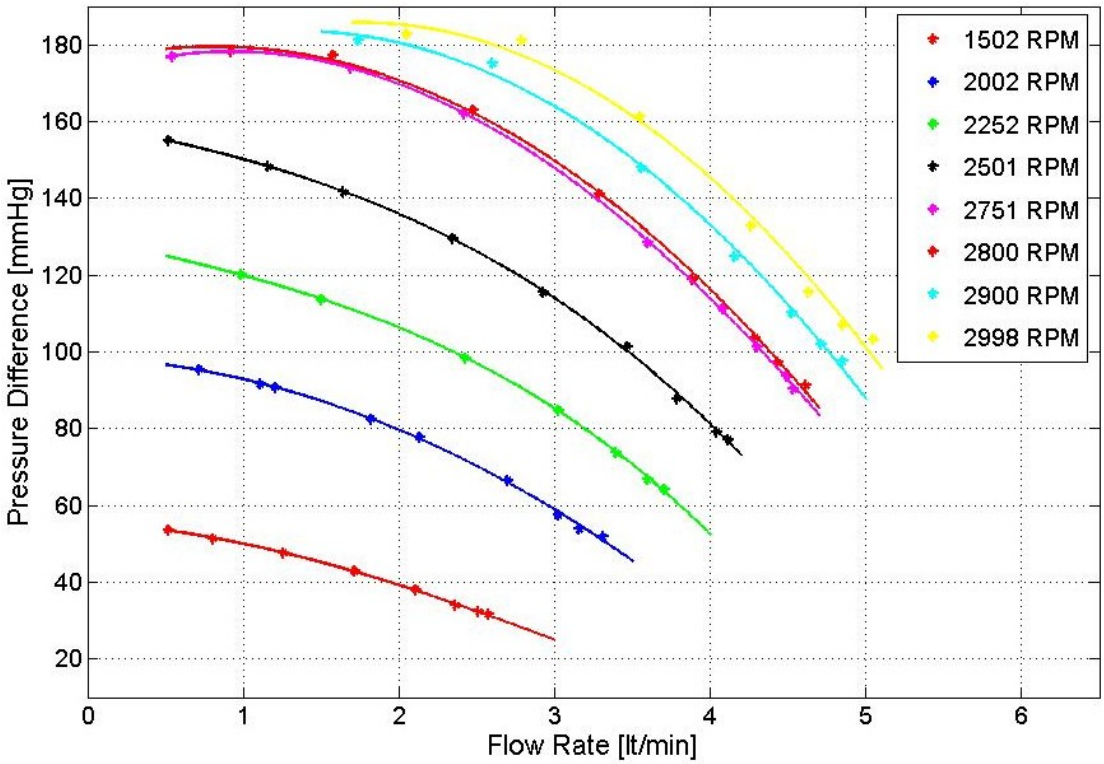

Figure 5.12: The performance curve of Pump Model 2

It is clearly seen that this pump gives satisfactory results, as it achieves the main objective because at rotational speeds higher than 2500 rpm, it reaches a pressure difference of 100 mmHg and a flow rate of 4.5 liters/min.

Figure 5.13 shows the comparison of experimental data with the simulation results. Experimental data fit well with the simulation values.

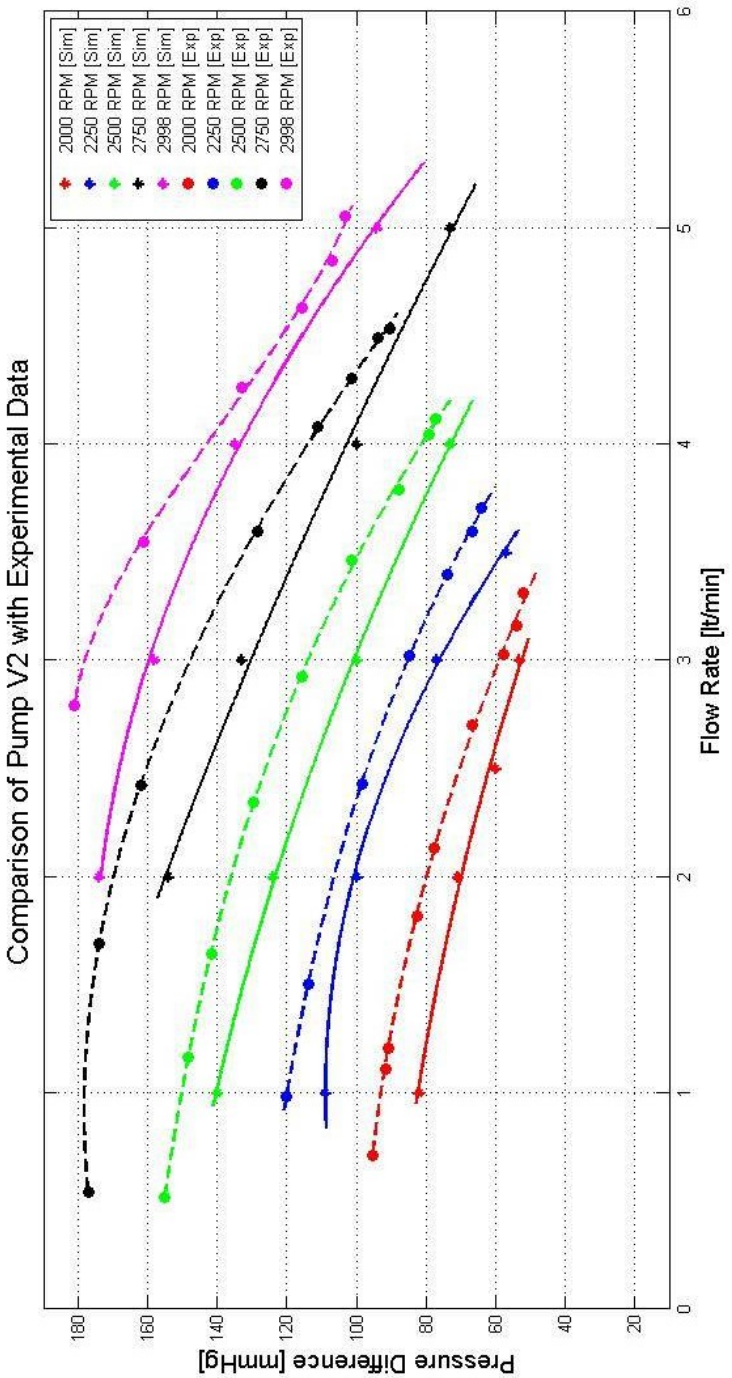

Figure 5.13: Comparison and validation of experimental data of Pump Model 2 with the simulation data

As described in Chapter 4, the hub height of the pump model 2 is reduced to 8 mm from 14 mm to investigate the effect of a smaller inside volume of the pump. Figure 5.14 shows the performance of the modified pump model 2. The comparison of the pumps with hub heights 8 and 14 mm are seen in Figure 5.15.

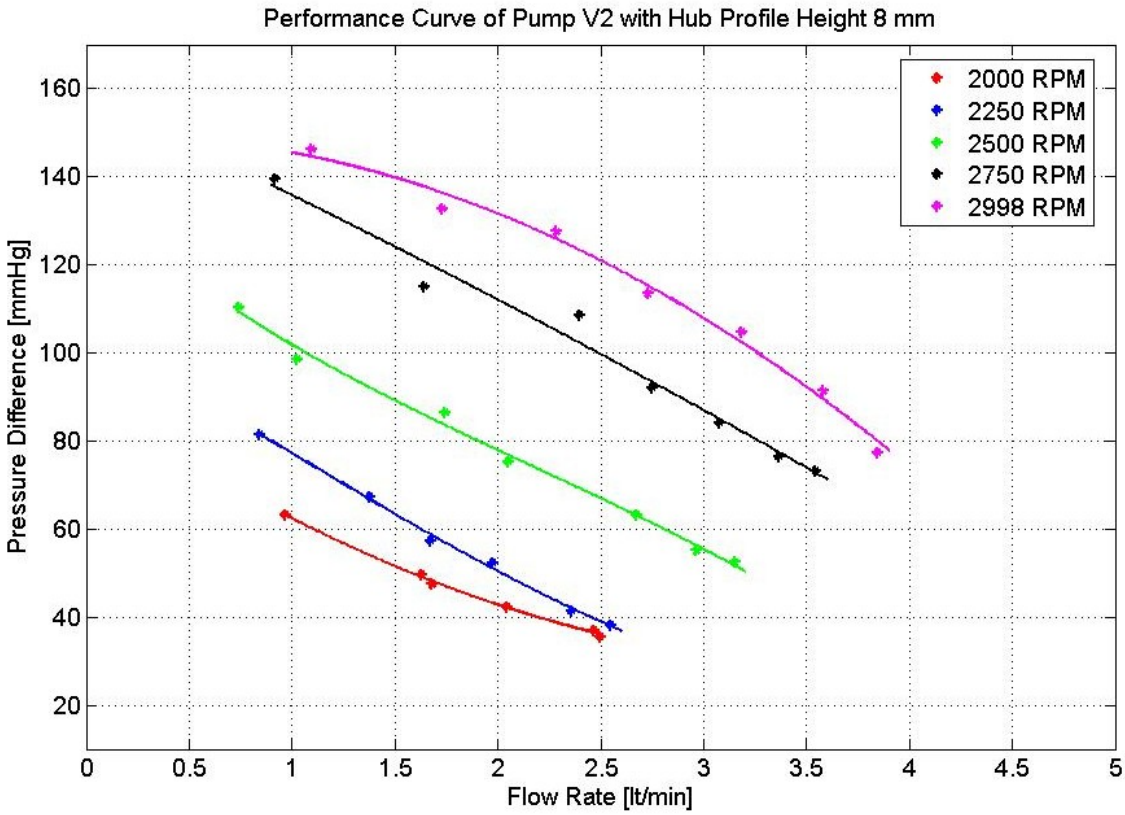

Figure 5.14: The performance curve of Pump model 2 with a hub height of 8 mm

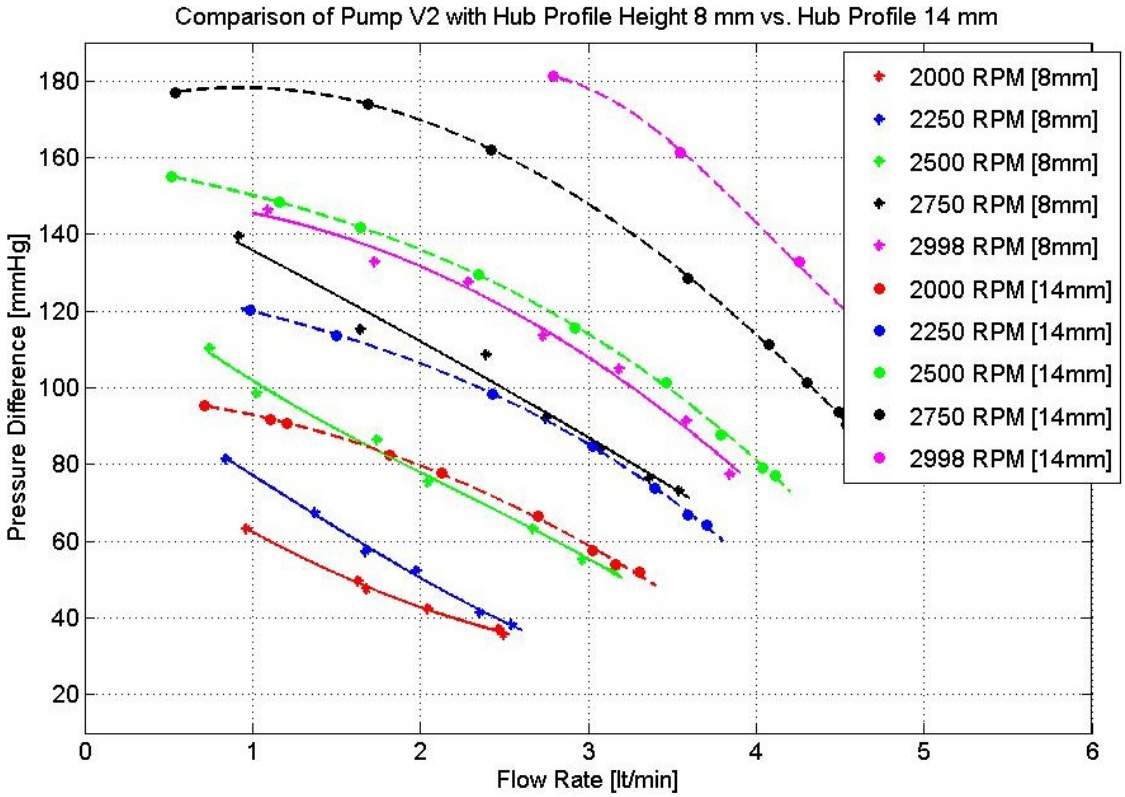

Figure 5.15: The comparison of performance curves of pumps with hub heights of 8 mm and 14 mm

From the comparison graph, it can be observed that the pump with a higher profile height is better than the pump with a hub profile height of 8 mm in terms of performance. This is directly proportional to the volume of the fluid that enters into the pump. When the hub height is 8 mm, less fluid enters the pump; hence less flow rate is achieved. This decreases the pressure at the exit of the pump. This is the result to the question why the pump with 14 mm hub height is preferable to the pump with 8 mm hub height.

If decreasing the volume inside the pump decreases the performance, then increasing the volume will increase to. The hub profile cannot be increased much because it is at the optimum value to be replaceable in human body. Instead, the height of the blades of Model 13 is doubled. Model 13 is selected because it is the pump that achieves best performance. The experimental results for Model 13 with blade height doubled is shown in Figure 5.16. Figure 5.17 shows the comparison graph of experimental data of Model 13 with 5 mm blade height and 10 mm blade height.

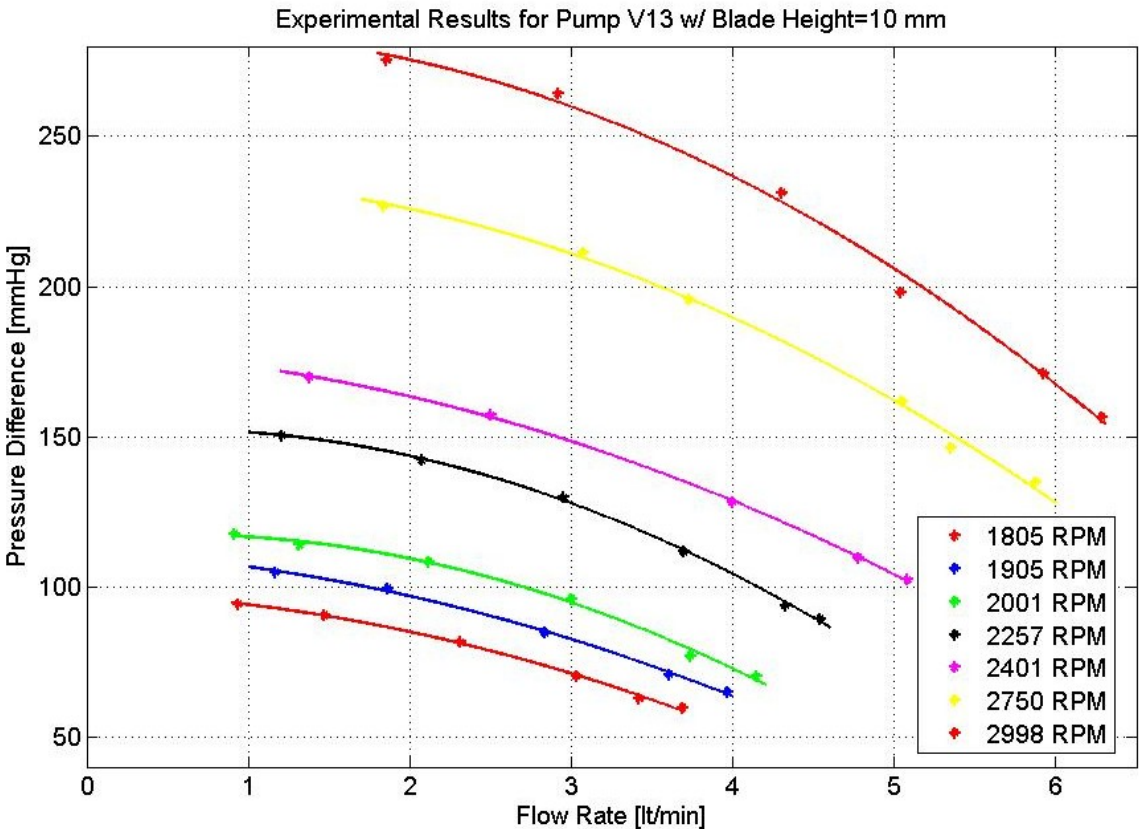

Figure 5.16: The performance curve of pump V13 with blade height 10 mm

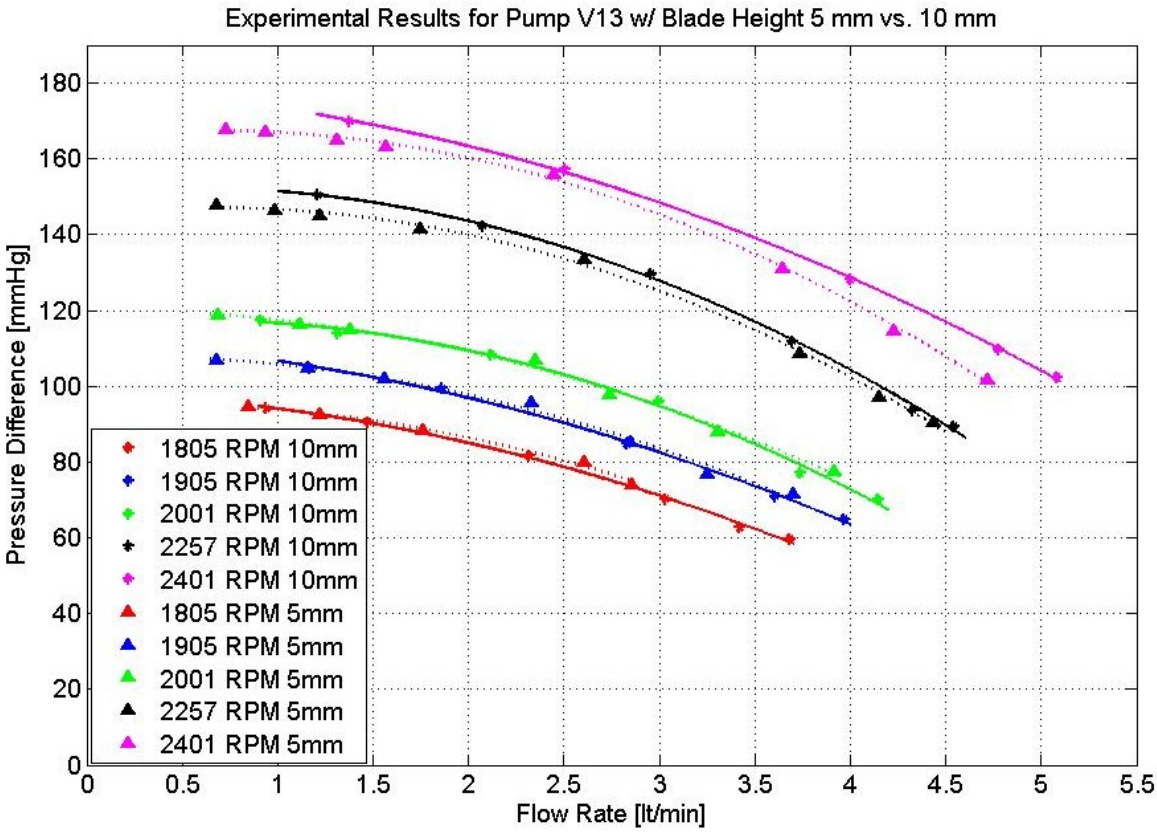

Figure 5.17: The comparison of performance curves of pump V13 with blade heights of 5 mm and 10 mm

There is not so much significant difference between the experimental data of Model 13 with blade height 5 mm and blade height 10 mm. But, it is obvious in the comparison graph that higher flow rates are achieved across the pump with bigger blade height.

The final design is made to analyze the effect of blades with hydrofoil shaped and constant thickness on the performance of the pump. Model 13 is selected to be re-designed. The comparison of pumps with hydrofoil shaped and constant thickness blades and the older version is shown in Figure 5.18.

Model 13 with constant blade thickness is better in terms of performance than the pump with variable blade thickness. Therefore, the pump with constant blade thickness achieves to replace a normal heart because at the rotational speeds higher than 2000 rpm, this pump can achieve a flow rate 4.5 liters/min with a pressure difference of higher than 100 mmHg. This pump is selected to be manufactured from titanium because it can provide the design condition of a LVAD and it is considerably lighter than the other pump. Having a smaller mass is important for a LVAD because the human can comfortably carry a pump up to 300-350 grams.

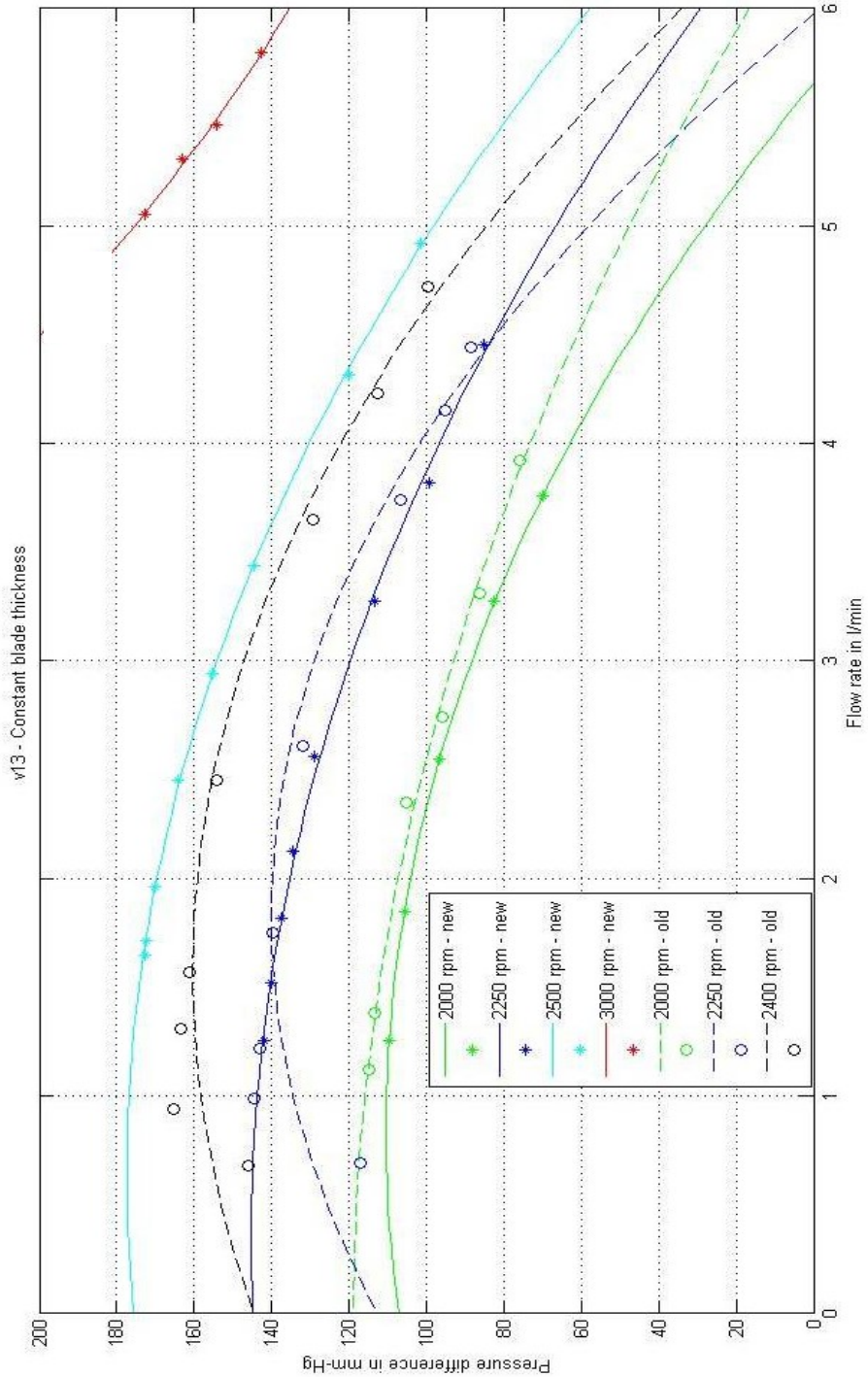

Figure 5.18: The comparison of performance curves of pump V13 with variable blade thickness (old) and constant blade thickness (new)

5.5 In-Vitro Experiments done with Glycerin Solution

Up to this point, all of the in-vitro experiments have been carried out by using water as the fluid passing through the pump. However, in actual case, the fluid passing through the pump is the blood. The main property that characterizes the flow of a fluid is its viscosity, which can be defined as the quantity describing the resistance of the fluid to flow. Viscosity is the most important thing to be considered when any measurement of flow of fluids is made.

As blood and water are different fluids, their viscosities are different. Blood is a shear thinning (which means viscosity decreases with increasing rate of shear), viscoelastic fluid (Cokelet 1987) that is often taken as Newtonian at sufficiently high shear rates (above 500 s^{*1}) [46]. Newtonian fluids flow regardless of the forces acting on it. The relative volume of red blood cells mostly affects the magnitude and relative importance of the viscous and elastic components of the complex viscosity. The kinematic viscosity for blood can often be estimated as 3.5 centistokes (cs), which is equivalent to approximately 4.2 centipoises (cP) [46]. In stead of using blood for visualizing the flow and measuring the pressure and flow rate, using fluids analogous to blood would be more practical.

The Brookfield DV-II+ programmable viscometer is used to measure the viscosity of the glycerin-water mixture. The viscosity experiment set-up is shown in Figure 5.19. On the screen of the viscometer, continuous display of viscosity (cP or mPa·s), temperature (°C or °F), shear Rate, shear Stress, % torque, and spindle speed is seen (Figure 5.20). The data collection and historical comparison of data is done by using Wingather software.

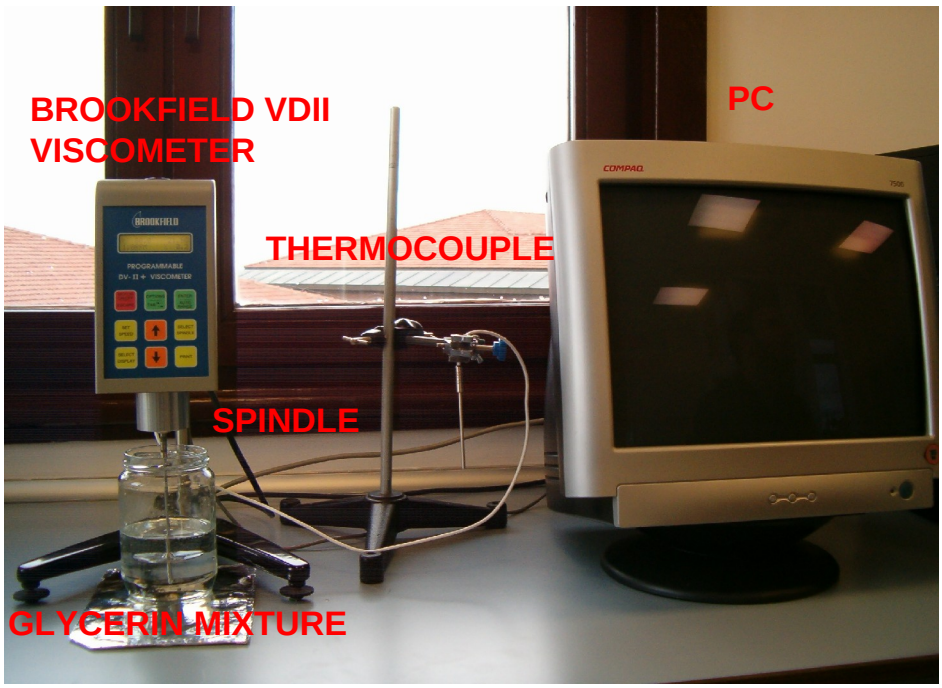

Figure 5.19: The Viscosity Experiment Set-Up

Figure 5.20: The Viscosity Experiment Set-Up Display

In order to be sure that accurate results will be obtained at the end of measurements, the experiments are decided to start by measuring the viscosity of pure glycerin. 300 ml of glycerin is used without adding any water. On the screen of viscometer, two different values are read for the viscosity; one for the lower value of viscosity, the other for the upper value of the viscosity. The viscosity of the mixture is a value between these upper and lower values. As post-processing, the graphs of lower and upper viscosities are drawn for each measurement. The average of these values is taken, and another graph is drawn showing the average value of the viscosity at that measurement conditions. In the tables for each measurement, both the lower and upper values of viscosity can be read.

The values obtained by the measurements can be seen in the following table and graph:

Spindle Speed (rpm)	***Viscosity (cP)***	***Torque (%)***	***Temperature ©***
0,5	880-960	1,1	20,8
1	920-980	2,3	20,8
2	920-940	4,6	20.9-21
2,5	928-944	5,8	21.0-21.1
4	920-930	9,3	21.0-21.2
5	920-928	11.5-11.6	21.1-21.2
10	920-924	23.0-23.1	21.1-21.2
20	924-926	46.2-46.3	21.0-21.1
50	EEE	EEE	EEE

Table 5.2: Measurement Data for 100% Glycerin Solution

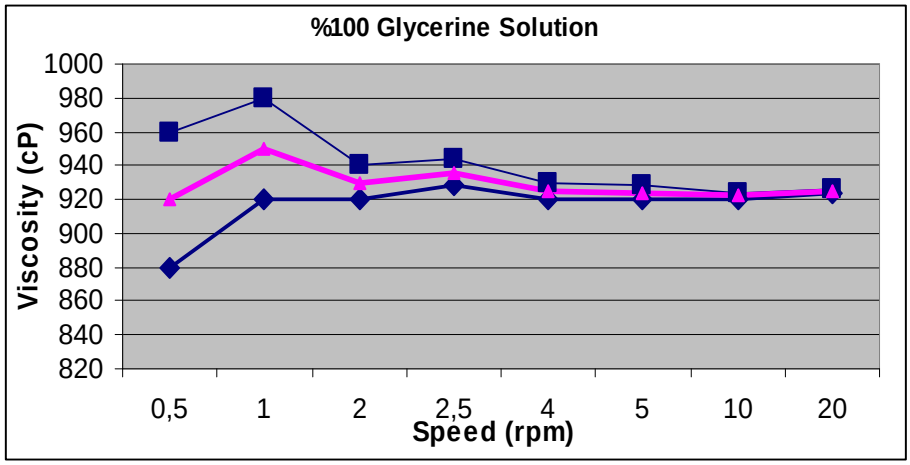

Figure 5.21: Viscosity vs. Spindle Speed Graph for 100% Glycerin Solution

Once the viscosity of pure glycerin is measured, water is added in the glycerin in order to achieve 60% glycerin solution in volume. The experiments have started by measuring the viscosity of 60% solution. Water is added and left to mix for about an hour. Hıowever, homogenous solution could not be obtained, because it is impossible to achieve perfect dilution. Dilution of water in glycerin also increases as time passes, so after waiting for an hour for water to mix with glycerin, experiments start over immediately. Lots of bubbles occur because of the heterogeneous solution. As the speed of the spindle increases, there exits more bubbles on the spindle. Moreover, so much run-out is observed on the spindle, which makes us to make the measurements at spindle speed of not more than 100 rpm. One more reason for not working more than 100 rpm is that boundary layer occurs at higher speeds at the surface of the spindle, which leads to turbulence flow.

Table 5.3 and the Figure 5.22 show the results of viscosity measurement of 60% glycerin solution, which consists of 12 ml of glycerin and 8 ml of water.

Spindle Speed (rpm)	*Viscosity (cP)*	*Torque (%)*	*Temperature ©*
0,5	115-192	0.8-1.3	21.6-21.7
1	64-128	1.3-1.7	21,7
2	19.2-35.2	0.6-1.1	21,7
2,5	15.4-28.2	0.6-1.1	21,7
4	16-19.6	1-1.2	21.6-21.7
5	11.5-15.4	0.9-1.2	21.7-21.8
10	10.9-12.2	1.7-2	21.7-21.8
20	10.6-11.2	3.3-3.5	21.7-21.8
50	10.6-10.9	8.4-8.5	21.6-21.7
100	10.8-10.9	16.9-17.1	21,7

Table 5.3: Measurement Data for 60% Glycerin Solution

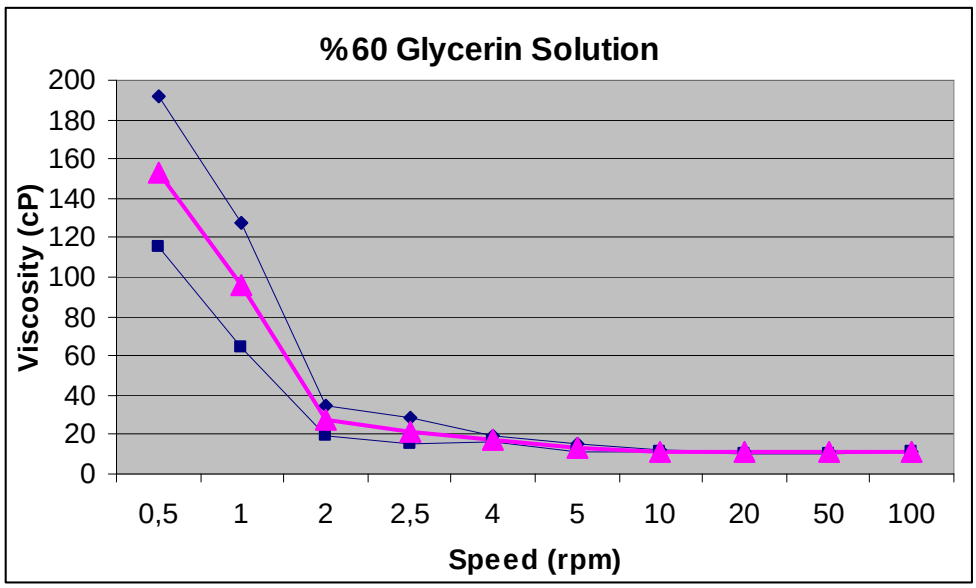

Figure 5.22: Viscosity vs. Spindle Speed Graph for 60% Glycerin Solution

In literature the actual value of 60% glycerin solution is given as 10.8 cP. It is seen from the results of the measurements that the viscosity of the solution is nearly 10.9 cP.

After this step, 50% glycerin mixture is prepared by adding 4 ml more water on the previous solution. The following are the results of 50% glycerin mixture:

Spindle Speed (rpm)	*Viscosity (cP)*	*Torque (%)*	*Temperature ©*
0,5	102.4-140.8	0.8-1.2	21.7-21.8
1	57.6-76.8	0.8-1.2	21,7
2	25.6-48	0.9-1.5	21,8
2,5	20.5-43.5	0.8-1.7	21.8-21.9
4	12.8-17.6	0.8-1.1	21,8
5	8.96-14.1	0.7-1.1	22-22.1
10	7.04-8.96	1.1-1.4	22.1-22.2
20	6.72-7.04	2.1-2.3	22,1
50	6.27-6.53	4.9-5.1	22,1
100	6.40-6.46	10-10.1	22,2

Table 5.4: Measurement Data for 50% Glycerin Solution

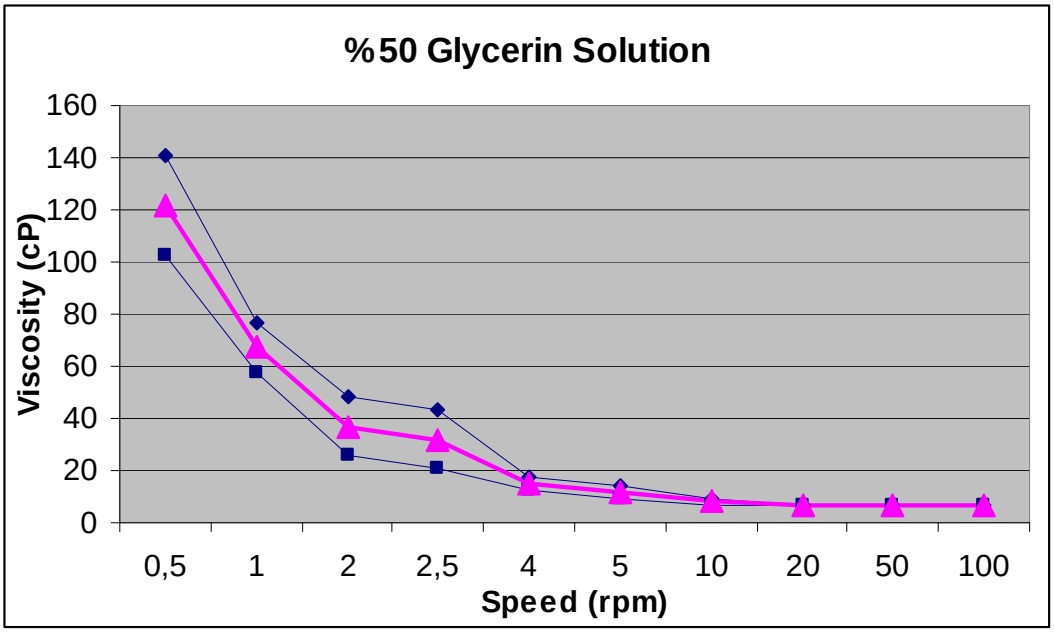

Figure 5.23: Viscosity vs. Spindle Speed Graph for 50% Glycerin Solution

In literature the actual value of 50% glycerin solution is given as 6.4 cP. It is seen from the results of the measurements that the viscosity of the solution is nearly 6.5 cP.

Next comes the preparation of 40% glycerin mixture by adding 6 ml more water on the previous solution. The following are the results of 40% glycerin mixture:

Spindle Speed (rpm)	***Viscosity (cP)***	***Torque (%)***	***Temperature ©***
0,5	89.6-153.6	0.8-1.2	22.1-22.2
1	64-89.6	1.0-1.4	22.1-22.2
2	38.4-60.8	1.2-1.8	22,1
2,5	30.7-53.6	1.1-2.1	22,1
4	11.2-22.6	0.7-1.6	22,1
5	7.68-21.8	0.6-1.7	22.0-22.1
10	5.76-8.32	0.9-1.4	22,1
20	4.80-5.44	1.4-1.7	22.0-22.1
50	4.10-4.35	3.2-3.5	22.0-22.1
100	4.16-4.22	6.5-6.6	22.0-22.1

Table 5.5: Measurement Data for 40% Glycerin Solution

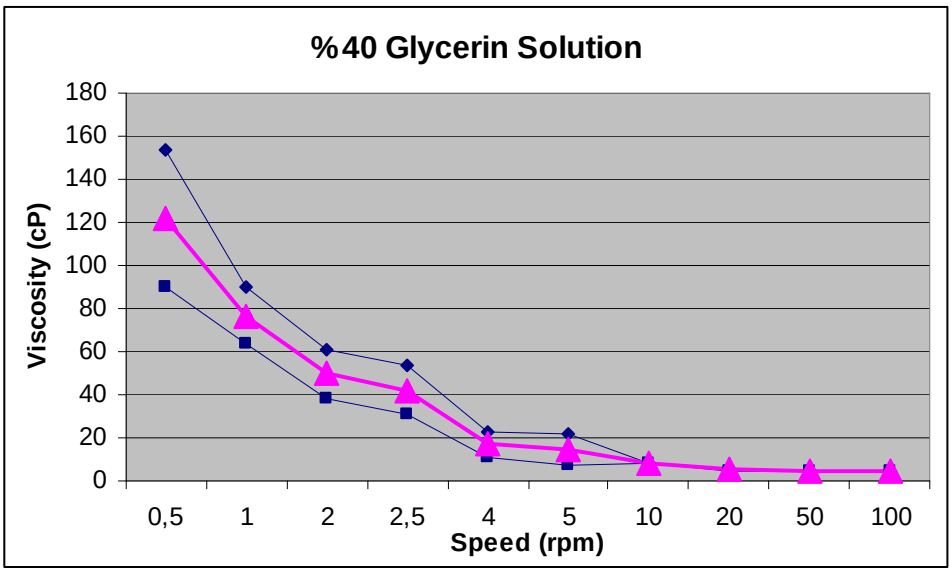

Figure 5.24: Viscosity vs. Spindle Speed Graph for 40% Glycerin Solution

40% glycerin solution with water can be used as the fluid analogous to blood because it nearly has the same viscosity with blood.

Once the fluid analogous to the blood is prepared, the experiments done with water are repeated by using glycerin-water mixture. Experiments are repeated again for pumps Model 13 and Model 14 with glycerin solution. Figures 5.25, 5.26, 5.27 and 5.28 show the performance curve of pump Model 13 and Model 14 for the experiments done by using glycerin-water mixture and the comparisons of experiments done with glycerin and done with water.

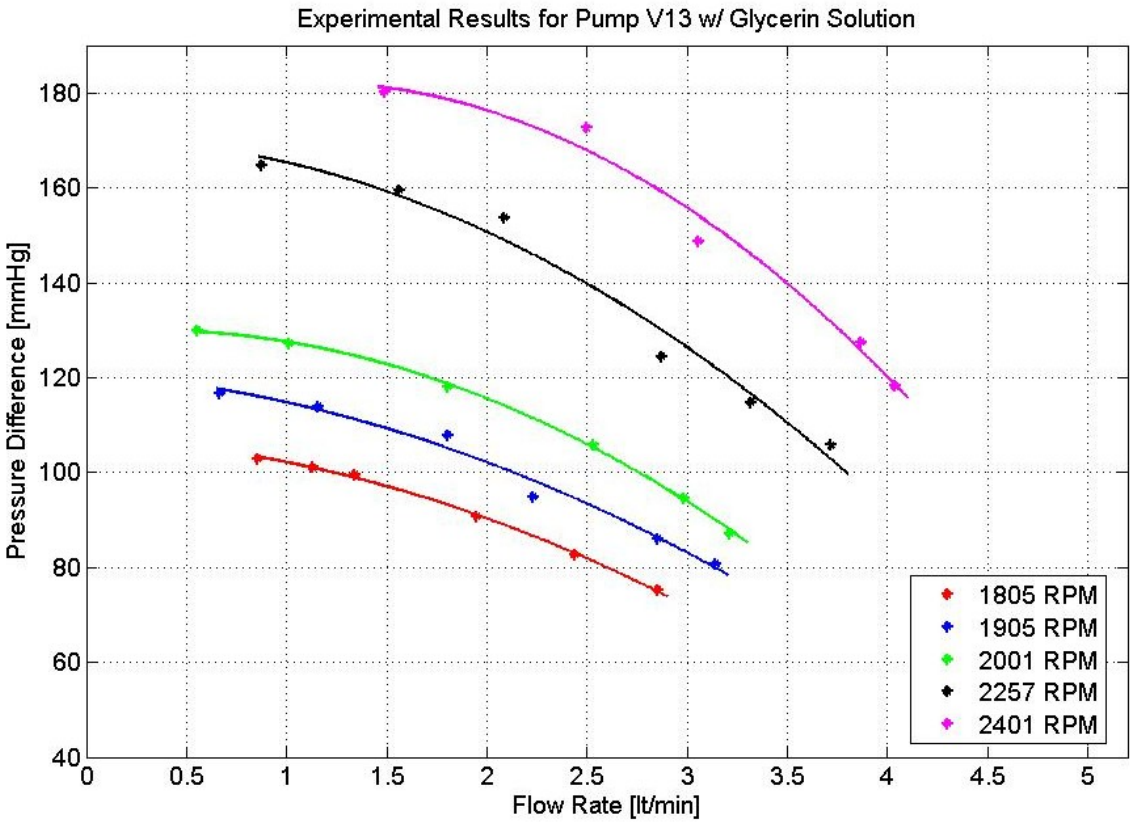

Figure 5.25: The performance curve of Model 13 for the experiments done with glycerin solution

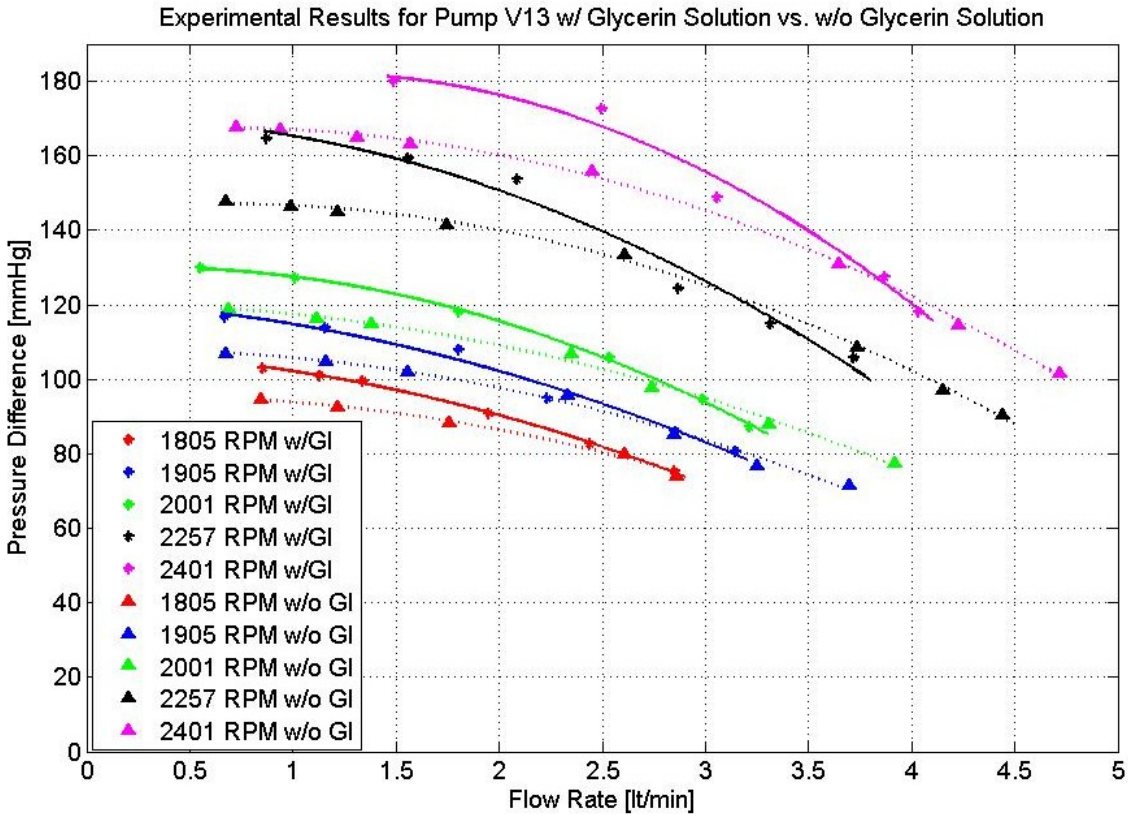

Figure 5.26: The comparison of experimental data of Model 13 for the experiments done with glycerin solution and with water

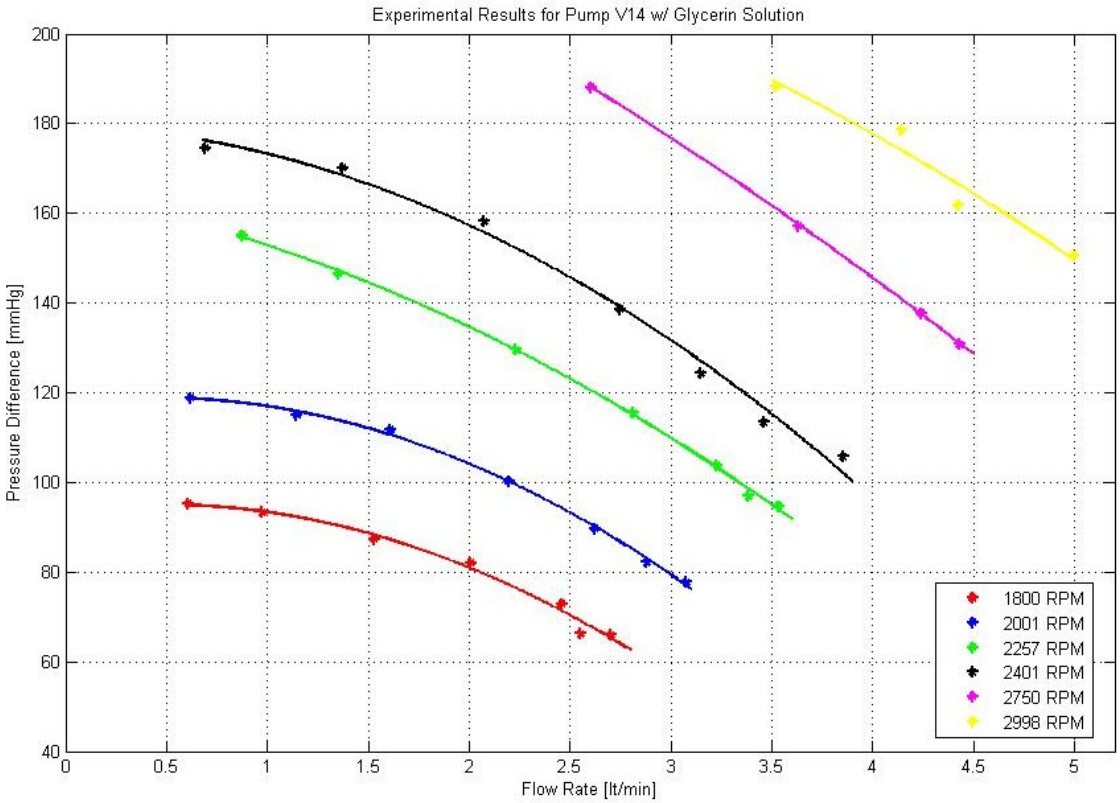

Figure 5.27: The performance curve of Model 14 for the experiments done with glycerin solution

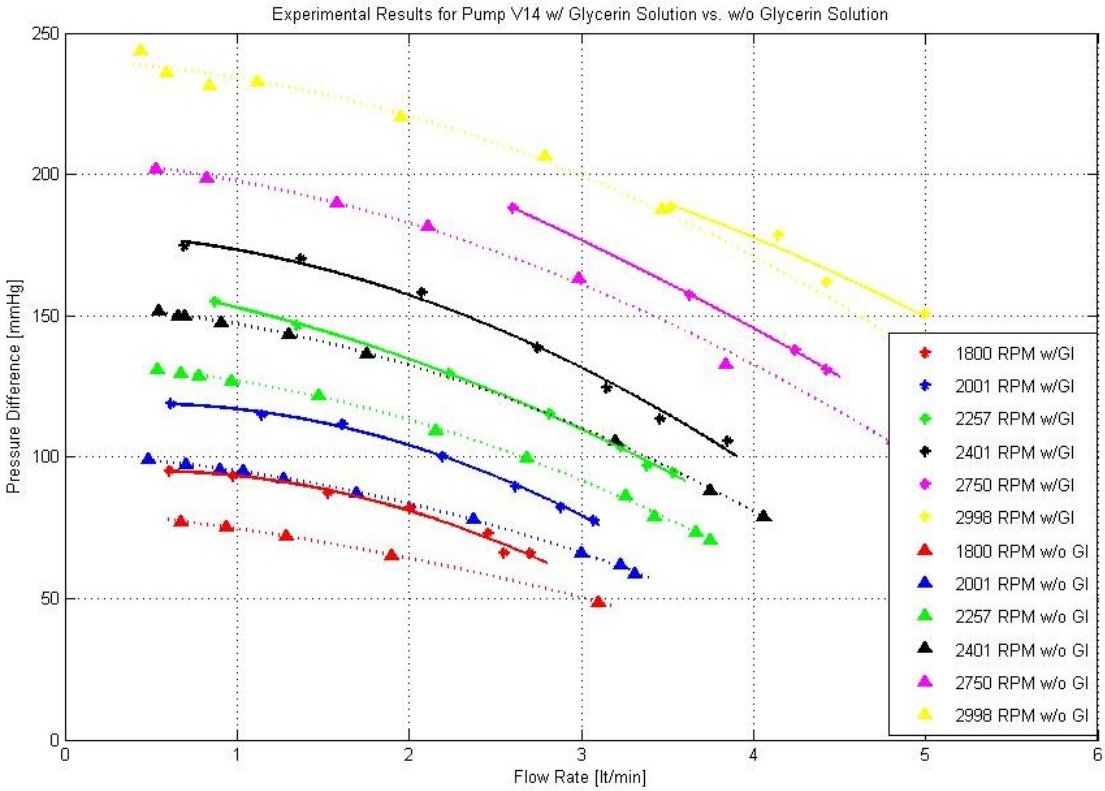

Figure 5.28: The comparison of experimental data of Model 14 for the experiments done with glycerin solution and with water

The pressure values do not change much regarding for the viscosity of fluid, there is not much significant difference between pressure values but higher pressure is obtained when the fluid is the glycerin-water solution. When it comes to compare the flow rates, it is obviously seen that there is approximately 15-20 % decrease with respect to the experiments done with water. This is expected because the viscosity is higher in this case and higher viscosity means there is a higher resistance shown to flow.

5.6 In-Vitro Experiments with Blood

Pump Model 13 with hydrofoil shaped blades that have constant blade thickness is selected to be manufactured from titanium to be used in in-vitro tests by blood and in-vivo tests in an animal. The pump has to be re-designed because the previous model has been designed for the prototype and consists of excess material that will cause the pump to be heavier and sharp edges that is unacceptable for implanting the pump in human body. In order to decrease the height at the back side of impeller, which is 10 mm because of the 8 mm height magnets used, smaller magnets are used. These magnets have diameters of 4 mm and heights of 4 mm. 1.5 mm parts of the magnets are embedded in to the shroud and the height of the back side of the impeller becomes 2.5 mm. This decreases the mass of the total assembly much because the volume of titanium cylinder with 48.3 mm diameter and 7.5 mm is removed, which means approximately 65 grams of excess material is eliminated. The final design of the impeller is shown in Figure 5.29.

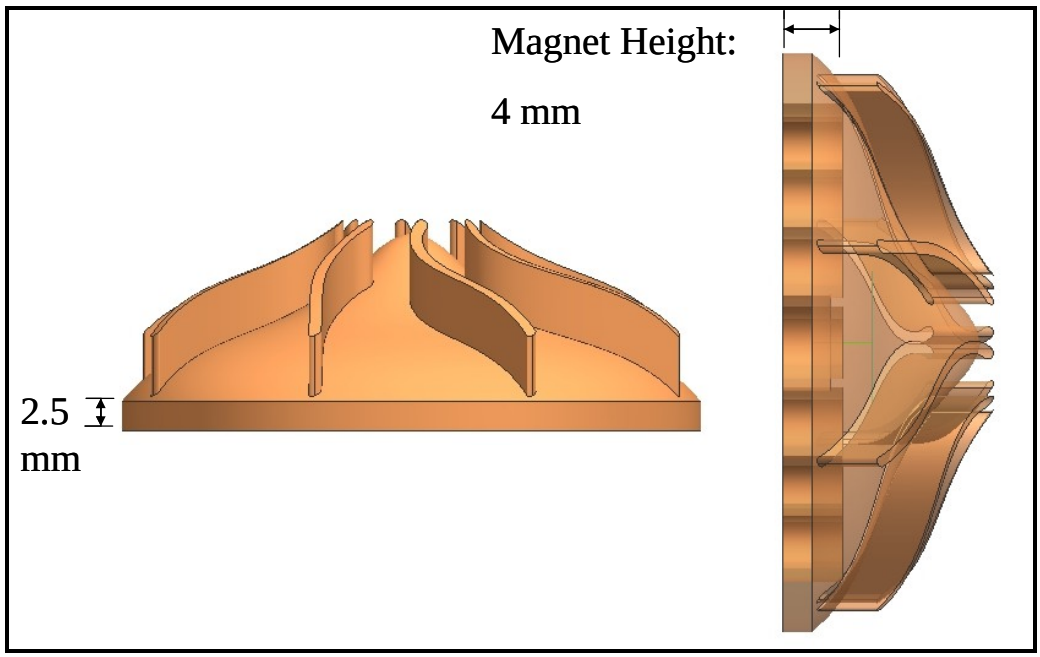

Figure 5.29: The final design of the impeller that will be manufactured from Ti6Al4V

17 holes are drilled on the back surface of impeller; 16 of them are for the magnets and one for the radial bearing. The bearing used for the prototypes of Heart Turcica was made of stainless steel. The same bearing cannot be used in in-vivo tests because the bearing also contacts with blood and has be a biocompatible material. The dimension of the bearing has to be minimum because as the diameter of bearing increases, the circumferential velocity at the contact surface of the impeller and bearing increases and this results in a larger frictional loss. The most suitable biocompatible material for the bearing is ceramic; and miniature ceramic bearing with dimensions of 3 mm inner diameter, 7 mm outer diameter and 2 mm height is used in Heart Turcica.

The casings have to be modified to eliminate all of the possible sharp edges that will cause the tearing of tissues inside the body. Blends are created on all over the sharp edges of casings because red blood cells will be destructed by crashing these zones. Moreover, the excess material is removed from the upper casing periphery and the final design of Heart Turcica Centrifugal is constructed (Figure 5.30).

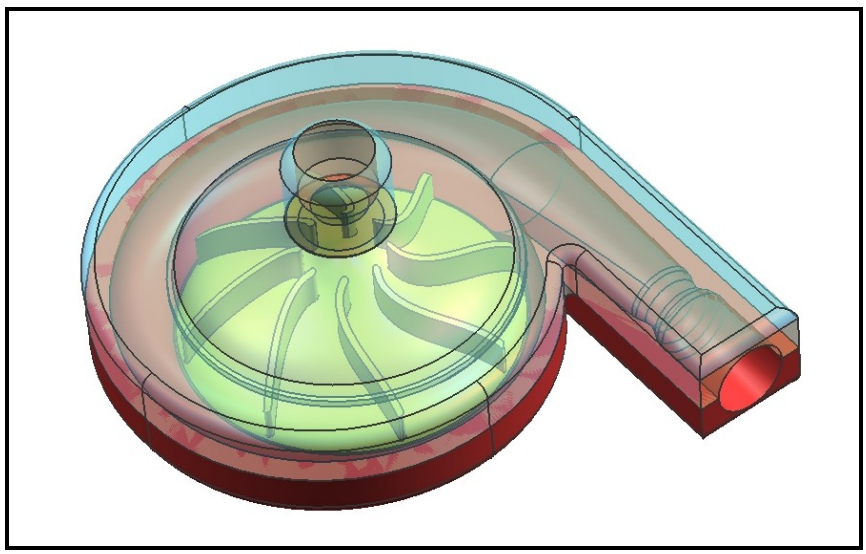

Figure 5.30: The final design of Heart Turcica Centrifugal that will be manufactured from Ti6Al4V

Once the pump is manufactured from Ti6Al4V alloy, next comes the testing of the pump with blood. Before the tests are performed, the pump needs to be coated. In fact Ti6Al4V is a biocompatible metal and it possesses good corrosion resistance, mechanical and electrochemical properties but coating should be done for two main reasons: (1) During the movements of red blood cells passive film can be destructed by crashing on hard tissues and repassivation rate results in delay of film repair on the surface (2) Ti6Al4V owns poor tribiological properties that can enhance both wear debris/metal particle and can give speed up the corrosion reaction of the implant [50]. For better biocompatibility a surface modification is a prerequisite because human body is very sensitive and hostile that the properties of the biomaterial must not disturb the various functions of human body. There are various surface modifications methodologies but mostly used surface modification techniques are titanium-nitride coating and diamond-like-carbon (DLC) coating. Laser alloying of titanium alloys with nitrogen is well-acceptable because of the biocompatibility of titanium nitride. In the most recent years surfaces coated with titanium nitride have been used in many devices such as heart valves, heart assist devices, blood pumps; that are in contact with blood in whole surfaces [51]. On the other hand, diamond-like-carbon also owes superior tribiological and mechanical properties with corrosion resistance, biocompatibility and hemocompatibility. DLC coating decreases the possibility of thrombus formation and which lessens the possibility of hemolysis. DLC coating is decided to be done on Heart Turcica Centrifugal.

Before coating, polishing of untreated and laser treated Ti6Al4V is performed to decrease the maximum roughness surface value to 0.2 μm.

Chapter 6

CONCLUSION & FUTURE WORK

The purpose of this study has been to design and develop an implantable, miniature centrifugal blood pump in order to meet the need of long-term ventricular assist for bridge to transplantation or bridge to recovery in Turkey. It is a fact that the design of the centrifugal pump of the ventricular assist device is quite important because it affects the performance of the pump. A centrifugal pump consists of volute and impeller which are the principal pumping units. The most essential design is performed for the impeller because the shape and the blades of impeller determine the performance and the efficiency of the pump and also the hemolysis index and thrombogenicity ratio. Therefore the impeller design is main concern of this study. In this thesis, a detailed design methodology and layout procedure has been constructed to contribute this design system in the literature. Depending on the simple fluid dynamic calculations, the impeller is carefully designed and the assembly of the pump is completed. Various impeller designs have been made by changing the blade angles. Beyond 17 different designs, Model 2 is selected to analyze and manufacture. The CAD data, CFD simulation results and experimental results of Model 2 have been presented. The experiments have been carried out by using water as the pumping fluid. Moreover, fluid analogous to blood, i.e. 40% glycerin-water solution, has been prepared because in actual case, blood will pass through the pump, water will not.

In order to validate with experimental results, CFD simulations were held and performance curve with theoretical results is obtained. The pump is prepared for the experiments and for the pump, 8 different rotational speeds were set: 1502 rpm, 2002 rpm,

2252 rpm, 2501 rpm, 2751 rpm, 2751 rpm, 2800 rpm, 2900 rpm and 2998 rpm. Measurements smaller than 1500 rpm were not tried because this not a pediatric pump, so it will not meet the needs of a normal heart. It is clearly seen that this pump gives satisfactory results, as it achieves the main objective because at rotational speeds higher than 2500 rpm, it reaches a pressure difference of 100 mmHg and a flow rate of 4.5 liters/min. The effect of shroud size is another subject to concern, so the hub height of the pump model 2 is reduced to 8 mm from 14 mm to investigate the effect of a smaller inside volume of the pump and it has been stated that larger inside volume results in a better performance. The effect of blade height on the pump performance has also been questioned and the pump which was designed and manufactured by Gökhan Yıldız, Model 13, has re-designed with blade heights doubled. Model 13 is selected because it is the pump that achieves best performance. The pressure head achieved by both of these pumps has not changed much, the main difference was larger flow rates have been achieved with higher blade heights. Finally, Model 13 is re-designed with hydrofoil geometry and constant blade thickness and the performance of Model 13 has increased. This pump has also been manufactured from titanium alloy, Ti6Al4V Grade 23, in order to be used inside the body. Ti6Al4V Grade 23 has been selected because after a detailed literature review, it has been seen that this alloy is the most suitable and biocompatible material.

The size of the actuator is not a big deal for the experiments that have been done, but in reality, it is obvious that this motor cannot be used in the body. For real applications, a brushless 50 watt micro motor which has a 45 mm diameter will be used and the pump will be manufactured from titanium alloy to be biocompatible. The experiments will be repeated using blood to observe the hemolysis ratio and thrombogenicity of the pump and finally in-vivo tests will be performed.

.

BIBLIOGRAPHY

[1] http://www.who.int/mediacentre/factsheets/fs317/en/index.html

[2] www.tkd.org.tr

[3] http://www.msnbcntv.com.tr/news/421303.asp

[4] Prof. Dr. Süha Küçükaksu, Türkiye'den Yapay Kalp Pompası Atağı, Anadolu Ajansı, 2006

[5] Sonna M. Patel, Amy L. Throckmorton, Alexandrina Untaroıu, Paul E. Allaire, Houston G. Wood, Don B. Olsen, The Status of Failure and Reliability Testing of Artificial Blood Pumps, American Society of Artificial Internal Organs, 50th year Anniversary Conference

[6] Jean-Raoul Montiés, The living organism and artificial organs, Artificial Organs, 22(5):358-361

[7] Progress of Rotary Blood Pumps: Presidential Address, International Society for Rotary Blood Pumps 2006, Leuven, Belgium, Artificial Organs, 31(5):329-344

[8] S. Ichikawa, K. Watanabe, Y. Nose, The Forth-Generation Centrifugal Blood Pump, Artificial Organs, 2002;5:208-210

[9] Don B. Olsen, The History of Continuous-Flow Blood Pumps, Artificial Organs, 2002;24(6):401-404

[10] Wesolowski SA., The role of the pulse in maintenance of the systemic circulation during heart-lung bypass, Artificial Organs, 1956;1:84-6

[11] Saxton, GA, Andrews CB, AN ideal pump analogous to the mammalian heart, Artificial Organs, 1960;6:288-9

[12] Michael Cotton, Internal Form and Finish Critical to Manufacture of Heart Pump, Artificial Organs, 2006;1:84-6

[13] www.me-server.mecheng.strath.ac.uk/group2004/group1/html/HADs.htm

[14] Yukihiko Nosé, Design and development strategy for the rotary blood pump, Artificial Organs, 1998;22(6):438-446

[15] Kenji Araki, Hirofumi Anai, Mitsuo Oshikawa, Kunihide Nakamura, Toshio Onitsuka, In Vitro Performance of a Centrifugal, a Mixed Flow, and an Axial Flow Blood Pump, Artificial Organs, 1998;22(5):366-370

[16] Takami Y, Makinouchi K, Nakazawa T, Glueck J, Benkowski R, Nosé Y, Effect of Surface Roughness on Hemolysis in a Pivot Bearing Supported Gyro Centrifugal Pump, Artificial Organs, 1996;20:1155-6189

[17] E.F. Bernstein, A.R. Castaneda, P.L. Blackshear, R.L. Varco, Prolonged Mechanical Circulatory Support: An Analysis of Certain Basic Physical and Physiological Considerations, Surgery, 1962;57:103

[18] E.F. Bernstein, L.C. Consentino, S. Reich, P. Stasz, I.D. Levine, D.R.Scott, F.D. Dorman, P.L. Blackshear, A Compact, Low Hemolysis Nonthrombogenic System for Nonthoracotomy Prolonged Left Ventricular Bypass, Artificial Organs, 1974;20:643-54

[19] Golding L.R., Loop F., Peter M., Jacobs G., Gill C., Groves L.K., Nosé Y., Use of a Temporary Left Ventricular Assist System Postoperatively, Artificial Organs 1979;3:394

[20] Losert U., Clogar D., Mayr H., Regonl Myocardial Blood Flow During Nonpulsatile Left Ventricular Bypass in Calves, Trans ASAIO 1982;28:86-92

[21] Natalie L. James, Carmel M.Wilkinson, Nicole L. Lingard, Anita L. van der Meer, and John C.Woodard, Evaluation of Hemolysis in the VentrAssist Implantable Rotary Blood Pump, Artificial Organs, 27(1):108-113

[22] Noon GP, Morley DL, Irwin S, et al., Clinical Experience with the MicroMed DeBakey Ventricular Assist Device, Ann Thorac Surg 2001; 71:S133

[23] Wieselthaler GM, Schima H, Hiesmayr M, et al: First Clinical Experience with the DeBakey VAD Continuous Axial Flow Pump for Bridge to Transplantation, Circulation 2000; 101:356

[24] Westaby S., Frazier OH, Banning A., Six years of continuous mechanical circulatory support, N Engl J Med 2006; 355:325-7

[25] Michael P. Siegenthaler Ju¨rgen Martin, Andreas van de Loo, Torsten Doenst, Wolfgang Bothe, Friedhelm Beyersdorf, Implantation of the permanent Jarvik 2000 Left Ventricular Assist Device, Journal of American College of Cardiology, Vol.39No.11, 2002

[26] Griffith BP, Kormos RL, Borovetz HS, et al: HeartMate II Left Ventricular Assist System: From Concept to First Clinical Use, Ann Thorac Surgery 2001; 71:S116

[27] O.H. Frazier, Reynolds M. Delgado III, Biswajit Kar, Vijay Patel, Igor D. Gregoric, Timothy J. Myers, First Clinical Use of the Redesigned HeartMate II Left Ventricular Assist System in the United States, Texas Heart Institute Journal, 2004;31:157-9

[28] Hideo Hoshi, Tadahiko Shinshi, Setsuo Takatani, Third-Generation Blood Pumps with Non-Contact Magnetic Bearings, Artificial Organs, 30(5):324-338

[29] El-Banayosy A, Koerfer R, Hetzer R, Wieselthaler G, Pavie A, Initial Results of a European multicenter Clinical Trial with the Duraheart Mag-Lev Centrifugal LVAD; J Heart Lung Transplant 2006;25:145

[30] Hetzer R, Weng Y, Potapov EV, First Experiences with a Novel Magnetically Suspended Axial Flow Left Ventricular Assist Device, Eur J Cardiothorac Surgery 204;25:964-70

[31] De Robertis F, Birks EJ, Rogers P, Dreyfus G, Pepper JR, Khaghani A, Clinical Performance with the Levitronix Centrimag Short-term VAD, J Heart Lung Transplant 2006;25:181-6

[32] Lisa Mielniczuk, Tofy Mussivand, Ross Davies, Thierry G. Mesena, Roy G. Masters, Paul J. Hendry, Wilbert J. Keon, Haissam A. Haddad, Patient Selection for Left Ventricular Assist Devices, Artificial Organs, 28(2):152-157

[33] Miller L, Patient Selection for the Use of Ventricular Assist Devices as a Bridge to Transplantation, Ann Thorac Surgery, 2003;75:S66-71

[34] Know and Understand Centrifugal Pumps, Larry Bachus and Angel Custodio, Elsevier, First Edition, 2003

[35] http://www.lightmypump.com/pump_glossary.htm

[36] Centrifugal Pumps Design & Application, Val S. Lobanoff Robert R. Ross, Gulf Professional Publishing, Second Edition

[37] Centrifugal Pump Design, John Tuzson, John Wiley and Sons Inc, 2000

[38] D.J. Vlaming, Optimum Impeller Inlet Geometry for Minimum NPSH Requirement for Centrifugal Pumps in Pumping Machinery, ASME FED Vol.81, pp.25-28

[39] Centrifugal Pump User's Guidebook Problems and Solutions, Sam Yedidiah, Chapman&Hall, 1996

[40] http://www.engineersedge.com/pumps/centrifugal_pump.htm

[41] Yuki Miyazoe, Toshio Sawairi, Kazuyuki Ito, and Junzo Yana, Development of the Small Caliber Centrifugal Blood Pump, Artificial Organs 1998, 22(6):461–465

[42] Eiji Okamoto, Shin-ichi Fukuoka, Eichi Iwazawa, Yoshinori Mitamura, Computer assisted design for the implantable left ventricular assist device (LVAD) blood pump using computational fluid dynamics (CFD) and computer-aided design and manufacturing (CAD/CAM), Artificial Organs (2001) 4:205-213

[43] http://www.wisegeek.com/what-is-computer-aided-manufacturing.htm

[44] MSc Thesis by Onur Demir, Development of an Implantable Left Ventricular Assist Device: Heart Turcica Centrifugal, Koç University Graduate School of Sciences and Engineering, June 2008

[45] Effect of surface modified layers on fretting fatigue damage of biomedical titanium alloys, A. Vadiraj, M. Kamaraj, U. Kamachi Mudali and A. K. Nath, Material Science and Technology, 2006, Vol.22 No.9

[46] Experimental Fluid Mechanics of Pulsatile Artificial Blood Pumps, The Annual Review of Fluid Mechanics 2006, 38:65-86, Steven Deutsch, John M. Tarbell, Keefe B. Manning, Gerson Rosenberg and Arnold A. Fontaine

[47] Flow Through an Outlet Cannula of a Rotary Ventricular Assist Device, Keefe B. Manning and Gerald E. Miller; Biomedical Engineering Program, Virginia Commonwealth University

[48] M.A. Langthjem, N. Olhoff, A numerical study of flow-induced noise in a two-dimensional centrifugal pump. Part I. Hydrodynamics, Journal of Fluids and Structures 19 2004;349–368

[49] L. Xian-hua et al., The Study of the k – ε Turbulence model for Numerical Simulation of Centrifugal Pump

[50] Raghuvir Singh, S. Ghosh Chowdhury, S.K. Tiwari, Narendra B. Dahotre, Laser surface processing of Ti6Al4V in gaseous nitrogen: corrosion performance in physiological solution, Material Sicence: Material Med (2008) 1):1363-1369

VITA

Çınar ERSANLI was born in İzmir, Turkey on October 5, 1984. He received his B.Sc. degree in Mechanical Engineering from Marmara University, İstanbul, ranked 1st in the department, in 2006. Since then, he has enrolled in the M.Sc program in Mechanical Engineering at Koc University, Istanbul as both a teaching and research assistant. He has mainly worked on development of a left ventricular assist device system which consists of a centrifugal pump, and he completed numerous works especially on the design and manufacturing steps of the pump. He is planning to continue his career as a mechanical engineer in the industry.